SAPIENZA
UNIVERSITÀ DI ROMA

Academic year 2012/2013

Facoltà di Farmacia e Medicina

Dipartimento di Chimica e Tecnologie del Farmaco

Dottorato in Scienze Farmaceutiche – XXV ciclo

Chiral Supramolecular Chemistry of Basket Resorc[4]arenes

Supervisor:
Prof. Antonello Filippi

PhD student:
Andrea Calcaterra

Ai miei genitori e a Carmelo Frisina

“Il fascino di una scienza che va crescendo sta nel lavoro dei pionieri che operano alle frontiere dell’ignoto, ma per raggiungere quelle frontiere bisogna percorrere strade molto battute…”

Gilbert Newton Lewis

Contenents

1. General Introduction

1.1 Supramolecular Chemistry

Jean-Marie Lehn, who won the Nobel Prize for his work in the area in 1987, defined supramolecular chemistry as the "chemistry of molecular assemblies and of intermolecular bonds".[1]

This kind of "chemistry beyond the molecule", considered in its simplest sense, regards the (non covalent) binding of a molecule (host) with another molecule (guest), producing a new entity, defined complex or supramolecule, with properties different from those of each single component.

Commonly the host is defined as the molecular entity possessing *convergent* binding sites (*e.g.* Lewis basic donor atoms, hydrogen bond donors *etc.*), while the guest is the entity possessing *divergent* binding sites (*e.g.* Lewis acidic metal cation or hydrogen bond acceptor halide anion). In turn a binding site is defined as a region of the host or guest capable of taking part in a non-covalent interaction.[2]

Generally the host appears as the largest component, such as an enzyme or synthetic cyclic compounds with a central hole or cavity, while the guest correspond to a small organic or inorganic ion, or ion

pair, or a little molecule with biological activity such as hormone or neurotransmitter.

Moreover the host-guest aggregate could be identified using different term, with respect to the forces occurring between the components:[3]

- if electrostatic interactions are the principal forces (including ion–dipole, dipole–dipole, hydrogen bonding *etc.*) the term *complex* is used;
- if less specific, weaker, non-directional interaction are involved (i.e. hydrophobic, van der Waals or crystal close-packing effects) the most appropriate terms are *cavitate* and *clathrate*: the former is constituted by the aggregation of guest and cavitand, host possessing permanent intramolecular cavities available for guest binding as intrinsic molecular property, both in solutions and in solid state; the latter is obtained by the aggregation of guest and clathrands, hosts possessing extramolecular recess that constitute a cavity only after aggregation in solid or crystalline state (Figure 1.1). The distinctions between these classes of supramolecular aggregates are blurred and often the word “complex” is used to cover all these phenomena.

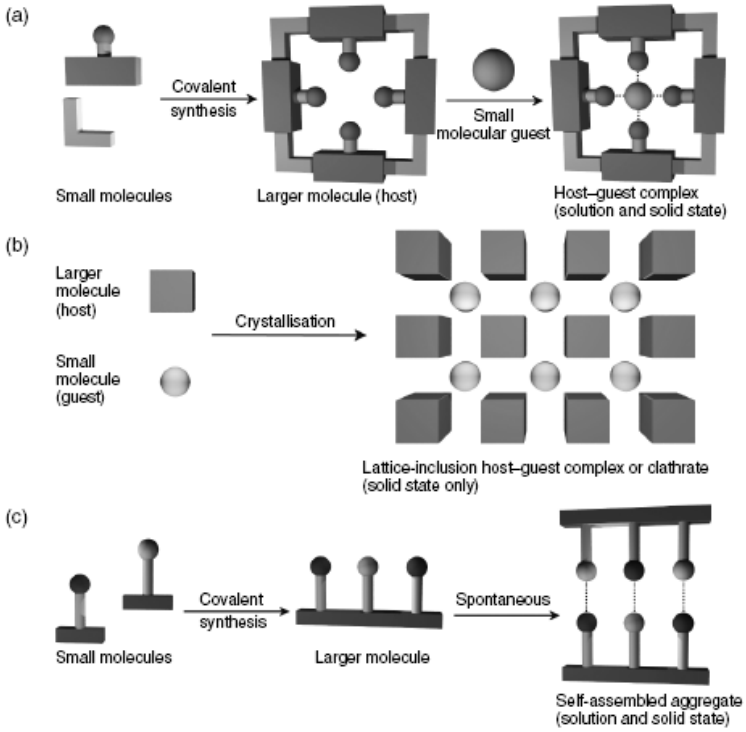

Figure 1.1. Illustration of the difference between a cavitate and a clathrate: (a) synthesis and conversion of a cavitand into a cavitate by inclusion of a guest into the cavity of the host molecule; (b) inclusion of guest molecules in cavities formed between the host molecules in the lattice resulting in the conversion of a clathrand into a clathrate; (c) synthesis and self-assembly of a supramolecular aggregate that does not correspond to the classical host-guest description.

The host-guest chemistry is based on three fundamental concepts: [4]

1. the recognition by Paul Ehrlich, at the beginning of 20th century, that molecules do not act if they do not bind, "*Corpora non agunt nisi fixate*"; in this way Ehrlich introduced the concept of a biological receptor;

2. the recognition in 1894 by Emil Fischer that binding must be selective, as part of the study of receptor–substrate binding by enzymes. He described this by a *lock and key* image of steric fit in which the guest has a geometric size or shape complementarity to the receptor or host. This concept laid the basis for *molecular recognition*, the discrimination by a host between a number of different guests;
3. the fact that selective binding must involve *attraction* or mutual affinity between host and guest. This is, in effect, a generalization of Alfred Werner's 1893 theory of coordination chemistry, in which metal ions are coordinated by a regular polyhedron of ligands binding by dative bonds.

1.2 Molecular Recognition and Host-Guest Chemistry

Associations between host (H) and guest (G) molecules are usually based on simultaneous non-covalent interactions between single binding sites, A (acceptor) and D (donor).[5] Exceptions are solvent-driven equilibria and enforced guest encapsulations within closed host cavities. The need for several binding sites is quite evident: non-covalent interactions are usually weak, and concerted interplay between many sites is the only way to achieve strong and specific complexation (recognition) of a guest molecule. The principle of

multi-site complexation is very general in living systems, where it ensures the efficiency of many important biological functions, including DNA replication, enzyme-substrate recognition, and antigen-antibody interactions.

Furthermore, one can view multi-site complexation as a generalized chelate effect, which is of course well known from coordination chemistry. An important requirement for multi-site binding is complementarity between binding sites of host and guest molecules. In other words, complexation will be more efficient when the shapes and arrangements of binding sites in host and guest molecules fit each other. This is the general lock and key principle of Emil Fischer, who had already explained the remarkable specificity of enzyme catalysis a century ago.

In order to bind, a host must have binding sites that present the correct electronic character (polarity, hydrogen bond donor/acceptor ability, hardness or softness *etc.*) to complement those of the guest. Hydrogen bond donors must match acceptors, Lewis acids must match Lewis bases and so on. Furthermore, those binding sites must be spaced out on the host in such a way as to make it possible for them to interact with the guest in the binding conformation of the host molecule. If a host fulfils these criteria, it is said to be *complementary*. The principle of complementarity has been summed up by Donald Cram:

”To complex, hosts must have binding sites which cooperatively contact and attract binding sites of guests without generating strong non-bonded repulsions”.[6]

An example of extremely efficient biological multi-site binding[7] of a low molecular weight guest (biotin) by a protein host (streptavidin) with an association constant $K= 2.5 \times 10^{13}\ M^{-1}$ is shown in Figure 1.2 (a). A very large binding free energy of -76 kJ mol^{-1} results here from simultaneous action of more than 10 weak pairwise van der Waals, electrostatic, H-bonding and some lipophilic interactions. For comparison, a synthetic receptor for biotin, shown in Figure 1.2 (b), uses only four hydrogen bonds for the guest recognition and therefore exhibits only $K = 9.3 \times 10^{3}\ M^{-1}$ even in the less polar solvent $CDCl_3$, which favors hydrogen bonds.[8] In some cases, however, synthetic host compounds approach the affinity of biological receptors. For example, a protonated azacrown ether[9] (Figure 1.3) can bind ATP (adenosine triphosphate) in water with an association constant of $K= 10^{11}\ M^{-1}$; ethyl adenine can be bound by an artificial receptor in chloroform essentially by multiple hydrogen bonds with $K = 4 \times 10^{5}\ M^{-1}$. [10] Some cyclophanes[11] and calixarenes[12] bind choline and acetylcholine with association constants of 10^{4}-$10^{5}\ M^{-1}$; crown ethers and cryptands can bind alkali cations with stability constants and selectivities similar or even higher than natural ionophores. [13] Some synthetic siderophores have

binding constants for Fe(III) ions around 10^{60} M^{-1}, generating severe problems to determine such values.

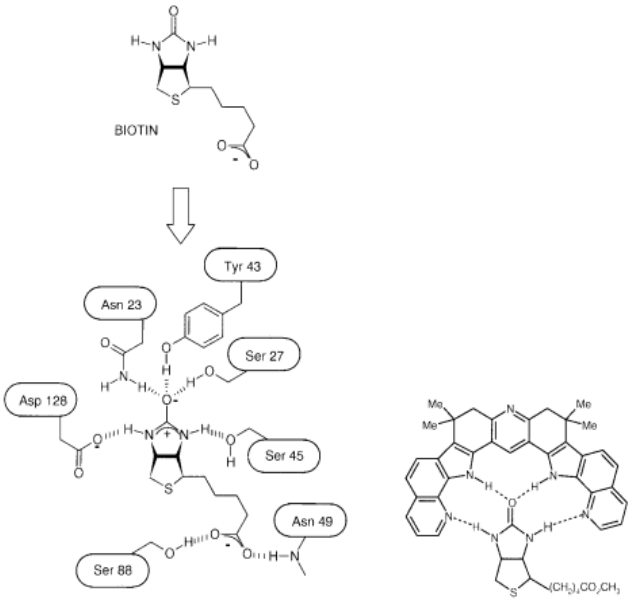

(a) (b)

Figure 1.2. (a) Schematic illustration of biotin binding to streptavidin;[7] (b) Binding of biotin methyl ester to a synthetic host. [8]

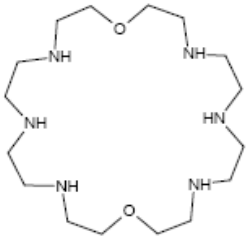

Figure 1.3. Azacrown ether able to complex ATP with an high stability constant.

Much of the emphasis in the construction of supramolecular host molecules concerns summative or even multiplicative interactions (Figure 1.4). This means that we can construct a stable host–guest complex using non-covalent interactions (often weak), if we ensure that there are as many as possible of these interactions stabilizing the complex. The small amount of stabilization energy gained by each of these interactions when added to all the other small stabilizations from the other interactions (*summative*), results in a significant binding energy and hence complex stability.

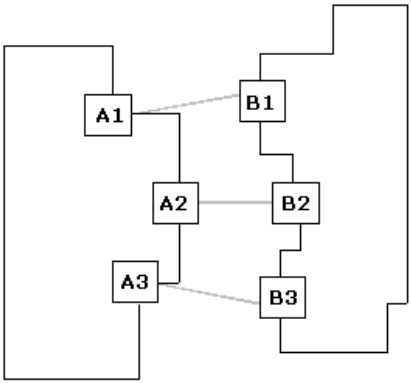

Figure 1.4. Schematic illustration of pairwise multisite host-guest interactions.

In some cases, the interaction of the whole system is synergically greater than the sum of the parts (multiplicative interaction). When two or more binding sites on a host cooperate in this way in binding a guest, the phenomenon is termed *cooperativity*. If the overall stability of the complex is greater than the sum of the energies of the

interactions of the guest with binding groups A and B individually then the result is termed *positive cooperativity*. On the other hand, if unfavourable steric or electronic effects, arising from the linking of A and B together into one host, cause the overall binding free energy for the complex to be less than the sum of its parts, then the phenomenon is termed *negative cooperativity*. Binding site cooperativity in a supramolecular host-guest interaction is simply a generalisation of the *chelate effect* found in classical coordination chemistry. The chelate effect relates to the observation that metal complexes of bidentate ligands (such as 1,2-diaminoethane) are significantly more stable than closely related complexed that contain unidentate ligands (such as ammonia).

1.3 Preorganisation and Macrocyclic Effect

Many supramolecular host–guest complexes are even more stable than what would be expected from cooperative/chelate effects alone. The hosts in these species are usually macrocyclic (large ring) ligands that chelate their guests, again *via* a number of binding sites. Such compounds are additionally stabilised by what is traditionally termed the *macrocyclic effect*. [6] This effect relates not only to the chelation of the guest by multiple binding sites, but also to the *organisation* of those binding sites in space prior to guest binding

(*i.e. preorganisation*). Furthermore the entropic and enthalpic penalty associated with bringing donor atom and lone pairs into close proximity to one another (with consequent unfavourable repulsion and desolvation effects) has been "paid in advance" during the synthesis of the macrocycle. This makes macrocycles difficult to make but stronger complexing agents than analogous non-macrocyclic hosts (podands).

The macrocyclic effect was first elucidated by Cabbiness and Margerum in 1969 who studied the Cu(II) complexes **1.5.a** and **1.5.b**.[14] Both ions benefit from the stability associated with four chelating donor atoms. However, the macrocyclic complex **1.5.a** is about 10^4 times more stable than the acyclic analogue **1.5.b** as a consequence of the additional preorganisation of the macrocycle.

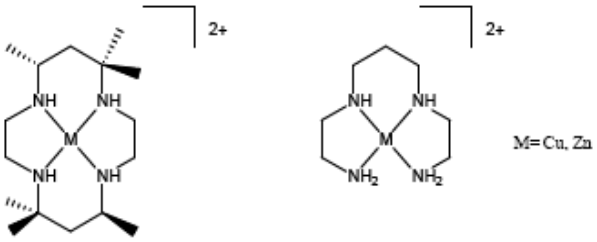

a) b)

Figure 1.5. Ion complexes **1.5.a** and **1.5.b** studied by Cabbiness and Margerum in 1969.[14]

The stabilisation by macrocyclic preorganisation has both enthalpic and entropic contributions. The enthalpic term arises from the fact that macrocyclic hosts are frequently less strongly solvated than their

acyclic analogues. This is because they simply present less solvent-accessible surface area. As a result there are fewer solvent–ligand bonds to break than in the extended acyclic case. Entropically, macrocycles are less conformationally flexible and so lose fewer degrees of freedom upon complexation.

In general, the relative importance of the entropic and enthalpic terms varies according to the system studied, although the enthalpy is frequently dominant. Bicyclic hosts such as *cryptands* are found to be even more stable than monocyclic *corands* for additional factors such as lone pairs repulsions. Historically this further additional stability is referred to as the *macrobicyclic effect* (Figure 1.6) and simply represents the more rigid, preorganised nature of the macrobicycle.

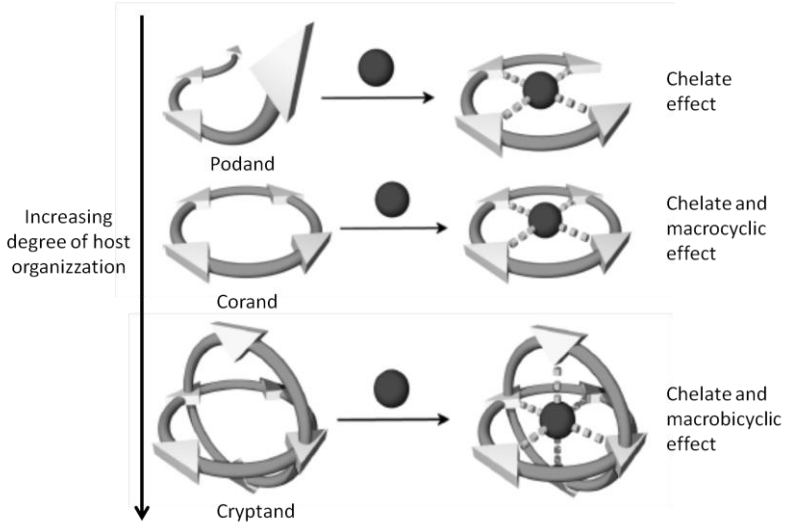

Figure 1.6. The chelate, macrocyclic and macrobicyclic effects.

The macrocyclic and macrobicyclic effects make an important contribution to hosts for alkali metal binding (Scheme 1.1). The macrocyclic and macrobicyclic effects are simply manifestations of increasing *preorganisation*. We can say that if a host molecule does not undergo a significant conformational change upon guest binding, it is *preorganised*. Host preorganisation is a key concept because it represents a major (in some cases decisive) enhancement to the overall free energy of guest complexation.

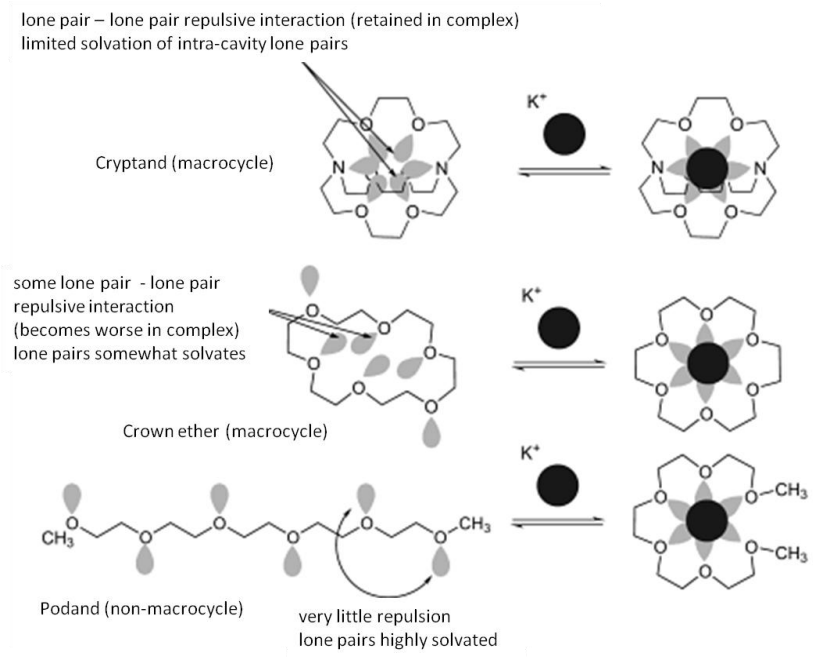

Scheme 1.1. Comparison of preorganisation effects in K^+ binding by a macrobicycle, macrocycle and non-preorganised podand.

Neglecting the effects of solvation, the host-guest binding process may be divided very loosely into two stages. First, there is an activation stage in which the host undergoes conformational readjustment; its binding sites must become complementary to the guest and at the same time unfavourable interactions between binding sites must be minimized. This is energetically unfavourable, and because the host must remain in this binding conformation throughout the lifetime of the host–guest complex, this energy is never paid back. In the second step, binding occurs; this is energetically favourable because of the enthalpically stabilising attraction between mutually complementary binding sites of host and guest.

The overall free energy of complexation represents the difference between the unfavourable reorganisation energy and the favourable binding energy. If the reorganisation energy is large, then the overall free energy is reduced, destabilising the complex. If the host is preorganised, this rearrangement energy is small.

The corollary of preorganisation is in the guest binding kinetics. Rigidly preorganised hosts may have significant difficulty in passing through a complexation transition state and so tend to exhibit slow guest binding kinetics. Conformationally mobile hosts are able to adjust rapidly to changing conditions, and both complexation and decomplexation are rapid. Solvation enhances the effects of preorganisation since the solvation stabilisation of the unbound host

is often greater than the case when it is wrapped around the guest, effectively presenting less surface area to the surrounding medium.

The preorganization[5] principle states that "the more highly hosts and guests are organized for binding and the lower is their solvation prior to their complexation, the more stable will be their complexes".[15]

To sum up both molecules will be optimally preorganized if:

a) all complementary binding sites geometrically match;
b) in the complexed state they are in the same lowest free energy conformation as in the free state;
c) polar binding sites do not need to change solvation.

In this case all distortions will be negligible and the complexation will be energetically most favorable, including only the sum of intrinsic binding free energies. One also may expect the interactions of such preorganized molecules to be highly selective since guests of different structures, such as cations of different sizes, will need different optimal host conformations.

Generally it is not easy to create an universally valid rule to generate a complex, independent from the nature of host and guest, the situation and specific condition. Moreover there are only few highly efficient preorganized hosts. We can say that creating a rigid host molecule, with the right conformation for the complex formation could be the solution, implying a high number of interactive sites in the good position, with a minor entropy loss due to the formation of

the complex. But usually the more rigidified is the conformation the more difficult is the synthesis.

Furthermore we can't forget that in the earlier phase of the complexation a little flexibility in the participants is required, to adapt each other and to get the best orientation for the weak non-covalent interaction to establish. Complexation with a rigid host can be kinetically slow, which is undesirable for many applications. Perfect biological protein receptors possess considerable conformational mobility. Fischer's lock-and-key hypothesis originally viewed protein binding sites as rigid structures. Only later the conformational mobility of proteins was discovered, and the induced-fit hypothesis was proposed: structures of free and bound proteins often endure considerable conformational changes upon binding (Figure 1.7).

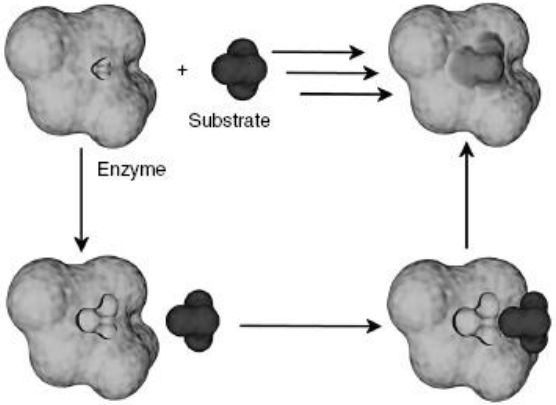

Figure 1.7. The induced-fit model of substrate binding. As the enzyme and the substrate approach each other, the binding site of the enzyme changes shape, resulting in a more precise fit between host and guest.

Inspection of structural data for complexes of proteins with low molecular weight guests (such as sugar, biotin and anion binding proteins, enzymes) shows the primary importance of a very large number of pairwise interactions, more than 10 for the small biotin molecule (see Figure 1.2), while a secondary importance is given to a rigid preorganization.

1.4 Interactions Playing Role in Supramolecular Chemistry

The nature of the interactions involved in supramolecular chemistry is non-covalent, as elucidated many times in this chapter, and they can be divided into three categories: electrostatic, van der Waals and solvofobic interactions. The most important interactions are explained below.

- *Charge-charge interactions*: ionic bonding is comparable in strength to covalent bonding (bond energy = 100-350 kJ mol^{-1}). A typical ionic solid is sodium chloride, which has a cubic lattice in which each Na^+ cation is surrounded by six Cl^- anions; this simple ionic lattice does illustrate the way in which a Na^+ cation is able to organise six complementary donor atoms about itself in order to maximize non-covalent ion–ion interactions. A supramolecular example of charge-charge interactions is the interaction of a

tetranionic cyclophan with an ammonium ion like acethylcoline (Figure 1.8).

The charge-charge interactions follow the physical rules of classical electrostatic with a force depending on: the charges of the interested species, their distance and the dielectric constant of their medium. Because of the directionless and long range character, this interactions play a fundamental role in the early stages of the complex formation.

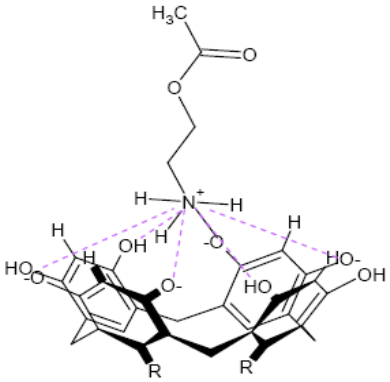

Figure 1.8. Charge-charge interactions between cyclophan and acethylcoline.

- *Hydrogen bond interactions*: these may be regarded as particular kind of dipole–dipole interactions in which a hydrogen atom attached to an electronegative atom such as O or N as the donor (D) is attracted by a similarly electronegative atom, often bearing a lone pair, as the acceptor (A).[16] Hydrogen bonds are commonly written D–H··A.

Because of its relatively strong and highly directional nature, hydrogen bonding has been described as the "masterkey interaction in supramolecular chemistry".[17] In particular, hydrogen bonds are responsible for the overall shape of many proteins, recognition of substrates by numerous enzymes, and (along with π-π stacking interactions) for the double helix structure of DNA.

Hydrogen bonds come in a wide range of lengths, strengths and geometries and can be divided into three broad categories: strong, moderate and weak interactions.

A strong interaction is somewhat similar in character to a covalent bond, whereby the hydrogen atom is close to the centre-point of the donor and acceptor atoms. Strong hydrogen bonds are formed between a strong acid and a good hydrogen bond acceptor, for example in the $H_5O_2^+$ ion or in complexes of "proton sponge", which are practically linear with the hydrogen atom between the two electronegative atoms.

Moderate strength hydrogen bonds are formed between neutral donor and neutral acceptor groups *via* electron lone pairs, for example the self-association of carboxylic acids, or amide interactions in proteins. Moderate hydrogen bond interactions do not have a linear geometry but are slightly bent.

Weaker hydrogen bonds play a role in structure stabilization and can be significant when large numbers act in concert. They tend

to be highly non-linear and involve unconventional donors and acceptors such as C–H groups, the π-systems of aromatic rings or alkynes or even transition metals and transition metal hydrides.

The types of geometries that can be adopted in a hydrogen bonding complex are summarized in Figure 1.9.

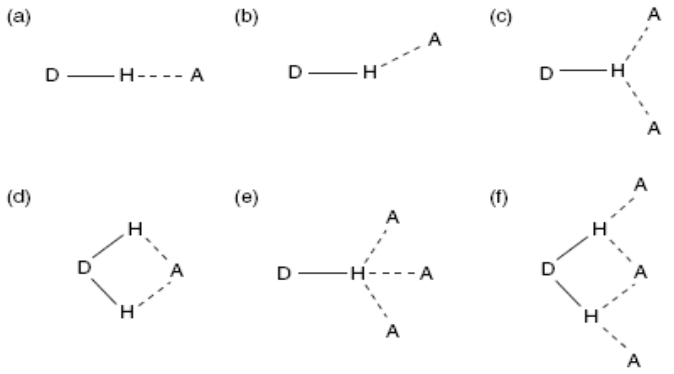

Figure 1.9. Various types of hydrogen bonding geometries; (a) linear, (b) bent, (c) donating bifurcated, (d) accepting bifurcated, (e) trifurcated, (f) three centre bifurcated.

These geometries are termed *primary hydrogen bond interactions*; this means that there is a direct interaction between the donor group and the acceptor group. There are also *secondary interactions* between neighbouring groups that must be considered. The partial charges on adjacent atoms can either increase the binding strength by attraction between opposite charges or decrease the affinity due to repulsion between charges. Figure 1.10 shows two situations in which arrays of hydrogen

bond donors and acceptors are in close proximity. An array of three donors (DDD) facing three acceptors (AAA) (Figure 1.10 a) has only attractive interactions between adjacent groups and therefore the binding is enhanced. Mixed donor/acceptor arrays (ADA, DAD) suffer from repulsions by partial charges of the same sign being brought into close proximity by the primary interactions (Figure 1.10 b).

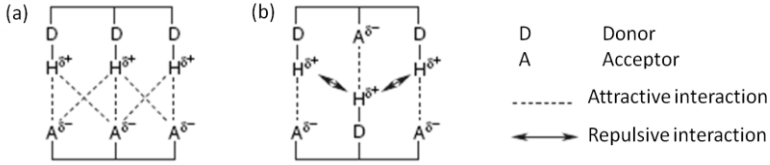

Figure 1.10. (a) Secondary interactions providing attractions between neighbouring groups between DDD and AAA arrays (primary interactions in bold) and (b) repulsions from mixed donor/acceptor arrays (ADA and DAD).

A real-life example of hydrogen bonding is the double helix of DNA. There are many hydrogen bond donors and acceptors holding base pairs together, as illustrated between the nucleobases cytosine (C) and guanine (G) in Figure 1.11. The CG base pair has three primary interactions and also has both attractive and repulsive secondary interactions.

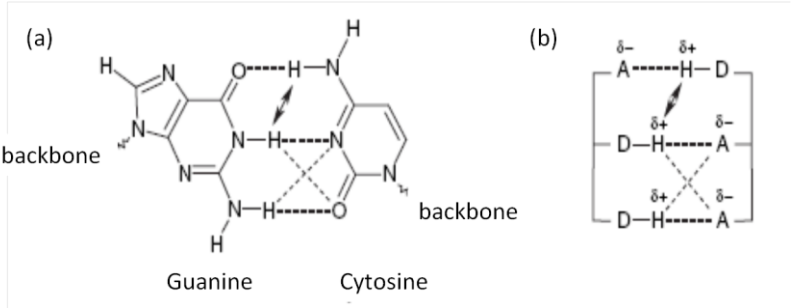

Figure 1.11. (a) Primary and secondary hydrogen bond interactions between guanine and cytosine base pairs in DNA and (b) a schematic representation.

- *Cation-π interactions*: transition metal cations such as Fe^{2+}, Pt^{2+} *etc*. are well known to form complexes with olefinic and aromatic hydrocarbons such as ferrocene $[Fe(C_5H_5)_2]$ and Zeise's salt $[PtCl_3(C_2H_4)]^-$.[18] The bonding in such complexes is strong and could be considered non-covalent, since it is intimately linked with the partially occupied *d*-orbitals of the metals. Even species such as $Ag^+\cdots C_6H_6$ (Figure 1.12) have a significant covalent component. The interaction of alkaline and alkaline earth metal cations with C=C double bonds is, however, a much more non-covalent "weak" interaction, and is suggested to play an important role in biological systems.

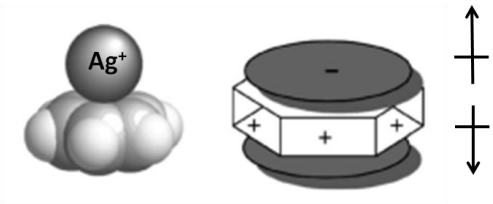

Figure 1.12. Cation-π interaction between a molecule of benzene and Ag^+.

Cation-π interactions are directly dependent on the distance; in fact the ion, because of its charge, has to induce polarization to the charge density of the near molecule. This explains why ammonium ion is not easily complexed by crown ethers and, instead, it interacts effectively with aromatic molecules: the electron density situated on the oxygen of the crown ethers is not sufficient to establish a purely electrostatic bond with a cation. On the contrary benzene, for example, represents a good interaction site because of its permanent electrostatic potential distributed above and below the plane, which is able to determine attraction towards small cationic species. Moreover from analysis of potential area of aromatic molecules, it was noticed that the maximum of this kind of interaction could be reached when the electron rich specie is positioned in perpendicular direction to the ion. This lead to the synthesis of receptor having an indefinite number of aromatic ring in blocked conformation so that the most favourable geometry is reached.

- *π-π interactions*: aromatic *π-π* interactions (sometimes called *π-π* stacking interactions) occur between aromatic rings, often in situations where one is relatively electron rich and one is electron poor.[19] There are two general types of *π*-interactions: face-to-face and edge-to-face, although a wide variety of intermediate geometries are known (Figure 1.13).

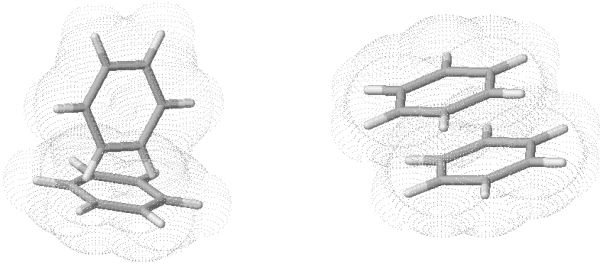

Figure 1.13. Edge-to-face and face-to-face interactions between two molecules of benzene.

Similar π-stacking interactions between the aryl rings of nucleobase pairs also help to stabilise the DNA double helix. Edge-to-face interactions may be regarded as weak forms of hydrogen bonds between the slightly electron deficient hydrogen atoms of one aromatic ring and the electron rich π-cloud of another ring.

Sanders and Hunter have proposed a simple model based on competing electrostatic and van der Waals influences, in order to explain the variety of geometries observed for π–π stacking interactions and to predict quantitatively the interaction energies. Their model is based on an overall attractive van der Waals interaction, which is proportional to the contact surface area of the two π-systems. This attractive interaction dominates the overall energy of the π–π interaction and may be regarded as an attraction between the negatively charged π-electron cloud of one molecule and the positively charged σ-framework of an adjacent

molecule. The relative orientation of the two interacting molecules is determined by the electrostatic repulsions between the two negatively charged π-systems (Figure 1.14). Sanders and Hunter stress the importance of the interactions between individual pairs of atoms rather than molecules as a whole.[20]

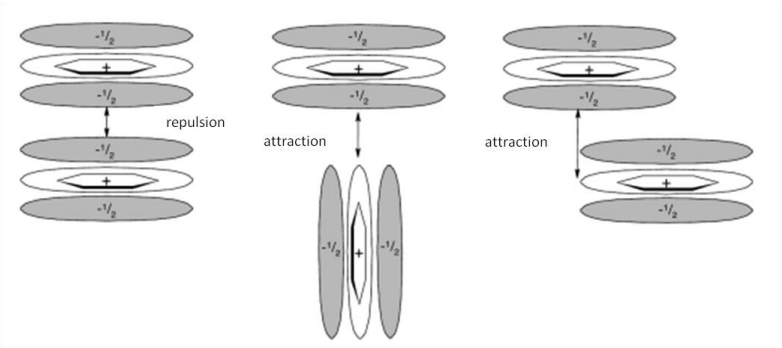

Figure 1.14. Interacting π- quadrupoles.

π-stacking interactions are of considerable interest and importance in the crystal structures of both organic and coordination compounds and have a marked influence on solution binding *via* the hydrophobic effect.

- *Charge transfer interactions*: these are short-range and site specific forces, arising from orbital overlap between the reacting species. They occur with an electron-transfer between high energy molecular orbitals (HOMO, highest occupied molecular orbital) of electron rich species and empty low energy molecular orbitals (LUMO, lowest unoccupied molecular orbital) of electron

deficient molecules.[21] A charge-transfer interaction[22] has two important effects on the complexation process:

a) it stabilizes (or destabilizes) complex formations, affecting the total interaction energy,
b) it results in the net partial transfer of charge (i.e., electrons) from one complexing molecule to the other.

Those kinds of interactions are involved in the complex between a calixarene, which is the electron rich specie because of the presence of hydroxylic groups as substituents, and the fullerene, which is the electron deficient specie (Figure 1.15).

Figure 1.15. Complex between fullerene C_{60} and a calix[4]arene.

- *Solvofobic interactions*: these play an important role in many cases, such as folding of proteins, protein-protein interactions and tensioactives interactions.

  The aggregation of two molecules in a polar medium through their apolar sites is caused by the balancing of two forces:

a) the necessary energy to create a cavity in the solvent and so to win the cohesion between the molecules of solvent;
b) the change of the solvating energy of the molecules participating to the process.

From a thermodynamic point of view the process is favoured by entropic contribute. In fact, considering Frank and Evans‘ theory, the hydratation of a molecule which passes from a gaseous phase to solution is a process characterized by a negative entropy – and so an unfavourable process – because a shell of organized solvent molecules is formed around the molecules to solubilize. Such entropic disadvantage is not filled by the favourable enthalpy due to van der Waals interactions between solute and solvent. So aggregation of apolar particles follows and the molecules of solvent, which form the shell of solvation, are freed.

Solvofobic interactions are directly proportional to the extension of the apolar area of the molecule, which represents the contact area of the complex. They are a good hint for the design of new host. In fact a new tendency is the synthesis of the so called "*deep"* cavitand,[23] i.e. a macrocyclic compound with deep hydrophobic cavity, which allows a better interaction with guest. As an example, calixarenes derivates are able to complex fullerene C_{60}, utilizing the large hydrophobic area beside the charge transfer (Figure 1.16). [24]

Figure 1.16. "*Deep*" cavitand interacting with fullerene C_{60}.

1.5 Supramolecular Chemistry in nature

One of the application of supramolecular chemistry is molecular recognition. It is one of the most sophisticated functions of numerous biological systems (enzymes, antibodies, DNA, etc.) (see for example Figure 1.17) and it has inspired many chemists to synthesize new receptors able to simulate such function.

The enantioselectivity of enzymes, namely the property of enzymes to recognize and metabolise only one of the two enantiomers of chiral molecules, is related to the chiral structure of the enzymes, reflecting the three-dimensional folding of the polypeptide backbone and the orientation of the amino acid side chains in the folded molecule. Enzyme structure may be divided into primary, secondary, tertiary and quaternary features.[25] The primary structure is the

sequence of amino acid residues on the polypeptide chain and is determined by the way in which the enzyme is synthesized. The secondary structure relates to ordering of the chains into discrete units or segments such as α-helices and β-sheets, while tertiary structure is the way in which the secondary structural features arrange themselves to produce the full globular protein. This occurs *via* hydrogen bonding, stacking interactions and hydrophobic forces,

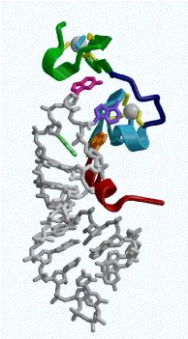

Figure 1.17. NMR structure of the complex between the HIV-1 nucleocapside protein and the SL3 stem loop recognition element of the genomic RNA packaging signal. Knowledge of the complex structure is fundamental for the development of inhibitors designed to interfere with the encapsidation of the virus genome.

and often involves the participation of water molecules buried deep within the enzyme, where they fill small cavities and act as a 'glue' holding secondary features together. In many cases more than one protein strand is involved in a fully functioning enzyme system and the supramolecular association of more than one protein molecule is termed quaternary structure (*e.g.* haemoglobin, a tetramer of four myoblobin units). The enzyme tertiary and quaternary structures are

responsible for the organisation of the binding site(s); they are also the most flexible components of the enzyme structure, allowing the binding site to deform in response to guest binding. Hydrophobic effects, resulting in an overall globular shape, are important like the steric effects, which may be responsible for most of the organisation. Specific, directional hydrogen bonds then determine which, among a small number of globular conformations, is the one favoured. The hydrophobic receptor site is usually located inside and the hydrophilic amino acid residues located on the surface of enzyme are heavily solvated by water molecules in aqueous solution. Then, the supramolecular interactions with specific coenzymes, substrates, and inhibitors inevitably accompany extensive dehydration and conformational change of both enzyme and ligand.

The antigen-specific supramolecular interaction of antibody is also made possible through cooperative weak interactions. Composed of the same components (amino acids), antibody behaves like enzyme upon interaction with its specific antigen. Thus, the binding of antigen to the concave hydrophobic pocket of antibody in aqueous solution induces considerable structural changes especially in antibody and extensive dehydration of both components around the receptor site.

DNA, RNA, and polynucleotides constitute the most sophisticated supramolecular systems that play the crucial, essential roles in living organisms. The basic components of DNA are *nucleotides*,

molecules that contain a nucleobase (either adenine (A), thymine (T), cytosine (C) or guanine (G)) attached to a sugar and a phosphate tail.[26] The A and T components are known as *purines*, while the C and G nucleobases are called *pyrimidines*. Polymerization of these nucleotides *via* the sugar–phosphate residues forms the backbone of a DNA single strand. Within the DNA double helix, the hydrogen-bonded pairs are of a very specific type termed Watson–Crick base pairs (after James Watson and Francis Crick who first described the structure of DNA in 1952). This interaction takes the form of very specific, mutually complementary hydrogen bonds between either adenine and thymine, or guanine and cytosine. No other combinations exist and it is this ability of each nucleic acid to recognise its complementary partner that is the basis for the mode of operation of DNA. In both combinations, more than one hydrogen bond is responsible for the mutual recognition of the complementary bases and the geometry is such that the overall lengths of the two pairs are equal. The hydrogen bond lengths of 2.8–2.9Å are typical of medium-strength N—H…O/N hydrogen bonds. The fact that the G-C pair has three hydrogen bonds while the A-T has only two, means that G-C rich regions of the DNA strand are more stable than A-T regions. The role of base pairing and π–π stacking in assembling the DNA double helix is an excellent example of supramolecular self-assembly, and enables DNA to replicate itself as well as passing on its encoded genetic information to transfer RNA. DNA possesses

several functions of transmission, transcription, and duplication of genetic information, and protein synthesis, all of which involve the equilibrium between single and double-stranded DNA. Hydrophobic domains of nucleic acid bases in single stranded DNA are known to associate together in aqueous solutions, while the hydrophilic phosphates and the carbonyl and amino groups of nucleic acid bases are exposed to aqueous solvent and therefore heavily hydrated. Hence, the duplex formation of DNA inevitably requires the initial dissociation of single-strand aggregation followed by the bimolecular association, which undoubtedly accompany drastic conformational changes and extensive dehydration. In double-stranded DNA, functional groups of nucleic acid bases are completely dehydrated and located inside the hydrophobic domain of duplex, forming efficient interhelix hydrogen bonds as shown in Figure 1.18.

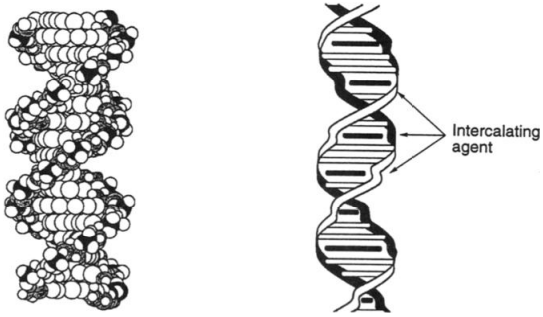

Figure 1.18. B-Type double-stranded DNA *(left)* and intercalated DNA.

Another type of supramolecular interaction of DNA is the intercalation of fused aromatic compounds into the stacked base

pairs in double-stranded DNA (see Figure 1.18). Intercalation induces not only dehydration from the polar groups in the intercalator but also concomitant unwinding, lengthening, dehydration, and stiffening of the DNA double helix.

Taking inspiration from nature, artificial enzymes, enzyme mimics and protein-protein interactions are the latest challenge in supramolecular chemistry.

Real enzymes are more than just highly evolved catalysts: they also recognize and respond to molecules other than their specific substrate and product, as part of the control mechanism of the cell. The evolution of artificial enzymes is at a much more primitive stage, with efficient catalysis as primary objective.[27] To be useful as an industrial catalyst, for example, an artificial enzyme does not need a sophisticated built-in feedback control or high-substrate specificity. A stable molecule that is an efficient catalyst for a key target reaction in a chemical reactor will not be required to select its substrate from many hundreds in the same solution, as enzyme routinely must in the cell. So the sensible design strategy is minimalist: just those features of enzymes that are essential for catalytic efficiency are considered. Enzyme mimics catalyze reactions by mechanism that are demonstrably enzyme-like.

Cyclodextrins have proved the most enduringly popular enzyme mimics. Their central hydrophobic cavity is lined with CH groups and glycosidic oxygen atoms, and carries arrays of functional

hydroxyl groups on both rims. The unmodified cyclodextrins are themselves good functional enzyme mimics, catalyzing various relatively rapid reactions: the basis of the catalysis is the positioning of the reactive secondary hydroxyl groups directly at the entrance to the molecular cavity. One of the most effective reactions catalysed by cyclodextrins is the hydrolysis of aryl and phosphate esters (esterase activity). For example, the rate of hydrolysis of *p*-nitrophenol esters is increased by factors of up to 750 000 by *β*-CD. The mechanism of action of the cyclodextrin is shown in Scheme 1.2.[28]

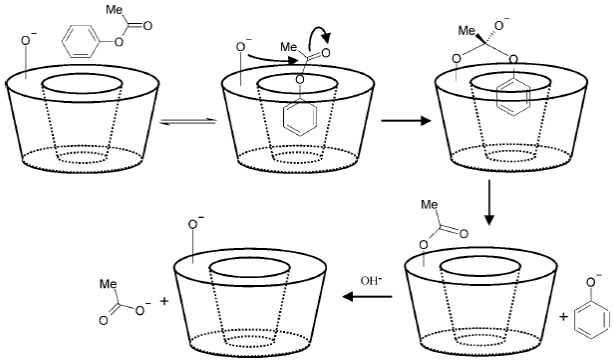

Scheme 1.2. Mechanism of ester hydrolysis by *β*-cyclodextrin.

The use of cyclodextrins as enzyme mimics has been extended to incorporate dimers and trimers of cyclodextrins, as well as a range of transition metal complexes (Figure 1.19).[29]

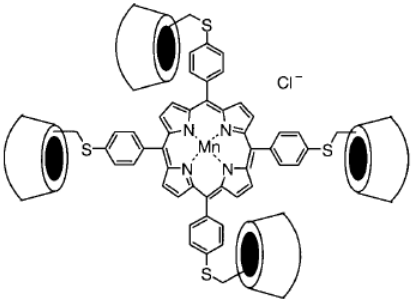

Figure 1.19. An example of cyclodextrins as enzyme mimics.[31]

Catalytic antibodies[30] are currently the most successful enzyme mimics. They are quite good at catalyze easy reactions, like the hydrolysis of *p*-nitrophenyl esters, and have been reported to catalyze the hydrolysis of benzyl[31] and other alkyl esters[32] but not that of ordinary amides at a useful rate.[33]

Protein-protein interactions play key roles in several biological processes, such as cell proliferation, growth and differentiation, and these interactions are therefore attractive targets for the chemical biologist.[34] There have been recent reports on protein surface recognition by peptide calixarenes. Cunsolo *et al.* have designed basic amino acid calyx[8]arenes receptors that behave as competitive inhibitors of recombinant human tryptase, probably binding the intended region of Asp residues near the active site of the tetrameric protein.[35] Neri *et al.* recently demonstrated the surface recognition of transglutaminase by their peptidocalix[4]arene diversomers (isomers comprising the same components that are arranged in

different orders).[36] Hamilton *et al.* have introduced 3,2',2'-functionalised terphenyl derivatives as structural and functional mimetics of α-helices with the preparation of two potent antagonists of calmodulin,[37] and inhibitors of the assembly of the hexameric HIV fusion protein gp41.[38]

1.6 Calixarenes as Artificial Receptors

The calixarenes are macrocyclic molecules containing phenolic rings bridged by methylene groups and are among the most ubiquitous host molecules in supramolecular chemistry.[39-44] The basic molecular scaffolds are, in general, simple to prepare in high yields from cheap starting compounds: they derive from the condensation of phenols and formaldehyde.

These compounds are characterized by an hydrophobic cavity which allows the interactions with neutral molecules,[45] but they can also be derivatized in the lower rim or in para positions on the aromatic nuclei (upper rim) with catalytic centers or other functional groups which favor interactions with ions (Figure 1.20).[46]

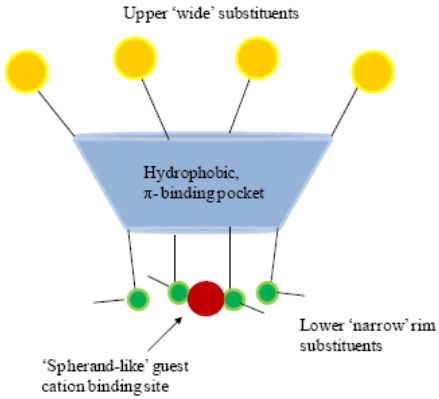

Figure 1.20. Anatomy of a calix[4]arene in the cone conformation.

The parent calixarenes are flexible during their high temperature synthesis, with rotation of the phenolic moieties about the bridging CH_2 groups possible, but the smallest members of the class "freeze out" upon cooling to ambient temperatures.[47] This is an important consideration when working with calix[4]arenes as they exist in four conformers that are hard to interconvert and become immobilized in a particular conformer if substituents are bound in the lower rim, even if re-heated to relatively high temperatures. Four principal conformers are observed at room temperature. If all four upper rim substituents are in the same orientation, then a cone conformer results, which is the average C_{4v} symmetry structure resulting from a fast equilibrium between two equivalent C_{2v} flattened cone conformers. [48] If one phenolic group is inverted with respect to the others, a partial cone conformer is found. Finally, two possibilities exist when two phenol rings are inverted: 1,2 alternate and 1,3

alternate. All four conformers are illustrated in Figure 1.21. Similar descriptions exist for larger calixarenes although these compounds are often conformationally dynamic and only frozen out in the solid state or in low temperature experiments.

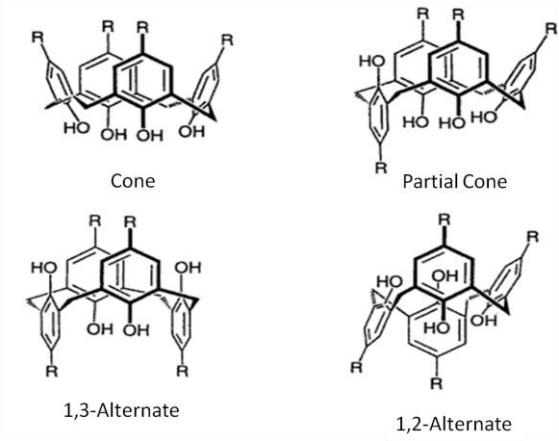

Figure 1.21. Calix[4]arene conformers.

The *resorcarenes* (or *calixresorcarenes*) (Figure 1.22) are closely related compounds. These are prepared in the similar way of calixarenes by condensation of resorcinol (3-hydroxyphenol) with aldehydes. In this case, acid-catalysed conditions are used and the preparation does not work with formaldehyde itself because of the consequent polymerisation reactions from the 2-position. However a wide range of other aldehydes are highly effective and commonly acetaldehyde (able to give a methyl ”feet” to the resorcarene bowl) or 2-phenylethanal (resulting in enhanced solubility of the product in organic solvents) are used.

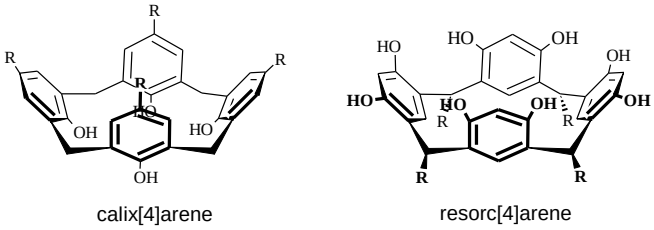

calix[4]arene resorc[4]arene

Figure 1.22. Nuclei of calix[4]arene and resorc[4]arene in cone conformation.

Also resorc[4]arenes possess a bowl-shaped conformation in their most stable form. This bowl is wider and shallower than in the calixarene analogues as a consequence of the presence of the "upper rim" hydroxy substituents, which stabilizes the bowl by intramolecular hydrogen bonding. Resorcarenes bearing small substituent groups are relatively conformationally mobile, adopting partial cone, 1,2-alternate and 1,3-alternate conformations as well as the cone form. (Figure 1.23)

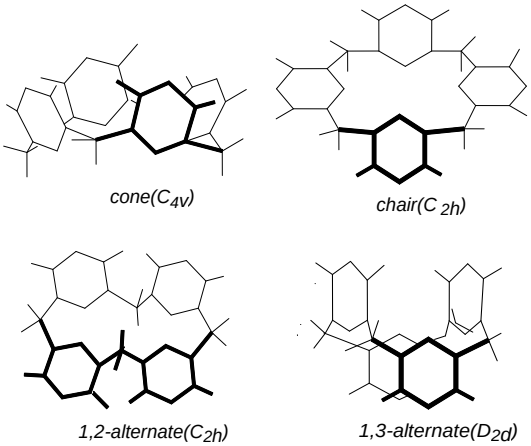

Figure 1.23. Principal conformations (and symmetry) for the resorc[4]arene.

Using the cone resorcin[4]arene as central macrocyclic scaffold, [49,50] functionalized on the lower rim by binding two bridged chains based on different diamines, a new class of resorc[4]arenes has been obtained, the basket bis-diamido resorc[4]arenes.

The presence of several idrogen-bond donors and acceptors inside these molecules makes them suitable for binding different guest, leading to the formation of a host-gest complexes. The loss of conformational entropy in the receptor, occurring during the formation of the complex, is limited by the structural preorganization offered by the same macrocyclic scaffold.

On these basis we decided to synthetize both enantiomer of two basket bis-diamido resorc[4]arenes, one already described in literature and one completely new. The synthesis will be described in the next chapter.

1.7 References

[1] J.-M. Lehn, *Supramolecular chemistry –scope and perspectives. Molecules, supermolecules, and molecular devices* (Nobel lecture), *Angew. Chem. Int. Ed. Engl*., **1988**, *27*, 90.

[2] E. P. Kyba, R. C. Helgeson, K. Madan, G. W. Gokel, T. L. Tarnowski, S. S. Moore, D. J. Cram, *J. Am. Chem. Soc*., **1977**, *99*, 2564-2571.

[3] J. W. Steed and J. L. Atwood, *Supramolecular Chemistry, 2nd edition*, John Wiley & Sons, Ltd, **2009**.

[4] J. P. Behr, *The Lock and Key Principle. The State of the Art – 100 Years on*, John Wiley & Sons, Inc., New York, **1994**.

[5] H. J. Schneider, A. Yatmirsky , *Principles and Methods in Supramolecular Chemistry*, Wiley, Chichester, **2000**.

[6] Cram, D. J., *Angew. Chem. Int. Ed. Engl.*, **1986**, *25*, 1039-1134.

[7] P. C. Weber, J. J. Wendoloski, M. W. Pantoliano, F. R. Salemme, *J. Am. Chem. Soc.*, **1992**, *114*, 3197.

[8] V. Hegde, C. Y. Hung, P. Madhukar, R. Cunningham, T. Hopfner, R. P. Thummel, *J. Am. Chem. Soc.*, **1993**, *115*, 872.

[9] M. W. Hosseini, J.-M. Lehn, *Helv. Chim. Acta*, **1987**, *70*, 1312.

[10] D. G. Lonergan, G. Deslongchamps, S. Tomás, *Tetrahedron Lett.*, **1998**, *39*, 7861.

[11] D. A. Dougherty, *Science*, **1996**, *271*, 163.

[12] (a) J.-M. Lehn, R. Meric, J. P. Vigneron, M. Cesario, J. Guilhem, C. Pascard, Z. Asfari, J. Vicens, *Supramol. Chem.*, **1995**, *5*, 97; (b) H. J. Schneider, D. Güttes, U. Schneider, *J. Am. Chem. Soc.*, **1988**, *110*, 6449.

[13] Y. Inoue, G.W. Gokel, *Cation Binding by Macrocycles*, Marcel Dekker, Inc., New York, **1990**, p. 761.

[14] D. K. Cabbiness, D. W. Margerum, *J. Am. Chem. Soc.*, **1969**, *91*, 6540-6541.

[15] D. J. Cram, *Angew. Chem, Int. Ed. Engl.*, **1988**, *27*, 1009.

[16] G. A. Jeffrey, *An Introduction to Hydrogen Bonding*, Oxford University Press, Oxford, **1997**.

[17] J.-M. Lehn, *Supramolecular Chemistry*. *1 ed.*, VCH, Weinheim, **1995**.

[18] J. C. Ma, D. Dougherty, *Chem. Rev.*, **1997**, *97*, 1303-1324.

[19] C. A. Hunter, K. R. Lawson, J. Perkins, C. J. Urch, *J. Chem. Soc., Perkin Trans. 2*, **2001**, 651-669.

[20] E.-I. Kim, S. Paliwal, C. S. Wilcox, *J. Am. Chem. Soc.*, **1998**, *120*, 11192.

[21] (a) R. L. Flurry, *J. Phys. Chem.*, **1965**, 69; (b) R. L. Flurry, *J. Phys. Chem.*, **1969**, 73.

[22] K. Kitaura, K. Morokuma, *Int. J. Quantum Chem.*, **1976**, *10*, 325-340.

[23] D. M. Rudkevich, J. Jr. Rebek, *Eur. J. Org. Chem.*, **1999**, *9*, 1991-2005.

[24] F. C. Tucci, D. M. Rudkevich, J. Jr. Rebek, *J. Org. Chem.*, **1999**, *64*, 4555-4559.

[25] D. H. Kim, "Supramolecular aspects of enzymes", in *Comprehensive Supramolecular Chemistry*, J. L. Atwood, J. E. D. Davies, D. D. MacNicol, F. Vögtle (Eds.), Pergamon, Oxford, **1996**, vol. 4, 503-526.

[26] C. R. Calladine, H. R. Drew, B. Luisi, A. Travers, *Understanding DNA: The Molecule and how it Works*, Academic Press, New York, 3rd ed., **2004**.

[27] A. J. Kirby, *Angew. Chem. Int. Ed. Engl*., **1996**, *35*, 707-724.

[28] a) F. Diederich, *Chem. Unserer Zeit*, **1983**, *17*, 105-119.; b) M. Komiyama, H. Hirai, *Chem. Lett.*, **1980**, 1251-1254.

[29] R. Breslow, S. D. Dong, *Chem. Rev.*, **1998**, *98*, 1997-2011.

[30] a) P. G. Schultz, *Angew. Chem.*, 1989, *101*, 1336; *Angew. Chem. Int. Ed. Engl.*, **1989**, *28*, 1283; b) U. K. Pandit, *Rec. Trav. Chim.*, **1993**, *112*, 431.

[31] D. S. Tawfik, B. S. Green, R. Chap, M. Sela, Z. Eshhar, *Proc. Natl. Acad. Sci. USA*, **1993**, *90*, 373-377.

[32] S. J. Pollack, P. Hsiun, P. G. Schultz, *J. Am. Chem. Soc.*, **1989**, *111*, 5961-5962.

[33] M. T. Martin, T. S. Angeles, R. Sugasawara, N. I. Aman, A. D. Napper, M. J. Darsley, R. I. Sanchez, P. Booth, R. C. Titmas, *J. Am. Chem. Soc.*, **1994**, *116*, 6508-6512.

[34] P. L. Toogood, *J. Med. Chem.*, **2002**, *45*, 1543-1558.

[35] T. Mecca, G. M. Consoli, C. Geraci, F. Cunsolo, *Bioorg. Med. Chem.*, **2004**, *12*, 5057-5062.

[36] S. Francese, A. Cozzolino, I. Caputo, C. Esposito, M. Martino, C. Gaeta, F. Troisi, P. Neri, *Tetrahedron Lett.*, **2005**, *46*, 1611-1615.

[37] B. P. Orner, J. T. Ernt, A. D. Hamilton, *J. Am. Chem. Soc.*, **2001**, *123*, 5382-5383.

[38] J. T. Ernt, O. Kutzki, A. K. Debnath, S. Jiang, H. Lu, A. D. Hamilton, *Angew. Chem. Int. Ed. Engl.*, **2002**, *41*, 278-281.

[39] C. D. Gutsche, in *Calixarenes Revisited*, J. F. Stoddart (Ed.); The Royal Society of Chemistry, Cambridge, **1998**.

[40] In *Calixarenes in Action*, L. Mandolini, R. Ungaro (Eds.); Imperial College Press, London, **2000**.

[41] In *Calixarenes 2001*, Z. Asfari, V. Böhmer, J. Harrowfield, J. Vicens (Eds.), Kluwer Academic Publishers, Dordrecht, The Netherlands, **2001**.

[42] A. Katsuhiko, K. Toyoki, *Supramolecular Chemistry-Fundamentals and Application*, Iwanami Shoten Publishers , Tokyo, Springer, **2006**.

[43] A. Casnati, F. Sansone, R. Ungaro, *Acc. Chem. Res.*, **2003**, *36*, 246-254.

[44] R. Ludwig, *Microchim. Acta*, **2005**, *152*, 1-19.

[45] A. Arduini, A. Pochini, A. Secchi, F. Ugozzoli, "Recognition of Neutral Molecules", In *Calixarenes 2001*, Z. Asfari, V. Böhmer,

J. Harrowfield, J. Vicens (Eds.), Kluwer Academic Publishers: Dordrecht, The Netherlands, **2001**, Chapter 25.

[46] A. Dalla Cort, L. Mandolini, "Calixarenes As Hosts for Quats", in *Calixarenes in Action*, L. Mandolini, R. Ungaro (Eds.), Imperial College Press, London, **2000**, Chapter 5.

[47] J. W. Steed, J. L. Atwood, *Supramolecular Chemistry, 2nd edition*, John Wiley & Sons, Ltd, **2009**.

[48] L. Abis, E. Dalcanale, A. Du Vosel, S. Spera, *J. Org. Chem.*, **1988**, *53*, 5475.

[49] B. Botta, I. D'Acquarica, G. Delle Monache, D. Subissati, G. Uccello-Barretta, M. Mastrini, S. Nazzi, M. Speranza, *J. Org. Chem.*, **2007**, *72*, 9283-9290.

[50] B. Botta, C. Fraschetti, I. D'Acquarica, M. Speranza, F. R. Novara, J. Mattay, M. C. Letzel, *J. Phys. Chem. A*, **2009**, *113*, 14625-14629.

2. Synthesis of chiral basket resorc[4]arenes

2.1 Introduction

Botta *et al.*[1] in 1997 synthesized double-spanned calix[4]resorcarenes treating a octamethyl tetraalcohol resorc[4]arene with glutaroyl, adipoyl and pimeloyl dichlorides in the presence of triethylamine. The insertion of two polymethylene bridges led to the formation of a cavity-shaped architecture resembling a basket which gave the name to these molecules. NMR characterization showed a C_{2v} symmetry with two parallel bridges: the formation of the bridge froze one of the two flattened cone conformations, which are normally in fast equilibrium to get the cone conformation as average (Figure 2.1).

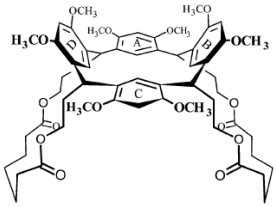

Figure 2.1. Chemical structures of a basket resorc[4]arene with two polymethylene bridges.

With the aim to build chiral rigidified hosts and to value their enantiodiscrimination ability, preorganized double-bridged resorc[4]arenes, resembling a basket, were synthesized by the

insertion of two bifunctional chiral molecules to four of the free functions of the resorcarenic cavity.

2.2 Results and Discussion

Resorc[4]arenes octamethyl ether tetraester **3** (*cone* conformation), was obtained following the synthetic procedures already published by Botta *et al.*[2] where the ability of ethereal BF_3 to convert (*E*)-2,4-dimethoxycinnamic acid derivatives to the corresponding mixture of tetraester was described. The *cone* conformer of **3**, isolated by column chromatography, was then hydrolyzed by treatment with NaOH (Scheme 2.1).

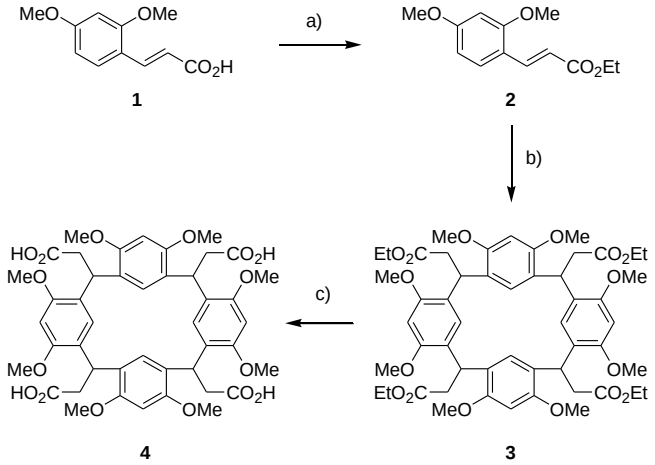

Scheme 2.1. Synthetic procedure for resorc[4]arene tetracid **4**; a) H_2SO_4, EtOH, reflux 4h, 98%; b) $BF_3{\cdot}Et_2O$, $CHCl_3$, reflux, 30 min, 20% of cone conformer; c) NaOH 2N, EtOH, reflux, 6h, than CH_3COOH glacial, 86%.

The corresponding tetraacid **4** was quantitatively converted into the tetrachloride derivative **5** by reaction with thionyl chloride. Treatment of dry THF solutions of **5** with diisopropylethylamine (DIPEA) and (1*R*,2*R*)-(+)-1,2-diphenylethylenediamine (DPEDA), under an atmosphere of argon, afforded compound (*all-R*)-**6** (31% yield, scheme 2.2). The same synthetic procedure with (1*S*,2*S*)-(–)-1,2-diphenylethylenediamine gave (*all-S*)-**6** (29% yield, with opposite $[\alpha]_D$ and coincident NMR and MS data) (Scheme 2.2).[3]

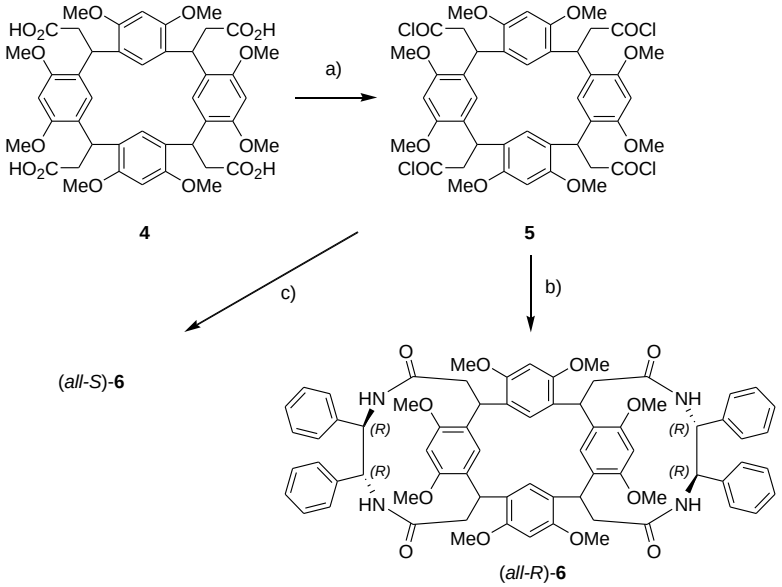

Scheme 2.2. Synthetic procedure for enantiomeric bis(diamido)-bridged basket resorc[4]arenes **6** [3]; a) $SOCl_2$, dry benzene, reflux 4h, quantitative yield; b) DIPEA, (1*R*,2*R*)-(+)-1,2-diphenylethylenediamine, dry THF, reflux overnight, 31%; c) DIPEA, (1*S*,2*S*)-(+)-1,2-diphenylethylenediamine, dry THF, reflux overnight, 29%.

These receptors have been extensively studied by spectroscopy both in gas and solution phase, because of their high capacity of forming complexes with several biological compounds, in particular nucleosides, and their ability to form diastereomeric complexes which show different interaction pattern giving a sort of chiral recognition.

In order to construct a chiral basket resorc[4]arene with less rigid side arms, we decide to synthetize a different diamine based on valine, to be used in the coupling reaction with tetrachloride derivative **5**. In this way, using L- or D-valine derivatives as starting material both enantiomers of resorc[4]arene **10** could be prepared.

Dimanine **9** was synthesized starting from N-Cbz-valine **7** which was commercially available in L- configuration and was prepared from D-valine and benzylchloroformiate according to the established procedures (scheme 2.3).[4]

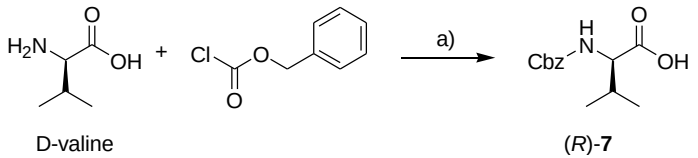

Scheme 2.3. Synthesis of (*R*)-**7**; a) Na_2CO_3, H_2O/1,4-dioxane overnight, 0°C → r.t., 99%.

N-Cbz-L-valine (*S*)-**7** was condensed with ethylene glycol in presence of benzotriazol-1-yloxytris(dimethylamino)-phosphonium (BOP) and triethylamine to afford compound (*S*,*S*)-**8**. Deprotection of amino groups of **8** by hydrogenolysis, using Pd supported on

carbon as catalyst, gave diamine (*S*,*S*)-**9** with 47% overall yield (scheme 2.4).

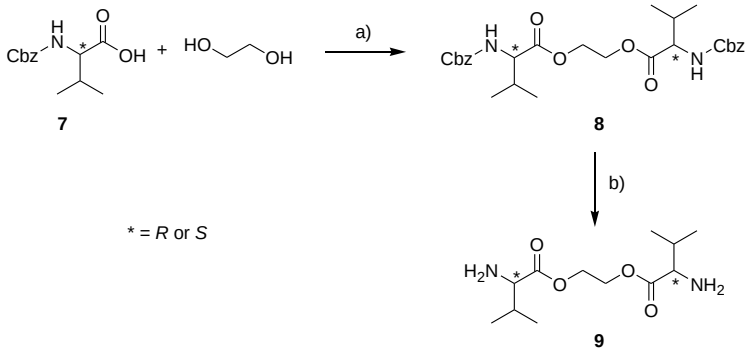

Scheme 2.4. Synthesis of enantiomeric diamines **9**; a) BOP, Et_3N, CH_2Cl_2, 4h, r.t., 54%; b) H_2, Pd/C, EtOH/THF 1:1, 94%.

The same synthetic procedures performed on N-Cbz-D-valine (*R*)-**7** gave diamine (*R*,*R*)-**9**. These enantiomeric diamines **9** was therefore employed in a coupling reaction with tetrachloride **5**, which was prepared as before by treatment of tetraacid **4** with thionyl chloride in dry benzene. Reaction of **5** with (*R*,*R*)-**9** in presence of DIPEA afforded basket resorc[4]arene (*all-R*)-**10** (42% yield). By treatment of **5** with (*S*,*S*)-**9** in the same experimental conditions (*all-S*)-**10** was obtained (22% yield with opposite $[\alpha]_D$ and coincident NMR and MS data) (scheme 2.5).

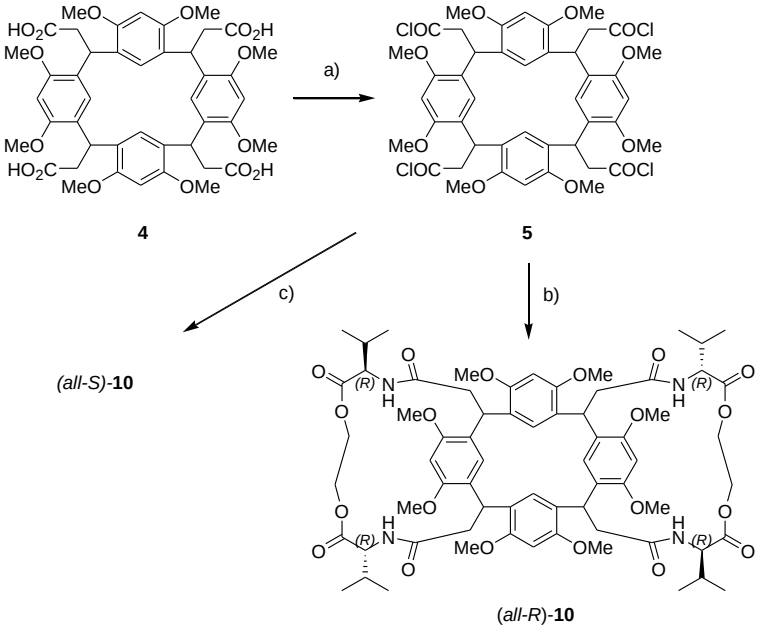

Scheme 2.5. Synthetic procedure for enantiomeric bis(diamido)-bridged basket resorc[4]arenes **10**; a) $SOCl_2$, dry benzene, reflux 4h, quantitative yield; b) DIPEA, (*R*,*R*)-**9**, dry THF, reflux overnight, 20%; c) DIPEA, (*S*,*S*)-**9**, dry THF, reflux overnight, 22%.

2.3 Studies on Enantiodiscrimination

Once supramolecular assembly has been established, a number of techniques in different phases can be used to generate data on the stoichiometry of the species involved and the affinity of host molecules for guests. In particular, both enantiomers of compounds **6** and **10** have been chosen as artificial receptors to perform host-guest

studies, both in the gas and in the solution-phase through mass spectrometry and NMR spectroscopy, respectively.

The emphasis was mainly put on the understanding of the fundamental interactions responsible of chiral discrimination by calixarenes. In particular ESI-MS experiments were performed using a quadrupole ion trap mass spectrometer equipped with an IR optical parametric oscillator/amplifier (OPO/OPA) system, pumped by a Nd:YAG laser for ESI-IRMPD analysis and an electrospray-ionization fourier-transform ion cyclotron resonance mass spectrometer (ESI-FT-ICR) to carry out our chiral recognition studies.

Enantiodiscrimination in solution-phase was studied determining the heteroassociation constants of the different complexes of calixarenes by ^{1}H NMR and DOSY (Diffusion Order SpectroscopY) techniques. Moreover some elucidations on the tridimensional conformation of the free host or of the complex were given through 1D and 2D ROESY (Rotating Overhauser Effect SpectroscopY) techniques.

Finally calixarenes are well known in literature as **CSA** (Chiral Solvating Agent),[5] so ^{1}H NMR experiments were carried out with different kinds of chiral molecules to differentiate enantiomeric mixtures.

2.3.1 Analytical Methods Based on Mass Spectrometry

Recently attention has been paid to the study of the physicochemical properties of chiral systems in solvent free conditions by mass spectrometry under suitable conditions.[6] Through this technique it is possible to measure the different stabilities of the diastereomers formed by interactions of enantiomers with a chiral reagent, which is added into the analyte solution in approximately the same relative amounts. Information obtained would include structural and chemical information alongside the chiral analysis and nearly every type of compound could be studied due to the vast array of ionization sources available.

Electrospray ionization, coupled with mass spectrometric detection (ESI-MS), proved very suitable, since it provides precious information on the stability of chiral clusters simply through the measurement of ion abundances.[6,7] A host molecule complex an analyte guest through various non-covalent interactions such as H-bonding or van der Waals.[8] The resulting complexes are diastereomeric with unique ionization efficiencies.[9] The differences in ionization efficiencies in turn produce unique abundances that can be normalized to provide e.e. (enantiomeric excess). Determination of e.e. may also be performed by collision-induced dissociation, where the MS/MS of diastereomeric adducts is performed.[10]

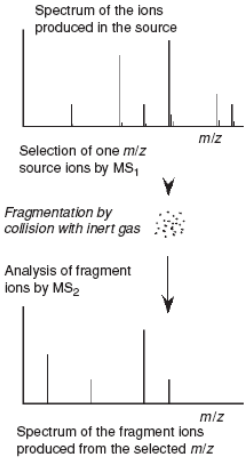

Figure 2.2. Principle of MS/MS: an ion M_1 is selected by the first spectrometer MS_1, fragmented through collision, and the fragments are analysed by the second spectrometer, MS_2. Thus ions with a selected *m/z* value, observed in a standard source spectrum, can be chosen and fragmented so as to obtain their product ions spectrum.

The success of ESI started when Fenn *et al.*[11] showed that multiply charged ions were obtained from proteins, allowing their molecular weight to be determined with instruments whose mass range is limited to as low as 2000 Th. Later on, its use was extended not only to other polymers and biopolymers, but also to the analysis of small polar molecules.

ESI[12] is produced by applying a strong electric field, under atmospheric pressure, to a liquid passing through a capillary tube with a weak flux (normally 1–10 μl min^{-1}). The electric field is obtained by applying a potential difference of 3–6 kV between this capillary and the counter-electrode, separated by 0.3–2 cm; the

electric fields produced are of the order of 10^6 V m^{-1} (Figure 2.3) and they induce a charge accumulation at the liquid surface located at the end of the capillary, which will break to form highly charged droplets. A gas injected coaxially at a low flow rate allows the dispersion of the spray; these droplets then pass either through a curtain of heated inert gas, most often nitrogen, or through a heated capillary to remove the last solvent molecules. The spray starts at an 'onset voltage' that, for a given source, depends on the surface tension of the solvent. In a source which has an onset voltage of 4 kV for water (surface tension 0.073 N m^{-2}), 2.2 kV is estimated for methanol (0.023 N m^{-2}), 2.5 kV for acetonitrile (0.030 N m^{-2}) and 3 kV for dimethylsulfoxide (0.043 N m^{-2}).[13] If one examines with a microscope the nascent drop forming at the tip of the capillary while increasing the voltage, as schematically displayed in Figure 2.4, at low voltages the drop appears spherical, then elongates under the pressure of the accumulated charges at the tip in the stronger electric field; when the surface tension is broken, the shape of the drop changes to a 'Taylor cone' and the spray appears. The solvent contained in the droplets evaporates, which causes them to shrink and their charge per unit volume to increase. Under the influence of the strong electric field, deformation of the droplet occurs.[14]

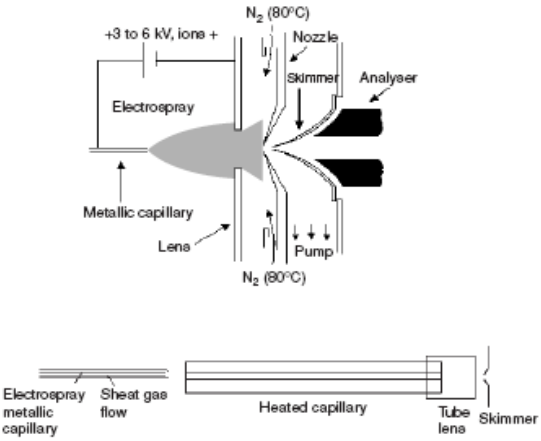

Figure 2.3. Diagram of electrospray sources, using skimmers for ion focalization and a curtain of heated nitrogen gas for desolvation (top), or with a heated capillary for desolvation (bottom).

The droplet elongates under the force resulting from the accumulation of charge, similarly to what occurred at the probe tip, and finally produces a new Taylor cone. From this Taylor cone, about 20 smaller droplets are released. Typically a first-generation droplet from the capillary will have a diameter of about 1.5 μm and will carry around 50 000 elementary charges, or about 10−14 C. The offspring droplets will have a diameter of 0.1 μm and will carry 300 to 400 elementary charges. The precursor droplet will shrink further by solvent evaporation and will produce other generations of offspring. These small, highly charged droplets will continue to lose solvent, and when the electric field on their surface becomes large enough, desorption of ions from the surface occurs.[13] The formation

of ions is a result of the electrochemical process and of the accumulation of charge in the droplets. The ESI currently is limited by the electrochemical process that occurs at the probe tip and is sensitive to concentration rather than to total amount of sample.

Figure 2.4. Effect of electrospray potential on the drop at the tip of the capillary, as observed with binoculars while increasing the voltage. Left: at low voltage, the drop is almost spherical. Centre: at about 1 or 2 kilovolts, but below the onset potential, the drop elongates under the pressure of the charges accumulating at the tip. Right: at onset voltage, the pressure is higher than the surface tension, the shape of the drop changes at once to a Taylor cone and small droplets are released. The droplets divide and explode, producing the spray.

CID is normally described as a two-step phenomenon[14-17] (Scheme 2.6); the first step is very fast (10−14 to 10−16 s) and corresponds to the collision between the ion and the target when a fraction of the ion translational energy is converted into internal energy, bringing the ion into an excited state. The second step is the unimolecular decomposition of the activated ion. The collision yield depends on the activated precursor ion decomposition probability, according to the theory of quasi-equilibrium or RRKM.[18] Several methods allow the activations of the ions through collisions, mostly by gas molecules as immobile targets. To achieve collisional activation in MS/MS instruments with spatially separate analysers, a collision cell is placed between the two mass analysers. This cell often corresponds simply to a small chamber with entrance and egress apertures and contains an inert target gas at a pressure sufficient for

collisions. In MS/MS instruments based on time-separated mass analysis steps, an inert gas is simply introduced into the ICR (Ion Cyclotron Resonance) or the ion trap.

$$M_1^+ + N \rightarrow M_1^{+*} + N$$
$$\downarrow M_2^+ + M_3$$

Scheme 2.6. Two steps mechanism of CID.

The *ion trap* consists of a doughnut-shaped ring electrode and two circular endcap electrodes, so that it is axially symmetrical and, ideally, has hyperbolic surfaces for maximum performance.[17] It is able to confine ions for long periods in a small volume close to the centre of the trap where ions may undergo reactions prior to mass analysis. As its name suggests, ions are stored within the trap and detection is accomplished by ejecting ions of a given mass-to-charge ratio to strike a conversion dynode before amplification of the signal by an electron multiplier. A mass spectrum is obtained by ramping a rf voltage, but ions that are not being ejected are stored rather than being lost, as in the scanning of a magnetic sector or quadrupole instrument. Since the ion trap is operated in a pulsed mode, it allows to store mass-selected ions between pulses, and then follow collisions by helium buffer gas. Since this is a very mild form of excitation, one can selectively promote fragmentation of almost all the precursor ions by the lowest energy process to give a single product ion in high yield.[19]

Another technique which finds numerous application in the field of enantiodiscrimination is *ESI-FTICR-MS* (Fourier Transform Ion Cyclotron Resonance Mass Spectrometry).

The first application of ion cyclotron resonance (ICR) to mass spectrometry is due to Sommer.[20] Irradiating with an electromagnetic wave that has the same frequency of an ion in the cyclotron allows resonance absorption of this wave. The energy that is thus transferred to the ion increases its kinetic energy, which causes an increase in the radius of the trajectory.

Ions excited by an AC (Alternated Current) irradiation at their own frequency and with the same energy (the same V_0 potential) applied during the same time T_{exc}, will have an orbit with the same radius, and with an appropriate radius[21] will all pass close to the detection plate:

$$r = (V_0 T_{exc})/B_0 \quad (1)$$

This equation is independent of the *m/z* ratio, though a broadband excitation will bring all the ions onto the same radius, but at frequencies depending on their *m/z* ratio.

In a magnetic field the trajectories of ions are curved differently. If the ion velocity is low and if the field is intense, the radius of the trajectory becomes small. The ion can thus be 'trapped' on a circular trajectory in the magnetic field: this is the principle of the ion cyclotron or Penning trap. Suppose that an ion is injected into a magnetic field B with a velocity v. The equations are:

Centripetal force : $F = q\ v\ B$ (2)

Centrifugal force : $F' = (mv^2)/r$ (3)

The ion stabilizes on a trajectory resulting from the balance of these two forces:

$q\ v\ B = (mv^2)/r$ or $q\ B = (mv)/r$ (4)

The ion completes a circular trajectory of $2\pi r$ with a frequency

$\nu = v/(2\pi r)$ (5)

Thus the angular velocity ω is equal to

$\omega_c = 2\ \pi\ \nu = v/r = (q/m)\ B$ (6)

As a result of this equation, the frequency and the angular velocity depend on the ratio (q/m)B, and are thus independent on the velocity. However, the radius of the trajectory increases, for a given ion, in proportion to the velocity. If the radius becomes larger than that of the cell, the ion is expelled.

The 'image current' that is induced by the ions circulating in the cell wall perpendicularly to the trajectory of the ions can be measured. In this case an ion excitation phase, targeting only ions with a given mass so as to have them fly close to the wall, alternates with a detection phase. To be detected, ions of a given mass must circulate as tight packets in their orbits. Ions of the same mass excited to the same energy will be in the same orbit and rotate with the same frequency, as shown above. If, however, they are located anywhere on the orbit, when one ion passes close to one of the detecting plate, then statistically there will be another ion of the same mass passing

close to the opposite detecting plate. The resulting induced current will be null. To avoid this, ions have to be excited in a very short time, so that they are all grouped together in the orbit, and thus in phase.

In practice, the ions are injected into a box (Figure 2.5) a few centimetres along its side, located in a magnetic field of 3 to 9.4 T produced by a superconducting magnet. For a 3 T field, the cyclotron frequency is 1.65 MHz at 28 Th and 11.5 kHz at 4000 Th. The frequency range is thus very large. Currently magnets giving a 15 T maximum field are used. The relationship between the frequency and the mass shows that determining the mass in this case consists of determining the frequency. The latter can be measured according to several methods, e.g. Fourier transforms.

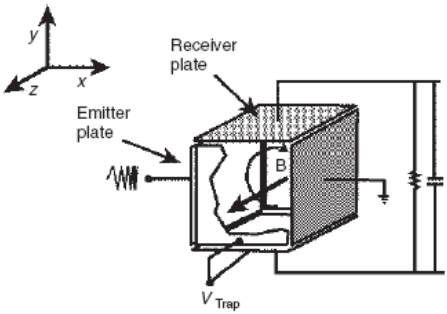

Figure 2.5. Diagram of an ion cyclotron resonance instrument. The magnetic field is oriented along the *z* axis. Ions are injected in the trap along the *z* axis. They are trapped along this axis by a trapping voltage, typically 1V, applied to the front and back plates. In the *xy* plane, they rotate around the *z* axis owing to cyclotron motion and move back and forth along the *z* axis, between the electrostatic trapping plates. The sense of rotation indicated is for positive ions. Negative ions will orbit in the opposite sense.

Fourier transform mass spectrometry (FT-MS) was first described by Comisarow and Marshall in 1974[22] and was reviewed by Amster[23] in 1996 and by Marshall *et al.*[21] in 1998. This technique consists of simultaneously exciting all of the ions present in the cyclotron by a rapid scan of a large frequency range within a time span of about 1 μs. This induces a trajectory that comes close to the wall perpendicular to the orbit and also puts the ions in phase. This allows transformation of the complex wave detected as a time-dependent function into a frequency-dependent intensity function through a Fourier transform (FT), as shown in Figures 2.6 and 2.7.

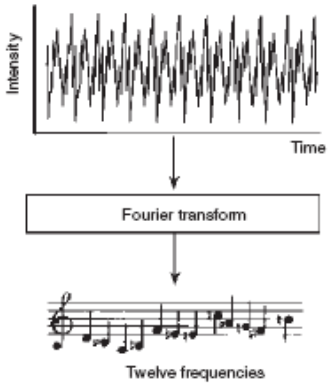

Figure 2.6. Principle of the Fourier transform: a sound signal whose intensity is measured as a time-dependent function is made up of many frequencies superposed one over the other, each with its own intensity. The Fourier transform allows to find the individual frequencies and their intensities.

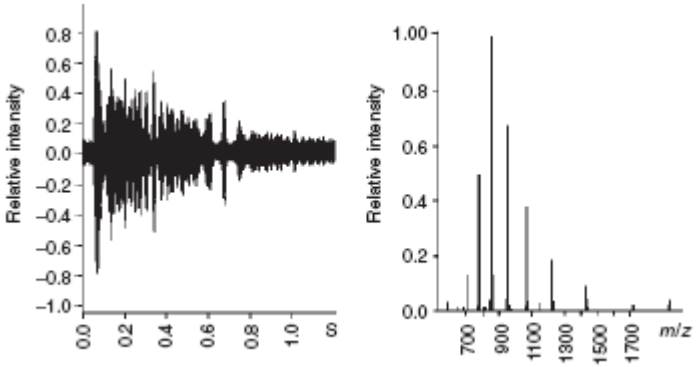

Figure 2.7. Signal intensity as a function of time is transformed, through a Fourier transform, into intensity as a function of frequency, and hence into an intensity to *m/z* relationship.

Ions both in a ion trap or in a ICR cell can be activated by photons to promove dissociation. Ions, infact can be excited by a laser and subsequently fragmented by the absorption of one or more photons. This type of activation of gaseous ions in a mass spectrometer has been performed with a range of photon energies, primarily by using lasers of different wavelengths. Historically, lasers emitting in the UV region, such as ArF excimer lasers (193 nm), and visible regions were used. Recently, there has been an increase in the use of IR lasers for photodissociation. These lasers are of lowenergies compared with UV lasers, where the absorption of only one photon provided enough energy to initiate dissociation of precursor ions. In IR, multiphoton processes are consequently needed to excite ions sufficiently for efficient fragmentation.

The chemistry of small molecules has been studied by *IRMPD* (infra red multi photon dissociation) for a long time.[24] The recent increase in applications for IRMPD as an activation technique in MS/MS is primarily due to the growth in popularity of trapping instruments, including quadrupole ion traps[25] and Fourier transform ion cyclotron resonance mass spectrometers. IRMPD is ideally suited to these instruments, given their ability to store ions for long times. Typically, ions in the ion trap (IT) or the ICR cell are activated by a low-power (<100 W) continuous-wave CO_2 (10.6 μm) laser for a selected irradiance time (usually on the order of 10-100 ms), followed by the detection of the resulting product ions (see Figure 2.8).

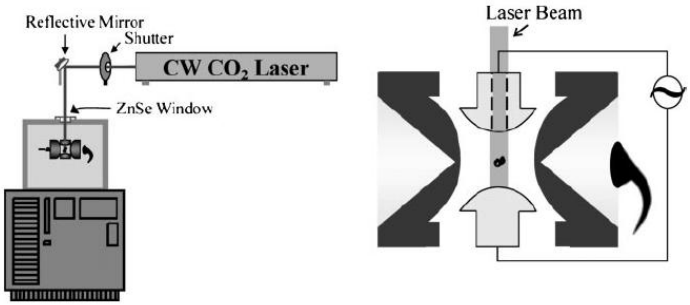

Figure 2.8. IRMPD in a quadrupole ion trap.

Photodissociation can be generally viewed by the following mechanism:

$$m_p^+ \xrightarrow{nh\nu} m_p^{+\neq} \xrightarrow{k_{diss}} m_f^+ + m_n$$

where *n* describes the number of absorbed photons, *hv* is the photon energy and k_{diss} is the rate constant for photodissociation. The mechanism of activation is assumed to be through the absorption of IR radiation by IR active modes present in the ion, followed by the rapid redistribution of energy over all the vibrational degrees of freedom. The outcome is a statistical internal energy distribution, similar to CID. The activation is stepwise, by subsequent absorption of photons, and dissociation occurs by low-energy pathways, often the lowest that is available. There are several important criteria for photodissociation to occur. The precursor ion must be able to absorb energy in the form of photons, producing excited states above the threshold of dissociation for the ion of interest. Competitive collisional and radiative cooling of ions also occurs, partially decreasing the energy gained by photon absorption and thus lowering the overall rate for dissociation. The energy gained by the absorption of photons must consequently overcome the energy lost by photon emission from the excited ions, as well as deactivation by collisions. The presence of gas in the activation region (storage device) increases the chances for deactivation of the excited ions. In an FTICR instrument, this fact does not pose a problem since extremely low pressures are maintained in the cell. Conversely, the quadrupole ion trap has a constant amount of helium buffer gas present in the trapping region at all times to help narrow the kinetic energy distribution of the ions, so collisional deactivation can become an

issue. A compromise is usually reached with a lower helium pressure than usual in the ion trap, as removing the helium altogether would cause peak resolution to suffer tremendously.

A very important advantage of IRMPD over CID in an ion trap comes from the fact that the trapping conditions, such as the r.f. voltages, do not need to be altered in the activation process. In a typical ion trap CID experiment, the precursor ion of interest is selectively accelerated by resonant excitation. Multiple collisions and stepwise energy deposition occur, until an energy threshold is surpassed and dissociation takes place. The necessary conditions for CID in an IT cause an inherent low-mass cut-off for the detection of product ions, so low-mass fragments are not observed even if they are easily formed. A tradeoff must be made between the amount of internal energy available, which depends on the potential well depth ($\propto q_z$), and the low-mass cut-off for product ions. Usually, CID conditions necessitate high q_z values. Photodissociation, however, can occur efficiently at very low q_z values.[26] IRMPD in ion traps allows for the storage of a wide m/z range of ions with less product ion mass discrimination. No fragments would be observable for CID under these trapping conditions.

The ion activation by photodissociation is rather non-selective, therefore all trapped ions are excited and secondary product ions can be observed.We therefore gain several new fragments compared with on-resonance or SORI CID, as product ions derived from the

precursor ion can be further excited into dissociative states. Keep in mind, though, that this outcome can also be disadvantageous if too many ions are formed and the resulting spectrum is a complicated collection of peaks. Moreover, the sequence of fragmentation pathways can easily be lost in such a situation. Fortunately, applying tailored excitation waveforms, such as 'stored waveform inverse Fourier transforms' (SWIFT), [27] may be used to eject specific product ions selectively from the trap. Fragment ions that disappear are concluded to be products of the ejected ions. This technique has been employed for IRMPD of macrolide antibiotics in a quadrupole ion trap.[24c]

The advantages of IRMPD are numerous. Particularly, the amount of available energy is well defined. In the case of a 10.6 μm CO_2 laser, the absorption of one photon corresponds to 0.117 eV of energy. The dissociation efficiency of this technique is good, given enough time for activation, and it can easily be implemented in routine analytical laboratories. Dissociation of precursor ions does not compete with scattering and ejection out of the trapping region. In the case of FTICR, gas does not need to be added to the cell. However, the cost of this technique is high and direct fragmentation pathways are often not easily determined, as in CID.

2.3.2 Analytical Methods Based on NMR Spectroscopy

Enantiorecognition involves complex phenomena which can be analyzed extensively by means of NMR spectroscopy. Especially over the last 10-20 years, NMR has assumed a leading role in this field, in part favored by the increasing use and accessibility of high field spectrometers. Furthermore this technique gives access to quite simple methods for enantiomeric excess and absolute configuration determinations,[28] the application of which requires a good basic knowledge of the data in the literature dealing with chiral auxiliaries specifically dedicated to NMR uses, together with the understanding of the mechanisms by which they act.

Each direct method of determination of the enantiomeric composition and/or absolute configuration of chiral compounds requires the knowledge of two different sets of parameters: those dependent on the structure, which assume distinct values for the two enantiomers, and those exclusively dependent on the relative amounts of them.

NMR spectroscopy gives a wide choice of parameters correlated to the structure, i.e. the chemical shifts (δ), the coupling constants (J) and the relaxation rates (R), and one parameter depending on the amount of substance (the integrated area of the NMR signal).[29] However, as a consequence of the intrinsic isochrony or equivalence of nuclei in enantiomeric environments (enantiotopic nuclei), these cannot be employed in the discrimination of the two enantiomers and

therefore in the determination of the enantiomeric excesses. On the other hand, corresponding nuclei of species in diastereoisomeric environments (diastereotopic nuclei) are intrinsically nonequivalent and could generate distinct resonances in NMR spectra, for which the magnitude of nonequivalence ($\Delta\delta$) (absolute value of the difference between the chemical shifts of diastereotopic nuclei) can be defined. This parameter depends on a number of factors: the nature of the groups in the molecule, conformational prevalence, temperature, concentration and solvent. The problem of the intrinsic equivalence of the enantiotopic nuclei can therefore be overcome by putting them into a diastereoisomeric environment by means of a suitable derivatization process in order to make them diastereotopic and hence distinguishable by NMR. Such a derivatization can be the result of the chemical reaction between an enantiopure substrate A [(+)-A, for example] and the two enantiomers of the chiral species B [(+)-B and (-)-B] and to obtain stable diastereoisomers. This process requires the formation of covalent bonds between A and B. Alternatively, the derivatization can be simply the consequence of labile attractive interactions between A and B, such as the formation of hydrogen bonds, the establishment of dipole-dipole or π-π interactions. On considering this last case, in solutions containing mixtures of the selected enantiomerically pure chiral auxiliary (B) and one or other of the enantiomers of the chiral substrate (A), two equilibria must be considered (Scheme 2.7) in which, frequently,

only one signal is observed for the bound and free form of each component.

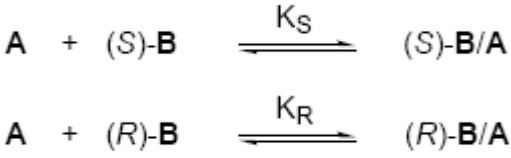

Scheme 2.7. Formation of a couple of diastereomers starting from a chiral auxiliary and a pair of enantiomers.

In these conditions, defined as fast exchange conditions, the selected observed NMR parameter (P_{obs}) is the molar fraction weighted average of the same parameters in the free (P_f) and bound (P_b) form (Eq. 7),

$$P_{obs} = x_f P_f + x_b P_b \quad (7)$$

where x_f and x_b are the molar fractions of the free and bound species, respectively.

Three important classes of chiral reagents have been developed: the chiral reagents employed in the formation of stable diastereoisomeric derivatives of the two enantiomers, Chiral Derivatizing Agents (**CDA**s); the chiral auxiliaries able to form labile diastereoisomeric adducts, Chiral Solvating Agents (**CSA**s); and paramagnetic chiral reagent named Chiral Lanthanide Shift Reagents (**CLSR**s). After the most suitable derivatization, the determination of the enantiomeric purity of the chiral substrate simply requires a routine NMR spectrum, the identification of the resonances due to corresponding

nuclei of the two diastereoisomers and, when sufficiently separated, their integration. Alternatively, the relative composition of the diastereoisomers can be determined by comparing the heights of the resonances, on condition that the half-height widths of the compared signals are nearly equal.

The success of the determination using **CDA**s depends on the strategy used in the synthesis of the diastereoisomers and on the nature of the groups deriving from the **CDA**. Indeed, it is not only essential that the **CDA** is easily available in enantiopure form and that no racemization or kinetic resolution occurs during the derivatization reaction, it is also mandatory that the **CDA** generates sufficient differentiation between the diastereotopic groups of the diastereoisomers, in order to obtain the magnitude of nonequivalence required to make accurate integrations of the diastereotopic resonances. Another essential feature of the **CDA** is that it should contain groups which produce simple resonances. The α-methoxyphenylacetic chloride, studied by Mislow and Raban,[30] satisfies completely the above requisites: it contains the phenyl group which gives rise to anisotropic effects and the two substituents, OMe and CH, which give rise each one to a singlet in the ^{1}H NMR spectrum.

In the course of the investigations into **CDA**s, the remarkable effect of the nature of the solvent on the measured nonequivalences was clearly shown and, hence, the ability of the solvent to interact with

the solutes was demonstrated. A direct consequence of these observations was the hypothesis, formulated by Mislow and Raban in 1965,[31] that the solvent, if optically active, could itself generate the chiral environment required to induce nonequivalence in the enantiotopic nuclei of two enantiomeric solutes. The first experiment was carried out soon after by Pirkle[32] in 1966: the racemic 2,2,2-trifluoro-1-phenylethanol in a chiral solvent, α-phenylethylamine (successively denoted as "chiral solvating agent"), showed non equivalence attributable to the formation of diastereoisomeric solvates. Similar nonequivalences could also be obtained by dissolving the enantiomeric mixture in an achiral solvent and adding some equivalents of the **CSA**. Obviously the achiral solvent should not compete with the **CSA** in the interaction with the enantiomeric substrate. The first experiments carried out by Pirkle clarified some fundamental peculiarities of the **CSA**s: *i*) the absolute configuration of the **CSA** affects exclusively the sense of nonequivalence (relative position of the resonances produced by the diastereotopic nuclei); *ii*) the enantiomeric purity of the **CSA** determines only the magnitude of nonequivalence: when the higher the enantiomeric purity of the **CSA** is, the greater the observed separations between corresponding signals of the two enantiomers of the solute are.

New developments are related to **CSA**s based on cyclodextrin,[33] chiral crown ethers and calixarenes.

The native cyclodextrins **2.9.1a** (Figure 2.9) induce nonequivalence in the ^{1}H NMR spectra in water of enantiotopic groups of polar molecules;[34] derivatized cyclodextrins, by virtue of their remarkably different solubility and complexing features, allow the extension of their use to the analyses of both polar and apolar chiral substrates. Thus, exhaustively methylated cyclodextrins **2.9.1b** are very efficient **CSA**s for trisubstituted allenes and aromatic hydrocarbons, whereas benzylated and/or benzoylated **2.9.1c**-**f** or carbamoylated **2.9.1g** systems are chiral auxiliaries that are very soluble in $CDCl_3$, being widely applicable to the analyses of polar substrates, derivatized or underivatized, insoluble in D_2O.

Chiral crown ethers, another class of cyclic compounds, are characterized by a polar cavity able to include positively charged polar groups, such as ammonium cations. Among these, (+)-(*R*)-18-crown-6-tetracarboxilic acid **2.9.2** (Figure 2.9) has been employed as chiral shift reagent for the enantiodiscrimination of amino acids, amines and amino alcohols.[35]

Also calixarenes have been used in NMR studies as **CSA** for the investigation of the stereochemistry, dynamics and thermodynamics of diastereomeric complexes. The bis(ethyl lactate) derivative of p-tert-butylcalix[4]arene is able to determine efficient enantiodiscrimination of simple amino acid derivatives.[36] Even if the two enantiomers of a guest are included by the same stereochemistries relative to the calixarene cavity, groups bound to

their stereogenic centres are, however, necessarily in different stereochemical environments with respect to lactate moieties at the lower rim. Accordingly, stability constants of the two diastereoisomeric complexes are slightly differentiated as stabilizing interactions must be quite similar.

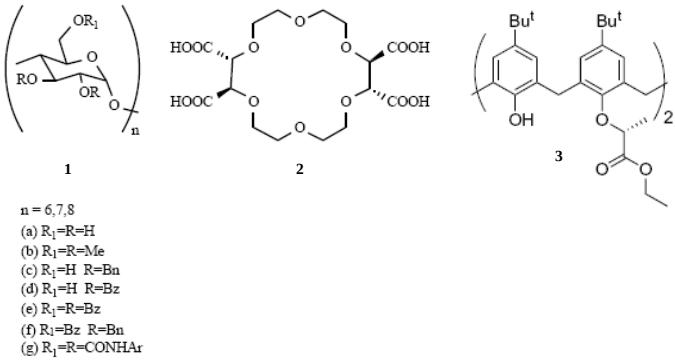

Figure 2.9. Examples of CSAs based on macrocyclic compounds like cyclodextrins (**1**), crown ethers (**2**) and calixarenes (**3**).

Lanthanide ions (Ln^{3+}) coordinate 1,3-diketones (dkts) to form hexacoordinate paramagnetic complexes ($Ln(dkt)_3$), which behave as Lewis acids and form addition complexes with a large variety of basic organic substrates.[37] When an optically active 1,3-diketone is employed in the formation of the lanthanide complexes, the interaction with the two enantiomers of a chiral organic substrate gives rise to diastereoisomeric species, which could produce different spectra. Although complexation processes involve fast exchanging species as in the case of **CSA**s, the rationalization of

enantiodiscriminating pathways involving **CLSR**s is strongly limited by the fact that each chiral lanthanide complex is itself a rapidly interconverting mixture of stereoisomers and each of them can offer different binding sites to the organic substrate. The remarkable feature of the **CLSR**s is their ability to induce not only nonequivalence in the enantiotopic nuclei of two enantiomers, but also very wide complexation shifts (Δδ, difference between the chemical shifts, for a given enantiomer, in the presence of the **CLSR** and in the free state) in the substrate nuclei, due to the magnetic moment of the unpaired electron. Unfortunately, most of these reagents also cause severe broadening of the signals, due to the efficient relaxation process provided by the unpaired electron. Being line-broadening dependent on B_0, the use of low magnetic field spectrometers is strongly recommended.

When studing host-guest system, the stoichiometry of the complex is usually determined from NMR data by means of Job's method,[38] analyzing the chemical shifts of solutions with different molar ratios of the two components, but with constant total concentration. The data are plotted in the form $x_B\Delta\delta^B$ ($\Delta\delta^B = \delta_{obs}{}^B - \delta_f{}^B$) versus x_A. The abscissa of the maximum is correlated to the stoichiometry of the complex (Figure 2.10). Alternatively, in the presence of strong complexes ($K>10^5$) the mole ratio method, involving the preparation of a series of solutions containing constant concentration of B and a suitable range of concentration of A, works well.[39] Two straight

lines, intersecting at the [A]/[B] ratio corresponding to the stoichiometry of complexation, are obtained plotting $\Delta\delta^B$ versus [A].

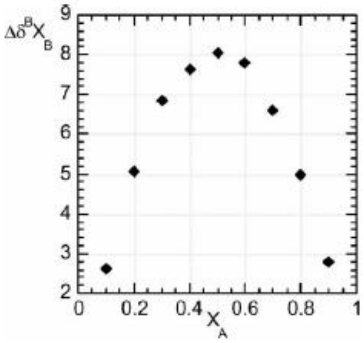

Figure 2.10. Job's plot for A/B mixture. Determination of a 1:1 stoichiometry.

Once the stoichiometry of complexation has been determined, separate NMR experiments must be carried out to measure the heteroassociation constants of the two diastereoisomeric complexes. Two different experimental conditions can be considered: a constant low concentration of one component in the presence of increasing excesses of the other or equimolar mixtures progressively diluted.

In fast exchange conditions, the measured chemical shift (δ_{obs}) represents the weighted average of the value corresponding to the uncomplexed (δ_f) and complexed (δ_c) forms (Eq. 8)

$$\delta_{obs} = x_f \delta_f + x_c \delta_c \qquad (8)$$

where x_f and x_c are the molar fractions of uncomplexed and complexed forms, respectively, with $x_f + x_c = 1$.

The data were fitted by equation 9 obtained combining equation 8 with the equation of association constant for 1:1 complexes:

$$C_0 = \frac{1}{K}\frac{(\delta_{obs} - \delta_f)(\delta_c - \delta_f)}{(\delta_c - \delta_{obs})^2} \quad (9)$$

Before determining complexation parameters, dimerization or self-association phenomena must be considered. The existence of self-association phenomena is clearly evaluated by analyzing the NMR spectra of the pure component in progressively diluted solutions: when the chemical shifts are dependent on the concentration, the self-association constant should be determined.

In the more simple and common autoaggregation case, i.e. the dimerization, the measured chemical shift (δ_{obs}) is defined as the weighted average of its value in the monomer (δ_m) and dimer (δ_d) (Eq. 10), while the dimerization constant (Eq. 11) depends on the initial concentration C_0.

$$\delta_{obs} = x_m \delta_m + x_d \delta_d \quad (10)$$

$$K_d = \frac{x_d}{2\, C_0 (1 - x_d)^2} \quad (11)$$

Recently the use of diffusion coefficients, obtained by NMR DOSY (Diffusion Order SpectroscopY) techniques,[40] are gaining increasing popularity in determining association constants. The diffusion coefficient (D), measured by NMR DOSY experiments, can be correlated to molecular size by means of hydrodynamic radius

(R_H) (Eq. 12), on the basis of the Stokes-Einstein equation (12) which strictly holds for spherical molecules:

$$D = \frac{kT}{6\pi\eta R_H} \tag{12}$$

where k is the Boltzmann constant, T the absolute temperature and η is the solution viscosity.

Complexation phenomena can be investigated efficiently by measurements of diffusion coefficients: an increase in the molecular size of complexed species is well reflected by a decrease in its diffusion coefficient. In fast exchange conditions, i.e. when diffusion of free and complexed species are undistinguishable by NMR, the measured diffusion coefficient (D_{obs}) represents the weighted average of the value corresponding to the uncomplexed (D_f) and complexed (D_c) forms (Eq. 13)

$$D_{obs} = D_f x_f + D_c x_c \tag{13}$$

where x_f and x_c are the molar fractions of uncomplexed and complexed forms, respectively, with $x_f + x_c = 1$.

Molar fraction of complexed species, and hence association constant K, can be obtained from equation 13. When complexation phenomena involve species with different sizes, it can be assumed that, in the complex, traslational diffusion is controlled mainly by the larger molecules, so D_c can be taken equal to the diffusion coefficient

of the larger molecule. In this way, from a single point measurement, the complexed molar fraction can be determined from equation 14.

$$x_c = \frac{D_{obs} - D_f}{D_c - D_f} \tag{14}$$

To carry out the NMR analysis of the conformational aspects, preliminary information regarding the intermolecular interactions can be obtained directly from the analysis of the ^{1}H NMR spectra in terms of the complexation shifts ($\Delta\delta = \delta_{obs} - \delta_f$) measured for all nuclei of the two species. However, the most important method of conformational analysis in the definition of the binding geometry is the detection of dipolar interactions (NOE),[41] which reflect the spatial proximity between nuclei and, therefore, allow us to impose proximity constraints between nuclei located inside the same molecule (intramolecular dipolar interactions) or belonging to different molecules (intermolecular dipolar interactions).

Intramolecular dipolar interactions allow the definition of the conformation of the chiral auxiliary or enantiomeric substrates both in the free state and in the diastereoisomeric complexes and, therefore, the identification of the nature of conformational changes due to complexation, if occurring. Intermolecular dipolar interactions allow the relative stereochemistry of the chiral auxiliary and one or other of the enantiomers in the two diastereoisomeric complexes to be defined. Dipolar interactions can be detected by measuring the NOE effects using mono- and bidimensional NOESY (Nuclear

Overhauser Effect Spectroscopy) and ROESY techniques. [41] The intensities of NOEs can be correlated to the interproton distances r_{ij} between *ij* protons.

2.4 Conclusion

On the basis of a well-known methodology, we synthesize both chiral resorc[4]arene **6** containing diphenilethylenediamine in the side chains which rigidify the structure of the resorcarene. Coumpond **6** already showed a good capacity to complex several small organic guest like aminoacids, nucleosides and alkaloids, and to give a chiral recognition towards this compounds. For this reasons we chose to synthesize this compound in order to investigate its molecular recognition properties towards nucleosides by IRMPD and NMR spectroscopy.

We also synthesized both enantiomer of a new resorc[4]arene derivative **10**. This compound, like **6** contains bis-diamido- side arms, but based on a dimer of valine (which was prepared by linking the carboxylic functions of valine by estherification with ethylene glycol). This side chains ensure less rigidity and more flexibility to the resorc[4]arene, keeping at the same time the capacity to recognize a chiral guest, but probably with a faster kinetic in the formation of complexes. Compund **10**, infact, contains four stereocenters arising from valine, which give to the molecule an

intrinsic chirality that is at the base of the enantidiscrimination towards chiral guests.

2.5 Experimental Section

General Remarks. All reagents and solvents were purchased from Sigma-Aldrich and used without further purification. ^{1}H and ^{13}C NMR spectra were recorded on a Bruker Avance 400 instrument operating at 400 and 75 MHz, respectively (TMS = 0 ppm as internal standard in $CDCl_3$ solutions), s = singlet; d = doublet; dd = double doublet; t = triplet; m = multiplet. Mass spectra (MS) were obtained with a Thermo Finnegan LCQ Deca XP-Plus ion-trap mass spectrometer equipped with an electrospray ionization (ESI) source. Conditions as follows: source voltage = +5.0 kV, sheath gas = 25 AU (Arbitrary Units), auxiliary gas = 10 AU, capillary voltage = +40.0 V, capillary temperature = 200 °C, tube lens offset = +15 V. HRMS were obtained with an APEX III (7 T Magnet) FTICR mass spectrometer equipped with an Apollo ESI source (Bruker Daltonik GmbH, Bremen). Optical rotations were measured with a Jasco P-1030 polarimeter.

Resorc[4]arene tetraacid 4. Compound **3** (1.6 g, 1.7 mmol), synthesized as described previously,[2] was dissolved in EtOH (10 mL), and 2 N NaOH solution (5 mL) was added. The reaction

mixture was stirred for 4 h at reflux. EtOH was removed in vacuo, and the aqueous solution was acidified with glacial acetic acid. The precipitate was filtered, rinsed several times with water and with Et_2O, and dried to give compound **4** in quantitative yield. ^{1}H NMR (400 MHz, $CDCl_3$, 298 K) δ (ppm): 9.57 (br. s, 1H), 6.52 (s, 4H), 6.30 (s, 4H), 4.95 (t, J = 7.0 Hz, 4H), 3.63 (s, 24H), 2.78 (d, J = 7.0Hz, 8H). ^{13}C NMR (75 MHz, $CDCl_3$, 298 K) δ (ppm): 175.86, 156.03, 125.88, 123.99, 96.28, 55.89, 36.25, 33.01.

Resorcin[4]arene Tetrachloride 5. $SOCl_2$ (2.4 mL, 33 mmol) was added under an atmosphere of argon to a solution of **5** (0.15 g, 0.18 mmol) in dry benzene (15 mL). The reaction mixture was heated at reflux whilst stirring for 4h. Final evaporation under an atmosphere of argon gave compound **5** as a dark green solid in quantitative yield, and the product was used without further purification in the following step.

Basket bis(diamidodiphenylethylene) resorc[4]arene (*all-R*)-6. DIPEA (0.062 mL, 0.36 mmol) was added, under atmosphere of argon, to a solution of **5** (0.054 g, 0.06 mmol) in dry THF (5 mL), and the mixture was stirred at room temperature for about 20 min. A solution of (1*R*,2*R*)-(+)-1,2-diphenylethylenediamine (0.038 g, 0.18 mmol) in dry THF (5 mL) was then added dropwise. The mixture was stirred and heated at reflux for 3h. Evaporation *in vacuo* and

purification of the crude product by column chromatography (silica gel; $CHCl_3$/MeOH, 99.5:0.5) gave compound (*all-R*)-**6** (31% yield) as a vitreous solid. $[\alpha]_D^{20} = -59.9$. ^{1}H NMR (400 MHz, $CDCl_3$, 298 K) δ (ppm): 7.62 (d, J = 7.2 Hz, 2H), 7.07 (br. s, 20H), 6.46 (s, 2H), 6.22 (s, 2H), 6.00 (s, 2H), 5.97 (dd, J = 8.0 Hz, J = 2.0 Hz, 2H), 5.43 (dd, J = 11.0 Hz, J = 8.0 Hz, 2H), 5.09 (dd, J = 11.0 Hz, J = 8.0 Hz, 2H), 4.90 (dd, J = 11.0 Hz, J = 7.5 Hz, 2H), 4.66 (dd, J = 13.0 Hz, J = 4.0 Hz, 2H), 5.09 (dd, J = 11.0 Hz, J = 8.0 Hz, 2H), 3.86 (s, 6H), 3.85 (s, 6H), 3.57 (s, 6H), 3.29 (s, 6H), 3.24 (dd, J = 14 Hz, J = 5.5 Hz, 2H), 3.00 (dd, J = 17.0 Hz, J = 4.0 Hz, 2H), 2.83 (dd, J = 17.0 Hz, J = 13.0 Hz, 2H), 2.39 (m, 2H). ^{13}C NMR (75 MHz, $CDCl_3$, 298 K) δ (ppm): 174.72, 171.65, 157.34, 156.62, 155.98, 154.88, 126.42, 126.24, 125.15, 124.30, 121.40, 97.81, 94.51, 60.27, 58.09, 55.93, 55.80, 55.34, 41.69, 40.09, 33.49, 33.27. ESI-MS (+): *m*/*z* = 1208.4 $[M•Na]^+$. $C_{72}H_{72}N_4O_{12}$ (M.W. 1185.38): calcd. C 72.95, H 6.12, N 4.73; found C 72.73, H 6.10, N 4.71.

Basket bis(diamidodiphenylethylene) resorc[4]arene (*all-S*)-6.

Treatment of **5** with (1*S*,2*S*)-(–)-1,2-diphenylethylenediamine under the same conditions as those used for the preparation of (*all-R*)-**6** afforded (*all-S*)-**6** (29% yield) as a vitreous solid. $[\alpha]_D^{20} = +59.9$ ($CHCl_3$). All spectroscopic data are coincident with those reported for (*all-R*)-**6**.

N-Cbz-D-valine (*R*)-7. D-Valine (0.661 g, 5.63 mmol) and Na_2CO_3 (1.5 g, 14.08 mmol) were dissolved in a solution of water/1,6-dioxane 1:1 (40 mL). The resulting solution was cooled to 0 °C in an ice bath and benzyl chloroformate (0.88 mL, 1.056 g, 6.19 mmol) was slowly added. The reaction mixture was stirred at room temperature overnight. The following morning, the solution was evaporated under reduced pressure in order to remove most of the dioxane. The acqueous residue was extracted with Et_2O (3 × 20 mL), and the organic layers were discarded. The aqueous layer was acidified with concentrated HCl (added dropwise) until the pH had reached 2 (as observed by pH paper). The aqueous solution was then extracted with EtOAc (3 × 30 mL). The collected organic layers were washed with brine and dried over anhydrous Na_2SO_4. Filtration and evaporation of the solvent under reduced pressure gave the crude product as a colourless oil. Purification by column chromatography (silica gel, eluent MeOH:CH_2Cl_2 15:1) afforded compound (*R*)-**7** in quantitative yield. ^{1}H NMR (400 MHz, $CDCl_3$, 298 K) δ (ppm): 7.27 (br. s, 5H), 5.09 (s, 2H), 4.31 (br., 2H), 2.05 (m, 1H), 0.87 (d, J = 6.8Hz, 6H). ESI-MS (+): *m*/*z* = 252.4 $[M•H]^+$, 275.3 $[M•Na]^+$.

N,N-Cbz-bis-valinethylenglycol esther 8. (*R*)-**7** (or (*S*)-**7**) (2.01 g, 8.0 mmol), ethylene glycol (0.248 g, 0.22 mL, 4.0 mmol), Et_3N (1.62 g, 2.22 mL, 16.0mmol) and BOP (3.54 g, 8.0 mmol) were dissolved in CH_2Cl_2 (120 mL) and the solution was stirred at room temperature

for 4h. After addition of brine (50 mL) the mixture was extracted with CH_2Cl_2 (3 × 50mL). The combined organic layers were washed tree times with HCl 2N and saturated Na_2CO_3 solution, then one time with brine. The organic layer was dried over anhydrous Na_2SO_4. Filtration and evaporation of the solvent under reduced pressure gave the crude product as a colourless oil. Purification by column chromatography (silica gel, eluent hexane:EtOAc 8:2) afforded compound (*R*,*R*)-**8** (or (*S*,*S*)-**8**) (54% yield). ^{1}H NMR (400 MHz, $CDCl_3$, 298 K) δ (ppm): 7.35 (br. s, 10H), 5.42 (d, J = 7.2 Hz, 2H), 5.10 (dd, J = 12 Hz, J = 18.4 Hz, 4H), 4.32 (br., 2H), 2.16 (m, 2H), 0.98 (d, J = 6.8Hz, 6H), 0.90 (d, J = 6.8Hz, 6H). ^{13}C NMR (75 MHz, $CDCl_3$, 298 K) δ (ppm): 171.89, 156.36, 136.29, 128.58, 127.78, 67.12, 62.62, 59.14, 50.74, 31.19, 19.01, 17.56. ESI-MS (+): *m*/*z* = 528.9 $[M•H]^+$, 551.2 $[M•Na]^+$.

Bis-valinethylenglycol esther 9.

Compound (*R*,*R*)-**8** (or (*S*,*S*)-**8**) (1.137 g, 2.15 mmol) was dissolved in a solution of EtOH/THF 1:1 (60 mL) under athmosphere of argon. Pd/C (10 wt.%, 0.73 g,) was added. The argon inside the flask was replaced with hydrogen (flushing two times) and the suspension was stirred overnight at room temperature. The next morning the mixture was filtered on celite and evaporation *in vacuo* of the solvent gave pure (*R*,*R*)-**9** (or (*S*,*S*)-**9**) (94% yield). ^{1}H NMR (400 MHz, $CDCl_3$, 298 K) δ (ppm): 4.10 (dd, J = 10.8 Hz, J = 13.6 Hz, 4H), 3.07 (d, J =

4.8 Hz, 2H), 1.78 (m, 6H), 0.73 (d, J = 7.2Hz, 6H), 0.66 (d, J = 6.8Hz, 6H). ^{13}C NMR (75 MHz, $CDCl_3$, 298 K) δ (ppm): 174.82, 62.14, 59.63, 31.83, 18.97, 17.08. ESI-MS (+): m/z = 261.1 $[M•H]^+$.

Basket bis(diamido-bis-D-valinethylenglycol) resorc[4]arene (*all-R*)-10.

DIPEA (0.35 mL, 2.0 mmol) was added, under atmosphere of argon, to a solution of **5** (0.118 g, 0.12 mmol) in dry THF (20 mL), and the mixture was stirred at room temperature for about 20 min. A solution of (*R,R*)-**9** (0.215 g, 0.83 mmol) in dry THF (15 mL) was then added dropwise. The mixture was stirred and heated at reflux for 5h. Evaporation *in vacuo* and purification of the crude product by column chromatography (silica gel; $CHCl_3$/MeOH, 99:1) gave compound (*all-R*)-**10** (20% yield) as a white solid. $[\alpha]_D^{20}$ = +73.9 (MeOH). ^{1}H NMR (400 MHz, $CDCl_3$, 298 K) δ (ppm): 7.40 (s, 2H), 6.56 (s, 2H), 6.33 (d, J = 9.2 Hz, 2H), 6.18 (d, J = 6.4 Hz, 2H), 6.13 (s, 2H), 6.12 (s, 2H), 4.93 (dd, J = 9.5, J = 5.1, 2H), 4.90 (dd, J = 11.3 Hz, J = 2.1 Hz, 2H), 4.56 (m, 2H), 4.33 (dd, J = 9.2 Hz, J = 5.9 Hz, 2H), 4.24 (m, 4H), 4.11 (t, J = 6.4 Hz, 2H), 4.00 (s, 6H), 3.96 (s, 6H), 3.74 (m, 2H), 3.38 (s, 6H), 3.37 (s, 6H), 2.89 (m, 6H), 2.75 (t, J = 12.8 Hz, 2H), 2.09 (m, 4H), 0.96 (d, J = 6.6Hz, 6H), 0.95 (d, J = 6.6Hz, 6H), 0.75 (d, J = 6.6Hz, 6H), 0.60 (d, J = 6.6Hz, 6H).

^{13}C NMR (75 MHz, $CDCl_3$, 298 K) δ (ppm): 173.36, 172.56, 171.29, 171.13, 156.96, 156.75, 155.65, 155.56, 128.06, 126.31, 125.92, 125.78, 122.25, 121.08, 98.14, 95.58, 61.78, 61.10, 58.14, 57.54,

56.24, 56.03, 55.98, 42.39, 40.13, 35.09, 33.65, 31.32, 30.17, 29.73, 29.68, 19.25, 19.14, 17.77, 17.62. ESI-HRMS (+): found *m*/*z* = 663.28902 $[M•Na_2]^{2+}$, 1303.58768 $[M•Na]^+$, $C_{68}H_{88}N_4O_{20}Na_2$ requires 663.28882 and $C_{68}H_{88}N_4O_{20}Na$ requires 1303.58841.

Basket bis(diamido-bis-L-valinethylenglycol) resorc[4]arene (*all-S*)-10.

Treatment of **5** with (*S*,*S*)-**9** under the same conditions as those used for the preparation of (*all-R*)-**10** afforded (*all-S*)-**10** (22% yield) as a white solid. $[\alpha]_D^{20}$ = -73.9 (MeOH). ESI-HRMS (+): found *m*/*z* = 663.28883 $[M•Na_2]^{2+}$, 1303.58734 $[M•Na]^+$, $C_{68}H_{88}N_4O_{20}Na_2$ requires 663.28882 and $C_{68}H_{88}N_4O_{20}Na$ requires 1303.58841. All the other spectroscopic data are coincident with those reported for (*all-R*)-**10**.

2.6 References

[1] B. Botta, G. Delle Monache, M. C. De Rosa, C. Seri, E. Benedetti, R. Iacovino, M. Botta, F. Corelli, V. Masignani, A. Tafi, E. Gács-Baitz, A. Santini, D. Misiti, *J. Org. Chem.*, **1997**, *62*, 1788-1794.

[2] B. Botta, M. C. Di Giovanni, G. Delle Monache, M. C. De Rosa, E. Gács-Baitz, M. Botta, F. Corelli, A. Tafi, A. Santini, E. Benedetti, C. Pedone, D. Misiti, *J. Org. Chem.*, **1994**, *59***,** 1532-1541.

[3] B. Botta, I. D'Acquarica, L. Nevola, F. Sacco, Z. Valbuena Lopez, G. Zappia, C. Fraschetti, M. Speranza, A. Tafi, F. Caporuscio, M. C. Letzel, J. Mattay, *Eur. J. Org. Chem.*, **2007**, 5995-6002.

[4] K. M. Engle, D. H. Wang, J. Q. Yu, *J. Am. Chem. Soc.*, **2010**, *132*, 14137-14151.

[5] a) T. J. Wenzel, J. D. Wilcox, *Chirality*, **2003**, *15*, 256-270; b) R. Rothchild, *Enantiomer*, **2000**, *5*, 457-471.

[6] K. Ve´key, G. Czira, *Anal. Chem*., **1997**, *69*, 1700-1705.

[7] A. Latini, D. Toja, A. Giardini Guidoni, A. Palleschi, S. Piccirillo, M. Speranza, *Chirality,* **1999**, *11*, 376-380.

[8] M. Sawada, Y. Takai, H. Yamada, S. Hirayama, T. Kaneda, T. Tanaka, K. Kamada, T. Mizooku, S. Takeuchi, K. Ueno,K.

Hirose, Y. Tobe, K. Naemura, *J. Am. Chem. Soc*., **1995**, *117***,** 7726.

[9] a) G. Hofmeister, J. A. Leary, *Org. Mass Spectrom.*,**1991**, *26*, 811; b) T. T. Dang, S. F. Pedersen, J. A. Leary, *J. Am. Soc. Mass Spectrom.*, **1994**, *5*, 452.

[10] a) K. Vekey, G. Czira, *Anal. Chem*., **1997**, *69*, 1700; b) W. A. Tao, D. Zhang, F. Wang, P. D. Thomas, R. G. Cooks, *Anal. Chem.*, **1991**, *71*, 4427.

[11] a) M. Mann, C. K. Meng, and J. B. Fenn, *Anal. Chem.*,**1989**, *61*, 1702-1708; b) J. B. Fenn, M. Mann, C. K. Meng *et al*., *Science*,**1989**, *246*, 64.

[12] a) R. D. Smith, J. A. Loo, C. G. Edmons *et al*., *Anal. Chem.*, **1990**, *62*, 882; b) M. Mann, *Org. Mass Spectrom.*, **1990**, *25*, 575.

[13] P. Kebarle,L. Tang, *Anal. Chem.*, **1993**, *65*, 972A.

[14] E. De Hoffmann, V. Stroobant, *Mass Spectrometry: Principles and Applications (Third Edition)*, John Wiley & Sons , Ltd., Chichester, **2007**.

[15] (a) R. G. Cooks (ed), *Collision Spectroscopy*, Plenum Press, New York, **1978**; b) K. L. Busch, G. L. Glish, S. A. McLuckey, *Mass Spectrometry/Mass Spectrometry: Techniques and Applications of Tandem Mass Spectrometry*,VCH: New York, **1988**; c) R. G. Cooks, J. H. Beynon, R. M. Caprioli, G. R. Lester, *Metastable Ions*, Elsevier, Amsterdam, **1973**; d) J.

Durup, in *Recent Developments in Mass Spectrometry*, K. Ogata, T. Hayakawa (Eds), University Park Press: Baltimore, **1970**, pp. 921-934; e) J. Los, *Ber. Bunsen. Phys. Chem.*, **1973**, *77*: 640; f) A. K. Shukla, J. H. Futrell, in: *Experimental Mass Spectrometry*, D. H. Russell (Ed), Plenum Press, New York, **1994**; g) A. K. Shukla, J. H. Futrell, *Eur. J. Mass Spectrom.* **1997**, *3*, 259.

[16] A. K. Shukla, J. H. Futrell, *J. Mass Spectrom.*, **2000**, *35*, 1069-1090.

[17] R. K. Jennings, *J. Mass Spectrom.*, **2000**, *200*, 479-493.

[18] H. B. Rosenstock, M. B. Wallenstein, A. L. Wahrhaftig, H. Eyring, *Proc. Nat. Acad. Sci. USA*, **1952**, *38*, 667.

[19] J. N. Louris, R. G. Cooks, J. E. P. Syka, P. E. Kelly, G. C. Stafford, J. F. J. Todd, *Anal. Chem.*, **1987**, *59*, 1677.

[20] R. B. Cole (ed), *Electrospray Ionisation Mass Spectrometry*, JohnWiley & Sons, Ltd., Chichester, **1997**.

[21] M. G. Ikonomou, A. T. Blades, P. Kebarle, *Anal. Chem.*, **1990**, *62*, 957.

[22] M. Yamashita, J. B. Fenn, *Phys. Chem.*, **1988**, *88*, 4451.

[23] J. A. Loo, H. R. Udseth, R. D. Smith, *Anal. Biochem.*, **1989**, *179*, 404.

[24] a) L. R. Thorne, J. L. Beauchamp, in: *Gas Phase Ion Chemistry*. Vol. 3: *Ions and Light*, MT Bowers (ed). Academic Press, London, **1984**, p. 41; b) W. J. van der Hart , *Int. J. Mass*

Spectrom. Ion Process., **1992**, *118/119*, 617; c) G. T. Uechi, R. C. Dunbar, *J.Chem. Phys.*, **1992**, *96*, 8897.

[25] J. S. Brodbelt, J. J. Wilson, *Mass Spectrom. Rev.*, **2009**, *28*, 390-424.

[26] A. Colorado, J. X. Shen, V. H. Vartanian,J. Brodbelt, *Anal. Chem.*, **1996**, *68*, 4033.

[27] A. G. Marshall, T. C. L. Wang, T. L. Ricca, *J. Am. Chem. Soc.*, **1985**, *107*, 7893.

[28] a) D. Parker, *Chem. Rev.*, **1991**, *91*, 1441-1457. b) M. D. McCreary, D. W. Lewis, D. L. Wernick, G .M. Whitesides, *J. Am. Chem. Soc.*, **1974**, *96*, 1038-1054. c) T. J. Wenzel, J. D. Wilcox, *Chirality*, **2003**, *15*, 256-270.

[29] G. Uccello-Barretta, F. Balzano, P. Salvadori, *Curr. Pharm. Des.*, **2006**, *12*, 4023-4045.

[30] M. Raban, K. Mislow, *Top. Stereochem.*, **1967**, *2*, 199-230.

[31] M. Raban, K. Mislow, *Tetrahedron Lett.*, **1965**, 4249-4253.

[32] W. H. I. Pirkle, *J. Am. Chem. Soc.*, **1966**, *88*, 1837.

[33] (a) H. Dodziuk, W. Kozminski, A. Ejchart, *Chirality*, **2004**, *16*, 90-105; (b) H. J. Schneider, F. Hacket, V. Ruediger, H. Ikeda, *Chem. Rev.*, **1998**, *98*, 1755-1785.

[34] G. Uccello-Barretta, F. Balzano, A. M. Caporusso, P. Salvadori, *J. Org. Chem.*, **1994**, *59*, 836-839.

[35] W. Lee, E. Bang, C. S. Baek, W. Lee, *Magn. Reson. Chem.*, **2004**, *42*, 389-395.

[36] G. Uccello-Barretta, M. G. Berni, F. Balzano, *Tetrahedron Asymmetry*, **2007**, *18*, 2565-2572.

[37] G. R. Sullivan, *Top. Stereochem.*, **1978**, *10*, 287-329.

[38] J. Homer, M. C. Perry, *J. Chem. Soc., Faraday Trans. 1*, **1986**, *82*, 533-543.

[39] L. Fielding, *Tetrahedron*, **2000**, *56*, 6151-6170.

[40] (a) P. Stilbs, *Prog. Nucl. Magn. Reson. Spectrosc.*, **1987**, 19, 1-45; (b) C. S. Jr. Johnson, *Prog. Nucl. Magn. Reson. Spectrosc.*, **1999**, *34*, 203-256.

[41] D. Neuhaus, M. Williamson, VCH Ed, *The Nuclear Overhauser Effect in Structural and Conformational Analysis*, Publishers Inc., New York, **1989**.

3. Basket resorc[4]arenes/nucleoside complexes in gas phase

3.1 Introduction

Enantioselectivity implies that a chiral receptor reacting with a chiral molecule yields preferentially one product enantiomer over the other. The nature of the enantioselectivity is one of the most fundamental and provocative problems in stereochemistry whose solution can be attempted only after disentangling all the factors involved, including:

1) the interference of the reaction environment in the receptor/molecule encounter and its evolution to products;
2) the specific configuration-dependent interactions in the unsolvated or partially solvated receptor/molecule complex;
3) the orientation of the functionalities in the receptor/molecule adducts affecting their reaction efficiency.[1,2]

In recent years, mass spectrometry (MS) proved to be a powerful means for investigating the stability and the reactivity of chiral complexes in the gas phase, i.e. in the absence of solvation and ion pairing phenomena.[3-24] Positive information on the structure and the conformation of covalently bonded diastereomeric ions[25] and their metal adducts,[26,27] has been gathered after the recent introduction of a very powerful and sensitive technique, namely the variable

wavelength InfraRed Multiple Photon Dissociation (IRMPD) spectroscopy.[28-36] In contrast, IRMPD-based stereochemical investigation of *noncovalent* chiral ion/chiral molecule complexes drew much less attention.[37,38] The major difficulty in these studies arises from the fact that their diastereomers are held together by the same strong electrostatic interactions (e.g. proton and hydrogen

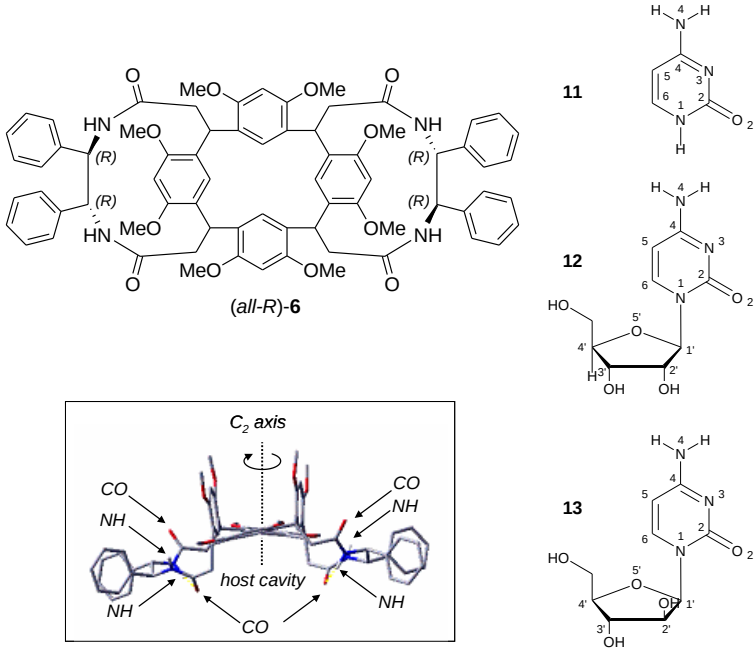

Figure 3.1. Structure of the flattened-cone bis(diamido)-bridged basket resorcin[4]arene (*all-R*)-**6** and of cytosine (**11**), cytidine (**12**), and cytarabine (**13**). The inset shows the side-view structure of the (*all-R*)-**6** enantiomer in the most stable *open-wings* conformation (see text and ref. [39]).

bonding) and any difference in their structure and stability is the result of much weaker factors, such as dispersion or repulsion interactions, charge transfer, and conformational effects. The

consequence is that noncovalent ion/molecule diastereomers often exhibit the same IRMPD spectral features, sometimes with small differences in the band intensities.[38]

We wish to report here a case of diastereomeric proton-bound receptor/molecule complexes showing IRMPD spectra with clearly different signatures. These findings outline an unprecedented effect of chirality on strong electrostatic interactions in gaseous ionic complexes.

As chiral receptor, we selected the *R,R,R,R*- and the *S,S,S,S*-enantiomers of the bis(diamido)-bridged basket resorc[4]arene of Figure 3.1 (hencefort denoted respectively as (*all-R*)-**6** and (*all-S*)-**6**) in the flattened cone conformation. Cytidine (**12**) and its epimer cytarabine (**13**) were used as chiral guests because of their ability to establish stable proton bonds with the amidocarbonyls of the basket resorcin[4]arene.[39-41] For comparison, the study has been also extended to cytosine (**11**), taken as a simplified achiral model of **12** and **13**. For the sake of clarity, the functional groups belonging to the host will be given in italic.

As shown in the inset of Figure 3.1, the most stable *open-wings* structure of the flattened-cone (*all-R*)-**6** and (*all-S*)-**6** hosts[39] display a slight distortion of the resorc[4]arene nucleus, probably due to the stereogenic centers (black dots in Figure 3.1) and to the resulting asymmetric orientation of the bridged side chains (the wings) holding two *vis a vis* phenyl rings. Each wing is connected to the rest

of the host frame through two adjacent -*NH*-*CO*- moieties whose carbonyls point either inward or outward the host cavity (Figure 3.1). The amidocarbonyls are connected to the adjacent *NH* group oriented in the same direction. An intramolecular hydrogen bond (henceforth denoted as *NH•••OC*) is formed within each wing between the *CO* and *NH* groups oriented inward the host cavity. The distance between the *NH* and *CO* groups oriented outward the host cavity is so large that a similar interaction is prevented.

3.2 Results

3.2.1 IRMPD spectra

The vibrational spectra of the ESI-formed proton-bound complexes are obtained using IRMPD spectroscopy. This technique is based on a multi-step absorption process followed by the fast intramolecular redistribution of the excess of the vibrational energy (IVR). If the IR photons are in resonance with an IR-active vibrational mode of the complex, energy can be transferred and, after several absorption steps, the ions undergo fragmentation by formal loss of the nucleosidic guest. By recording the intensity of the residual fragment, i.e. the protonated host (I_F) while varying the wavelength of the IR photons, an IRMPD spectrum is obtained. The IRMPD fragmentation efficiency is defined as $-\log[I_F/(I_P+I_F)]$, where I_P is the intensity of the parent complex.[42]

Figure 3.2 illustrates the IRMPD spectrum of [(*all-R*)-**6**•H•**11**]$^+$. Figure 3.3 shows the IRMPD spectra of the diastereomeric complexes with **12** and **13** as guests, respectively.

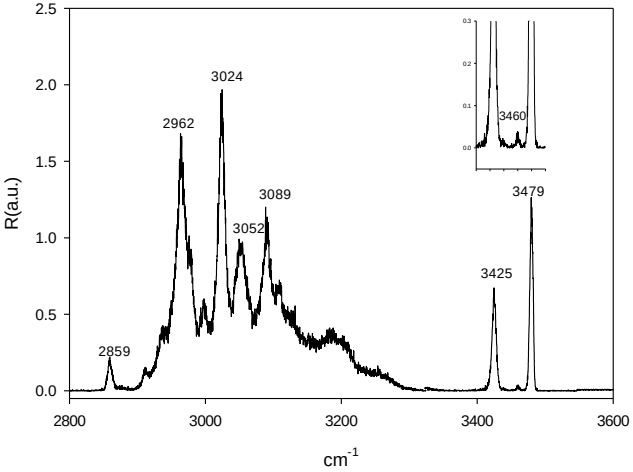

Figure 3.2. IRMPD spectra of the ESI-formed [(*all-R*)-**6**•H•**11**]$^+$ complex. The irradiation time is maintained constant throughout the entire frequency range.

Common features of all the spectra of Figures 3.2 and 3.3 are the packet of sharp resonances from ca. 2960 to ca. 3100 cm^{-1} and more or less intense broad structured resonances in the 3100-3300 cm^{-1} range. Besides this, all the IRMPD spectra display a sharp peak at 3420 cm^{-1} (with **13** as guest) or at 3425 cm^{-1} (with **11** or **12** as guest). The same signal is accompanied in the [(*all-R*)-**6**•H•**11**]$^+$ spectrum by an intense peak at 3479 cm^{-1} and a tiny one at 3460 cm^{-1} (Figure 3.2). Only some differences in signal shape and intensity are observed between the [(*all-S*)-**6**•H•**12**]$^+$ and [(*all-R*)-**6**•H•**12**]$^+$ diastereoisomers

in the 3100-3300 cm^{-1} region (Figure 3.3a,b). In contrast, the spectrum of [(*all-R*)-**6**•H•**13**]$^+$ displays also a pronounced signal at 3354 cm^{-1} which is conspicuously absent in the spectrum of [(*all-S*)-**6**•H•**13**]$^+$ (Figure 3.3d,c).

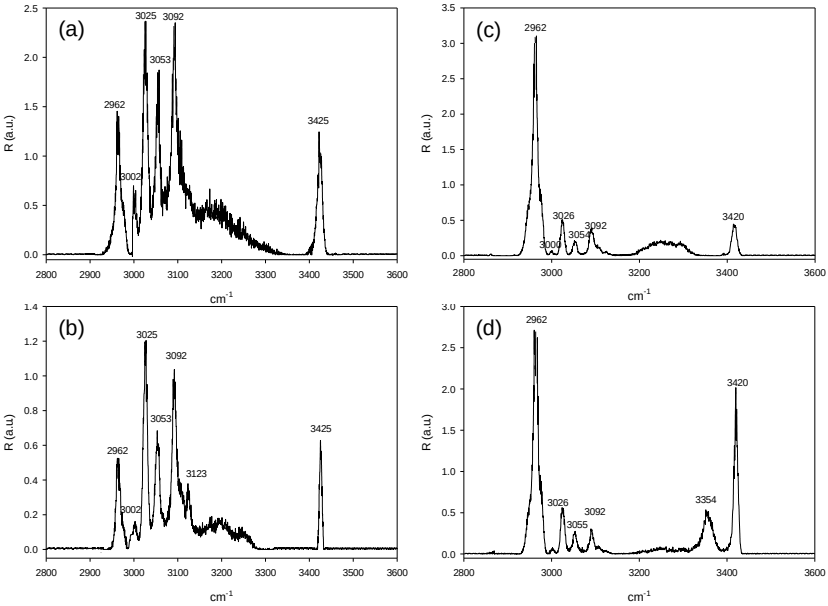

Figure 3.3. IRMPD spectra of the ESI-formed diastereomeric [(*all-S*)-**6**•H•**12**]$^+$ (a), [(*all-R*)-**6**•H•**12**]$^+$ (b), [(*all-S*)-**6**•H•**13**]$^+$ (c), and [(*all-R*)-**6**•H•**13**]$^+$ (d) complexes. The irradiation time is maintained constant throughout the entire frequency range.

3.2.2 Computational results

The presence of several basic centers in the flexible nucleosides and the large size of their proton-bound complexes with the basket resorcin[4]arene make a full exploration of the potential energy surface of the corresponding proton-bound complexes extremely

challenging, if not virtually inaccessible. Therefore, to determine their equilibrium geometry and harmonic vibrational frequencies, we decided to adopt a multi-step strategy. First, the relative proton affinities (PA's) of the most basic n-centers of the nucleoside have been calculated using the Lee–Young–Parr (B3LYP)[43,44] correlation functional and the 6-311++G(d,p) basis set as implemented in the Gaussian03 set of program suites.[45] At this level of theory, the most basic centers of **11**, **12**, and **13** are their the N(3) and the O(2) atoms (the numbering of the nucleoside atoms are reported in Figure 3.1). The N(3) center of **11** is calculated to be less basic than the O(2) one by 0.2 kcal mol^{-1}, in good agreement with previous estimates.[46,47] The PA gap between the same centers in **12** and **13** appreciably depends upon their specific sugar puckering and orientation relative to the aglycone. Extensive computational study on this dependence indicates that N(3) center of **12** is always more basic than the O(2) one by at least 0.2 kcal mol^{-1} and that this gap increases to over 1.7 kcal mol^{-1} for **13**.[48]

The second step moves from the notion that MCMM docking and constant temperature MD simulation on analogous proton-bound complexes with the basket resorcin[4]arene converge unambiguously towards several stable local minima with the guest located either at the lower rim of the host (henceforth denoted as *in*) or outside its cavity but always proton bonded to the *CO* groups (henceforth denoted as *out*) (Figure 3.4).[49]

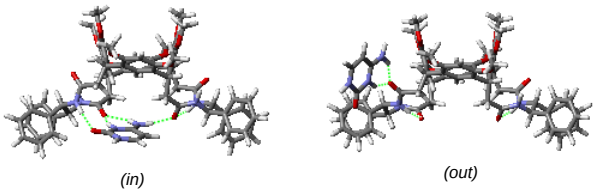

Figure 3.4. Side-view of typical *in* and *out* structures of [(*all-R*)-**6**•H•**11**]$^+$.

Assuming similar *in* and *out* arrangements for the N(3) and O(2) protonated nucleosides, we could calculate the optimized geometry, the relative stability, and the harmonic vibrational frequencies of the corresponding complexes at the ONIOM (B3LYP/6-31(d):UFF) level of theory. In all cases, thermochemical calculations indicate a distinct preference of their guests to be protonated at their N(3) centers, rather than to the O(2) ones, when interacting with the host amidocarbonyls.

This conclusion is further supported by a better correspondence between the experimental spectral pattern of a given complex and the calculated harmonic vibrational frequencies of its most stable N(3)-protonated structure. Therefore, from now on, the discussion will be restricted to the ONIOM (B3LYP/6-31(d):UFF)-calculated structures and harmonic frequencies of the complexes involving the N(3)-protonated guests (Tables 3.1-3.5).

3.3 Discussion

The experimental IRMPD spectra of Figures 3.2 and 3.3 are invariably characterized by sharp signals accompanied by very broad features. It is a well-known feature of the IRMPD spectra of noncovalent adducts involving NH and OH hydrogen-bond donors that their stretching vibrations can be more or less red-shifted and broadened, depending upon the relevant dissociation threshold.[34,46,47,50-56] The 3100-3300 cm^{-1} broad resonance structures of Figures 3.2 and 3.3 could be well a signature of these effects. However, it is also possible that the same broad feature arises from the co-existence in the ESI source of several different conformers of the complexes.

Inspection of Figures 3.2 and 3.3 reveals also that the relative intensity of the IRMPD peaks does not always reflect the relative intensity of the calculated absorption frequencies of the various structures (Tables 3.1-3.5). In few cases, several calculated frequencies appear even missing in the IRMPD spectra. It should be considered that the intensity of the experimental IRMPD signals is determined by the probability of depositing enough excess energy into the specific bond(s) involved in the complex fragmentation. This does not depend only on the efficiency of resonant photon absorption, but also on the efficiency of the IVR process as well as on the dissociation energy barrier.[56] Thus, it is possible that the

resonant absorption by a given IR-active vibrational mode in a complex could produce a signal with a relative intensity different from the corresponding calculated linear IR absorption intensity.

Table 3.1. Experimental and ONIOM (B3LYP/6-31(d):UFF)-calculated vibrational frequencies for the most stable [(*all-R*)-**6**•H•**11**]$^+$ structures

Experiment (cm^{-1})	ONIOM (B3LYP/6-31(d):UFF)-calculated frequencies (cm^{-1})[a]			Mode description[b]	Symbol
	in-1 (0.0)[c]	*out-1* (0.9)[c]	*out-2* (1.2)[c]		
3100-3300 (broad)	3129 (vs)	3090 (vs)	3158 (s)	N(3)-H•••*OC*	ν_1
		3188 (vs)	3187 (vs)	N(4)H•••*OCN-H*[d]	ν_2
	3179 (vs)	3261 (vs)	3226 (vs)	*symm* H-N(4)-H•••*OC*	ν_3
	3349 (vs)	3527 (w)	3523 (w)	*asymm* H-N(4)-H•••*OC*	ν_4
3425 (sharp)	3422 (s)			*N-H*•••OC[d]	ν_5
3460 (sharp)	3452 (vw)	3385 (w)	3384 (w)	*N-H*•••*OC*[d]	ν_6
3479 (sharp)	3466 (s)	3462 (w)	3463 (w)	N(1)-H	ν_7
	3478 (vw) 3498 (vw)	3488 (vw) 3506 (vw)	3487 (vw) 3505 (vw)	*N-H*[e]	ν_8

[a] Scaled by 0.961, absorption intensity: very weak (vw), weak (w), strong (s), very strong (vs); [b] the groups belonging to the host are denoted in italic; the predominant stretching mode is denoted by the arrow(s); [c] relative ΔH_{300} values in kilocalories per mol; [d] N-H oriented inward the host cavity; [e] N-H oriented outward the host cavity.

Table 3.2. Experimental and ONIOM (B3LYP/6-31(d):UFF)-calculated vibrational frequencies for the most stable [(*all-S*)-**6**•H•**12**]$^+$ structures.

Experiment (cm^{-1})	ONIOM (B3LYP/6-31(d):UFF)-calculated frequencies (cm^{-1}) [a]					Mode descr. [b]
	in-1 (5.1)[c]	*in-2* (13.0)[c]	*out-1* (10.3)[c]	*out-2* (12.0)[c]	*out-3* (18.6)[c]	
3100-3300 (broad)	3165 (vs)	3276 (s)	3170 (s)	3172 (vs)	3177 (s)	ν_1
			3230 (s)	3198 (vs)	3212 (vs)	ν_2
	3261 (vs)	3144 (vs)	3195 (vs)	3251 (vs)	3262 (vs)	ν_3
	3378 (vs)	3392 (s)	3525 (w)	3529 (w)	3529 (w)	ν_4
3425 (sharp)	3415 (s)					ν_5
	3448 (w)	3444 (w) 3456 (w)	3385 (w)	3386 (w)	3456 (vw)	ν_6
	3486 (vw) 3502 (vw)	3481 (vw) 3498 (vw)	3488 (vw) 3505 (vw)	3489 (vw) 3506 (vw)	3489 (vw) 3502 (vw)	ν_8

[a] See footnote [a] in Table 3.1; [b] See mode descriptions in Table 3.1; [c] ΔH_{300} values in kilocalories per mol relative to the global minimum *out-1* in Table 3.3.

Table 3.3. Experimental and ONIOM (B3LYP/6-31(d):UFF)-calculated vibrational frequencies for the most stable [(*all-R*)-**6**•H•**12**]$^+$ structures.

Experiment (cm^{-1})	ONIOM (B3LYP/6-31(d):UFF)-calculated frequencies (cm^{-1}) [a]				Mode description[b]
	in-1 (9.1)[c]	*in-2* (12.5)[c]	*out-1* (0.0)[c]	*out-2* (7.1)[c]	
3100-3300 (broad)	3158 (vs)	3253 (s)	3059 (s)	3184 (vs)	ν_1
			3262(s)	3217 (vs)	ν_2
	3217 (vs)	3164 (vs)	3289 (vs)	3278 (vs)	ν_3
	3370 (vs)	3406 (s)	3532 (w)	3534 (w)	ν_4
3425	3402 (s)				ν_5
	3449 (w)	3438 (w) 3450 (w)	3381(w)	3385 (w)	ν_6
	3480 (vw) 3500 (vw)	3489 (vw) 3493 (vw)	3489 (vw) 3505 (vw)	3488 (vw) 3506 (vw)	ν_8

[a] See footnote [a] in Table 3.1; [b] See mode descriptions in Table 3.1; [c] See footnote [c] in Table 3.2.

Table 3.4. Experimental and ONIOM (B3LYP/6-31(d):UFF)-calculated vibrational frequencies for the most stable [(*all-S*)-**6**•H•**13**]$^+$ structures.

Experiment (cm^{-1})	ONIOM (B3LYP/6-31(d):UFF)-calculated frequencies (cm^{-1}) [a]					Mode description[b]
	in-1 (6.3)[c]	*in-2* (11.6)[c]	*out-1* (7.4)[c]	*out-2* (20.8)[c]	*out-3* (22.4)[c]	
3180-3300 (broad)	3169 (vs)	3280 (s)	3087 (vs)	2890 (vs)	3127 (vs)	ν_1
			3192 (s)	3261 (s)	3204 (s)	ν_2
	3230 (vs)	3136 (vs)	3258 (vs)	3413 (s)	3275 (vs)	ν_3
	3377 (vs)	3392 (s)	3531 (w)	3550 (w)	3515 (w)	ν_4
3420 (sharp)	3403 (s)					ν_5
	3447 (w)	3454 (w) 3458 (w)	3384 (w)	3438 (w)	3443 (vw)	ν_6
	3482 (ww) 3502 (ww)	3482 (ww) 3497 (ww)	3488 (vw) 3504 (vw)	3506 (vw) 3510 (vw)	3484 (vw) 3500 (vw)	ν_8

[a] See footnote [a] in Table 3.1; [b] See mode descriptions in Table 3.1; [c] See footnote [c] in Table 3.2.

Table 3.5. Experimental and ONIOM (B3LYP/6-31(d):UFF)-calculated vibrational frequencies for the most stable [(*all-R*)-**6**•H•**13**]$^+$ structures.

Experiment (cm^{-1})	ONIOM (B3LYP/6-31(d):UFF)-calculated frequencies (cm^{-1}) [a]							Mode description[b]
	in-1 (8.7)[c]	*in-2* (10.8)[c]	*out-1* (0.4)[c]	*out-2* (5.9)[c]	*out-3* (6.9)[c]	*out-4* (8.6)[c]	*out-5* (10.9)[c]	
3180-3300 (broad)	3171 (vs)	3251 (s)	3075 (vs)	3184 (vs)	3029 (vs)	3296 (w)	3134 (s)	ν_1
			3253(s)	3215(s)	3210 (s)	3252 (s)	3273 (s)	ν_2
3354 (broad)	3227 (vs)	3161 (vs)	3282 (s)	3276 (vs)	3354 (s)	3349 (vs)	3255 (vs)	ν_3
	3374 (vs)	3407 (s)	3533 (w)	3534 (w)	3542 (w)	3541 (w)	3530 (w)	ν_4
3425 (sharp)	3405 (s)							ν_5
	3447 (w)	3441 (w) 3452 (ww)	3382(w)	3386 (w)	3391 (w)	3370 (w)	3383 (w)	ν_6
	3484 (vw) 3502 (vw)	3487 (ww) 3491 (ww)	3494 (vw) 3505 (vw)	3488 (vw) 3505 (vw)	3486 (vw) 3506 (vw)	3496 (vw) 3497 (vw)	3479 (vw) 3506 (vw)	ν_8

[a] See footnote [a] in Table 3.1; [b] See mode descriptions in Table 3.1; [c] See footnote [c] in Table 3.2.

The 2960-3100 cm^{-1} sharp resonances observed in all the spectra of Figure 3.2 and 3.3 can be essentially attributed to the host *C-H* stretching modes and will not be discussed further. Concerning the [(*all-R*)-**6**•H•**11**]$^+$ spectrum, the unresolved 3100-3300 cm^{-1} bands of Figure 3.2 cannot be taken as a signature of the *in* and *out* structures of Table 3.1 since their N(3)-H•••*OC* (ν_1), N(4)H•••*OCN-H* (ν_2), and *symm* H-N(4)-H•••*OC* (ν_3) stretching vibrations fall in the same broad range. A similar conclusion can be reached as regards to the intense sharp resonance at 3479 cm-1, attributed to the strong N(1)-H stretching (ν_7) of cytosine in [(*all-R*)-**6**•H•**11**]$^+$.[46,47] As expected, this band is absent in the spectra of Figures 3.2 and 3.3.

In contrast, the small IRMPD peak at 3460 cm^{-1} and the intense signal at 3425 cm^{-1} can be exclusively assigned to the *in-1* structure since corresponding respectively to the coordinated *N-H•••OC* (ν_6) and *N-H•••*OC stretchings (ν_5) (see the *in-1* structure in Figure 3.4). A similar ν_5 mode is obviously prevented in the *out-1* and *out-2* regioisomers (see, for instance, the *out-2* structure in Figure 3.4). It is concluded that, a significant fraction of the ESI-formed [(*all-R*)-**6**•H•**11**]$^+$ complex has the *in-1* structure, although the occurrence of other regioisomers, i.e. *out-1* and *out-2*, cannot be excluded. It should be noted, in this context, that no appreciable signals are observed around 3349 or 3525 cm^{-1} (Figure 2.2) which can be assigned to the strong *asymm* H-N(4)-H•••*OC* stretching (ν_4; Table 3.1). Possible reasons for these findings have been presented earlier in the text. The diastereomeric [(*all-R*)-**6**•H•**12**]$^+$ and [(*all-S*)-**6**•H•**12**]$^+$ complexes show almost identical IRMPD spectra, except for some differences in the peak shape and intensity (Figure 3.3a,b). Apart from the obvious absence of the ν_7 signal, the spectra of [(*all-R*)-**6**•H•**12**]$^+$ and [(*all-S*)-**6**•H•**12**]$^+$ are very similar to that of [(*all-R*)-**6**•H•**11**]$^+$. Indeed, they exhibit a pronounced 3425 cm^{-1} signal which can be attributed to the ν_5 stretching in the corresponding *in-1* structure. This assignment is supported by the fact that the *in-1* [(*all-S*)-**6**•H•**12**]$^+$ structure is the most stable one (Table 3.2). The same cannot be said for the [(*all-R*)-**6**•H•**12**]$^+$ diastereomer, since here is *out-1* the most stable calculated structure (Table 3.3). The formation

and the detection of structures other than the most stable ones is by no means unusual in ESI-MS. It may happen that aggregates, which are not stable in solution, are formed in the ESI microdroplets and released in the gas phase as kinetically trapped isomers.[53,57] It is therefore plausible to assign the sharp 3425 cm^{-1} signal of Figure 3.3a,b to the *in-1* structures of [(*all-R*)-**6**•H•**12**]$^+$ and [(*all-S*)-**6**•H•**12**]$^+$, possibly accompanied by the *out* regioisomers.

The same view applies to the [(*all-S*)-**6**•H•**13**]$^+$ complex whose spectrum is qualitatively similar to those of [(*all-R*)-**6**•H•**12**]$^+$ and [(*all-S*)-**6**•H•**12**]$^+$ (cfr. Figure 3.3a,b,d). In contrast, the spectrum of [(*all-R*)-**6**•H•**13**]$^+$ displays a signal at 3354 cm^{-1} which has never been observed in the spectra of its isomers (cfr. Figure 3.3d with Figures 3.2 and 3.3a,b,c). At this point, several questions arise: 1) what is the origin of this new peak; 2) why is this signal absent in the spectra of all the [(*all-R*)-**6**•H•**13**]$^+$ isomers studied?

In Figure 3.5, the calculated N(3)-H•••*OC* (ν_1) and *symm* H-N(4)-H•••*OC* (ν_3) frequencies of the *out* isomers of Tables 3.2-3.5 are reported as a function of the corresponding N(3)H•••*OC* proton-bond distance. As expected, the N(3)-H•••*OC* (ν_1) frequency is found to decrease with the distance of the N(3)H•••*OC* hydrogen bond (Figure 3.5).

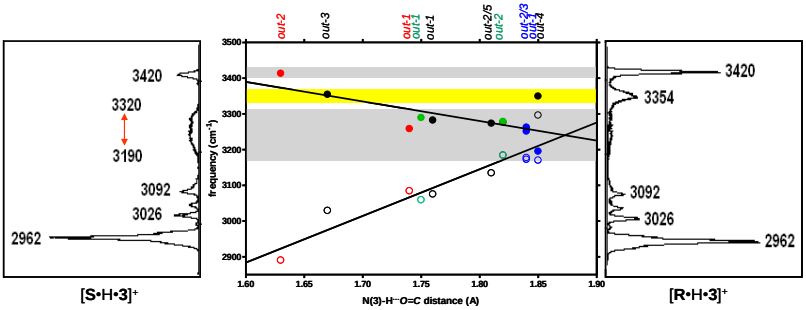

Figure 3.5. Dependence of the N(3)-H•••*OC* (ν_1) (open circles) and *symm* H-N(4)-H (ν_3) frequencies (full circles) of the calculated *out* structures of [(*all-R*)-**6**•H•**12**]$^+$ (green), [(*all-S*)-**6**•H•**12**]$^+$ (blue), [(*all-R*)-**6**•H•**13**]$^+$ (black), and [(*all-S*)-**6**•H•**13**]$^+$ (red) (Tables 2.2-2.5), as a function of the corresponding N(3)H•••*OC* proton-bond distance (in Å); (left) IRMPD spectrum of the ESI-formed [(*all-S*)-**6**•H•**13**]$^+$; (right) IRMPD spectrum of the ESI-formed [(*all-R*)-**6**•H•**13**]$^+$.

The trend is opposite for the corresponding *symm* H-N(4)-H•••*OC* (ν_3) frequency. This means that, in the *out* structures, more intense is the N(3)H•••*OC* interaction, less intense is the HN(4)H•••*OC* one. Besides, Figure 3.5 indicates that, in general, the N(3)H•••*OC* bond is stronger in the *out* structures of [(*all-S*)-**6**•H•**13**]$^+$ (red circles) and [(*all-R*)-**6**•H•**13**]$^+$ (black circles) than in those of [(*all-S*)-**6**•H•**12**]$^+$ (blue circles) and [[(*all-R*)-**6**•H•**12**]$^+$ (green circles). Besides, compared to the corresponding complexes with (*all-R*)-**6**, as host, the [(*all-S*)-**6**•H•**13**]$^+$ and [(*all-S*)-**6**•H•**12**]$^+$ complexes exhibit a large difference in the N(3)H•••*OC* distances ($\geq$ 0.1 Å). These findings may be ascribed to repulsive forces between the aglycone oxygen of the guest and the aromatic rings of the host (the C=O•••π repulsion),

which depend on the orientation of the C2'-OH bond in the sugar moiety of the guest (Figure 3.6).

In **13**, the C(2')-OH bond is oriented in such a way to allow hydrogen bonding with the aglycone oxygen (green broken line in Figure 3.6c,d) and, therefore, to lower its C=O•••π repulsion. No hydrogen bonding is allowed in **12** between the aglycone oxygen and the C(2')-OH bond because of the unfavourable orientation of the latter. Therefore, the C=O•••π repulsion is more intense and the N(3)H•••*OC* interaction weaker. Furthermore, Figure 3.6 illustrates the opposite disposition of the sugar moiety of the guest relative to the aromatic wings of the (*all-R*)-**6** and (*all-S*)-**6** hosts which may account for the comparatively large difference in the N(3)H•••*OC* strength in the complexes with (*all-S*)-**6**, as host.

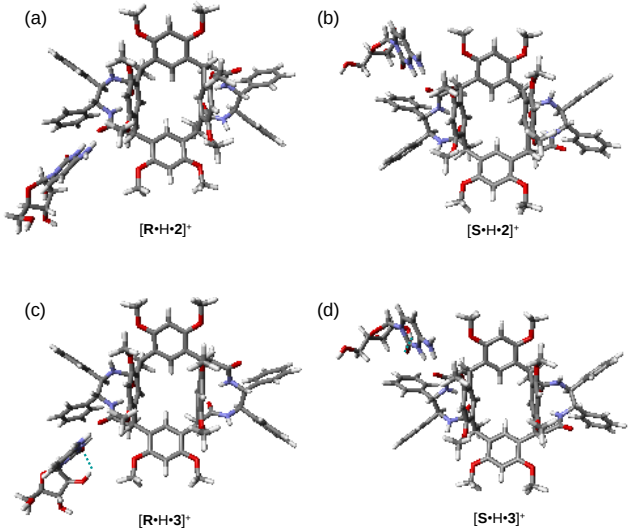

Figure 3.6. Comparison among some top-view *out* structures of (a) [(*all-R*)-**6**•H•**12**]$^+$, (b) [(*all-S*)-**6**•H•**2**]$^+$, (c) [[(*all-R*)-**6**•H•**13**]$^+$, and (d) [(*all-S*)-**6**•H•**13**]$^+$. Note the opposite disposition of the phenyl rings at the open wings of the (*all-R*)-**6** and (*all-S*)-**6** hosts. Note the intramolecular C(2')OH•••O(2)=C bonding (green broken line) in **13** and its absence in **12**. Note the different orientation of the sugar moiety in (*all-R*)-**6** vs. (*all-S*)-**6** complexes and its effect on the distortion of the proton-bonding between the nucleoside and the amidocarbonyl of the host.

The plot of Figure 3.5 explains why the spectra of both the [[(*all-R*)-**6**•H•**12**]$^+$ (Figure 3.2b) and [(*all-S*)-**6**•H•**12**]$^+$ (Figure 3.2a) complexes show broad bands peaking at ca. 3190 and ca. 3250 cm^{-1}. The first can be attributed to the N(3)-H•••*OC* (ν_1) stretching (e.g. the blue and green open circles in Figure 3.5) and the second to the *symm* H-N(4)-H•••*OC* (ν_3) one (e.g. the blue and green full circles in Figure

3.5). The N(3)-H•••*OC* (ν_1) stretching in the [(*all-R*)-**6**•H•**13**]$^+$ and [(*all-S*)-**6**•H•**13**]$^+$ structures is located beneath the *C-H* stretching region (2960-3100 cm^{-1}) (the black and red open circles in Figure 3.5). Instead, the *symm* H-N(4)-H•••*OC* (ν_3) stretching in [(*all-S*)-**6**•H•**13**]$^+$ mingles either in the unresolved 3200-3300 cm^{-1} band (the red full circles at ca. 3250 cm^{-1} for *out-1*) or in the 3420 cm^{-1} peak of its *in-1* structure (the red full circles at 3413 cm^{-1} for *out-2*).

As illustrated by the black full circles of Figure 3.5, the calculated *symm* H-N(4)-H•••*OC* (ν_3) stretchings of the *out-1, out-2*, and *out-5* regioisomers of [(*all-R*)-**6**•H•**13**]$^+$ mingle in the unresolved 3200-3300 cm^{-1} band as well. However, those of the *out-3* and *out-4* isomers fall at ca. 3350 cm^{-1}, i.e. in the spectral region where [(*all-S*)-**6**•H•**13**]$^+$, [(*all-R*)-**6**•H•**12**]$^+$, and [(*all-S*)-**6**•H•**12**]$^+$ do not exhibit any signals.

These assignments confirm the idea that ESI of the selected nucleoside/resorcin[4]arene methanolic solutions generates several co-existing regioisomers of their proton-bound complexes where the nucleosidic guest is kinetically trapped either inside or outside the host cavity. The strength of noncovalent interactions involved in these complexes depends on the possibility of hydrogen bonding in the nucleoside from the C(2')-OH group and the oxygen of the aglycone. The presence of this H-bond moderates the repulsive interactions between the aglycone oxygen and the aromatic rings of the host. The *symm* H-N(4)-H•••*OC* (ν_3) frequency in the *out*

complexes is significantly affected by the subtle interplay among host/guest attractive and repulsive interactions. While the ν_3 frequencies of the isomers of [(*all-S*)-**6**•H•**13**]$^+$, [(*all-S*)-**6**•H•**12**]$^+$, and [(*all-R*)-**6**•H•**12**]$^+$, cohalesce in broad bands, those of several *out* [(*all-R*)-**6**•H•**13**]$^+$structures are blue-shifted from the same region and, therefore, can be discerned.

3.4 Conclusions

The first case of diastereomeric noncovalent complexes showing clearly different IRMPD spectral patterns are reported in this chaper. The complexes are generated in the gas phase by electrospray ionization (ESI) of mixtures containing a chiral host, i.e. the pure enantiomers of the bis(diamido)-bridged basket resorcin[4]arene **6**, and achiral and chiral guest molecules, such as cytosine, cytidine, and its epimer cytarabine. The proton-bound complexes with cytosine, as guest, exhibits an IRMPD spectrum which, in the light of ONIOM (B3LYP/6-31(d):UFF) calculations, is consistent with the occurrence of several isomeric structures, where the N(3)-protonated guest is accommodated either inside the host cavity (the *in* structure) or outside it (the *out* structures). A similar picture holds for the ESI-formed diastereomeric proton-bound complexes with cytidine and cytarabine, as guests. However, the cytarabine complex with the *R,R,R,R*-enantiomer of the host exhibits a spectral pattern clearly

different from the others. This difference is attributed to the effects of the intramolecular hydrogen bonding between the C(2')-OH group and the aglycone oxygen of the nucleosidic guest upon the repulsive interactions between the same oxygen and the aromatic rings of the host.

The results presented in this chapter have been published:
A. Filippi, C. Fraschetti, S. Piccirillo, F. Rondino, B. Botta, I. D'Acquarica, A. Calcaterra, M. Speranza, *Chem. Eur. J.*, **2012**, *18*, 8320-8328.

3.5 Experimental Section

3.5.1 Chemicals

Enantiomerically pure basket resorcin[4]arenes (*all-R*)-**6** and (*all-S*)-**6**, in their flattened-cone conformation, were synthesized and purified according to established procedures[39], as showed in chapter 2. Compounds **11-13** were purchased from a commercial source and used without further purification.

3.5.2 IRMPD spectroscopy

All the proton-bound complexes have been generated in a modified Bruker Esquire 6000 quadrupole ion trap by electrospray ionization

(ESI) of methanolic mixtures containing the basket resorcin[4]arene and the nucleoside. The IR beam has been focused in the ion trap through a conical hole in the ring electrode. IR spectroscopy in the 2800-3600 cm^{-1} wavenumber range was performed using an IR optical parametric oscillator/amplifier (OPO/OPA) system, pumped by 10 Hz Nd:YAG laser (650 mJ per pulse, 8 ns pulse duration). In the presently covered wavenumber range, the typical output energy is ca. 23 mJ per pulse with a spectral bandwidth of ca. 5 cm^{-1}.[58]

3.5.3 Computational details

All the calculations for the noncovalent adducts between the (*all-R*)-**6** and (*all-S*)-**6** hosts and the O- and N-protonated **11**, **12** and **13** guests were performed using the hybrid quantum mechanics/molecular mechanics (QM/MM) ONIOM method [59] as implemented in the Gaussian 03 package.[45] The QM region included both the CO-NH-CH-CH-NH-CO sequences of the host and the entire protonated guest. It was calculated using the DFT B3LYP functional[43] and the 6-31G(d) basis set.[60] The rest of the host molecule constituted the MM region, where the UFF force field[61] was used. All the above ONIOM(B3LYP/6-31G*:UFF) geometry optimizations were full, without restrictions and the stationary points found were characterized as true minima through vibrational analysis. The value 0.961 was used as a scaling factor for the calculated harmonic frequencies.

3.6 References

[1] R. Bentley, *Archiv. Biochem. Biophys.*, **2003**, *414*, 1-12.

[2] V. Davankov, *Chirality*, **1997**, *9*, 99-102.

[3] M. Sawada, *J. Mass Spectrom. Soc. Japan*, **1997**, *45(3)*, 439-458.

[4] W. Shen, P. S. H. Wong, R. G. Cooks, *Rapid Commun. Mass Spectrom.*, **1997**, *11(1)*, 71-74.

[5] W. Tao, D. Zhang, F. Wang, P. D. Thomas, R. G. Cooks, *Anal. Chem.*, **1999**, *71(19)*, 4427-4429.

[6] A. Filippi, A. Giardini, S. Piccirillo, M. Speranza, *Int. J. Mass Spectrom.*, **2000**, *198(3)*, 137-163.

[7] D. V. Dearden, Y. Liang, J. B. Nicoll, K. A. Kellersberger, *J. Mass Spectrom.*, **2001**, *36*, 989-997.

[8] A. Schalley, *Mass Spectrom. Rev.*, **2002**, *20(5)*, 253-309.

[9] M. Sawada, *J. Mass Spectrom. Soc. Japan*, **2002**, *50(6)*, 311-329.

[10] W. A. Tao, R. G. Cooks, *Anal. Chem.*, **2003**, *75(1)*, 25A-31A.

[11] M. Shizuma, *J. Mass Spectrom. Soc. Japan*, **2003**, *51(1)*, 330-333.

[12] M. Speranza, *Adv. Phys. Org. Chem.*, **2004**, *39*, 147-281.

[13] M. Speranza, *Int. J. Mass Spectrom.*, **2004**, *232*, 277-317.

[14] K. A. Schug, W. Lindner, *J. Sep. Sci.*, **2005**, *28(15)*, 1932-1955.

[15] M: Speranza, M. Satta, S. Piccirillo, F. Rondino, A. Paladini, A. Giardini, A. Filippi, D. Catone, *Mass Spectrom. Rev.*, **2005**, *24(4)*, 588-610.

[16] A. Di Tullio, S. Reale, F. De Angelis, *J. Mass Spectrom.*, **2005**, *40(7)*, 845-865.

[17] S. C. Nanita, R. G. Cooks, *Angew. Chem. Int. Ed. Engl.*, **2006**, *45(4)*, 554-569.

[18] A. Zehnacker, M. A. Suhm, *Angew. Chem. Int. Ed. Engl.*, **2008**, *47(37)*, 6970-6992.

[19] M. Speranza, F. Rondino, M. Satta, A. Paladini, A. Giardini, D. Catone, S. Piccirillo, *Chirality*, **2009**, *21(1)*, 119-144.

[20] M. Speranza, F. Gasparrini, B. Botta, C. Villani, D. Subissati, C. Fraschetti, F. Subrizi, *Chirality*, **2009**, *21(1)*, 69-86.

[21] A. B. Wijeratne, K. B. Schug, *J. Sep. Sci.*, **2009**, *32(10)*, 1537-1547.

[22] M. Vairamani, S. Kumari, in *Chiral Recognition in the Gas Phase*, (Ed. A. Zehnacker) CRC Press, Taylor & Francis, **2010**, pp. 143-166.

[23] V. Dearden, N. Fang, in *Chiral Recognition in the Gas Phase*, (Ed. A. Zehnacker) CRC Press, Taylor & Francis, **2010**, pp. 133-142.

[24] M. Speranza, in *Chiral Recognition in the Gas Phase*, (Ed. A. Zehnacker) CRC Press, Taylor & Francis, **2010**, pp. 87-131.

[25] Y. M. E. Fung, T. Besson, J. Lemaire, P. Maitre, R. A. Zubarev, *Angew. Chem. Int. Ed.*, **2009**, *48*, 8340-8342.

[26] N. C. Polfer, J. J. Valle, D. T. Moore, J. Oomens, J. R. Eyler, B. Bendiak, *Anal. Chem.*, **2006**, *78*, 670-679.

[27] R. C. Dunbar, J. D. Steill, J. Oomens, *J. Am. Chem. Soc.*, **2011**, *133*, 1212-1215.

[28] M. Peiris, J. M. Riveros, J. R. Eyler, *Int. J. Mass Spectrom.*, **1996**, *159*, 169-183.

[29] J. J. Valle, J. R. Eyler, J. Oomens, D. T. Moore, A. F. G. van der Meer, G. von Helden, G. Meijer, C. L. Hendrickson, A. G. Marshall, G. Blakney, *Rev. Sci. Instrum.*, **2005**, *76*, 023103/1-023103/7.

[30] G. von Helden, D. van Heijnsbergen, G. Meijer, *J. Phys. Chem. A*, **2003**, *107*, 1671-1688.

[31] D. T. Moore, J. Oomens, J. R. Eyler, G. von Helden, G. Meijer, R. C. Dunbar, *J. Am. Chem. Soc.*, **2005**, *127*, 72437254-.

[32] P. Maitre, S. Le Caer, A. Simons, W. Jones, J. Lemaire, H. Mestdag, M. Heninger, G. Mauclaire, P. Boissel, R. Prazeres, F. Glotin, J. M. Ortega, *Nucl. Instrum. Methods A*, **2003**, *507*, 541-546.

[33] X. L. Kong, I. A. Tsai, S. Sabu, C. C. Han, Y. T. Lee, H. C. Chang, S. Y. Tu, A. H. Kung, C. C. Wu, *Angew. Chem. Int. Ed. Engl.*, **2006**, *45*, 4130-4134.

[34] A. Kamariotis, O. V. Boyarkin, S. R. Mercier, R. D. Beck, M. F. Bush, E. R. Williams, T. R. Rizzo, *J. Am. Chem. Soc.*, **2006**, *128*, 905-916.

[35] T. D. Vaden, T. S. J. A. de Boer, J. P. Simons, L. C. Snoek, *Phys. Chem. Chem. Phys.*, **2008**, *10*, 1443-1447.

[36] R. Wu, T. B. McMahon, *J. Phys. Chem. B*, **2009**, *113*, 8767-8775.

[37] As a matter of fact, some IRMPD spectroscopic studies on proton-bound amino acid adducts have been carried out in McLafferty's (see: H. B. Oh, C. Lin, H. Y. Hwang, H. Zhai, K. Breuker, V. Zabrouskov, B. C. Carpenter, F. W. McLafferty, *J. Am. Chem. Soc.*, **2005**, *127*, 4076-4083; X. Kong, C. Lin, G. Infusini, H. B. Oh, H. Jiang, K. Breuker, C. C. Wu, O. P. Charkin, H. C. Chang, F. W. McLafferty, *ChemPhysChem*, **2009**, *10*, 2603-2606) and Chang's groups (ref. 33). However, in these studies, no spectroscopic differences between diastereomeric complexes have been reported.

[38] Very recently, an IRMPD study on the protonated dimers of Cinchona alkaloids carried out in Zehnacker's group (see: D. Scuderi, K. Le Barbu-Debus, A. Zehnacker, *Phys. Chem. Chem. Phys.*, **2011**, *13*, 17916-17929) revealed small differences in the intensities of the ν(OH) stretches, attributed to the presence of a weak CH···O interaction on the neutral part of the heterochiral complex.

[39] B. Botta, I. D'Acquarica, L. Nevola, F. Sacco, Z. Valbuena Lopez, G. Zappia, C. Fraschetti, M. Speranza, A. Tafi, F. Caporuscio, M. C. Letzel, J. Mattay, *Eur. J. Org. Chem.*, **2007**, *36*, 5995-6002.

[40] B. Botta, C. Fraschetti, I. D'Acquarica, F. Sacco, J. Mattay, M. C. Letzel, M. Speranza, *Org. Biomol. Chem.*, **2011**, *9*, 1717-1719.

[41] B. Botta, A. Tafi, F. Caporuscio, M. Botta, L. Nevola, I. D'Acquarica, C. Fraschetti, M. Speranza, *Chem. Eur. J.*, **2008**, *14*, 3585-3595.

[42] J. M. Bakker, J. Y. Salpin, P. Maitre, *Int. J. Mass Spectrom.*, **2009**, *283*, 214-221.

[43] C. Lee, W. Yang, R. Parr, *Phys. Rev. B*, **1988**, *37*, 785-789.

[44] A. D. Becke, *J. Chem. Phys.*, **1993**, *98*, 5648-5652.

[45] M. J. Frisch, G. W. Trucks, H. B. Schlegel, G. E. Scuseria, M. A. Robb, J. R. Cheeseman, J. A. Montgomery,T. Vreven, K. N. Kudin, J. C. Burant, J. M. Millam, S. S. Iyengar, J. Tomasi, V. Barone, B. Mennucci, M. Cossi, G. Scalmani,N. Rega, G. A. Petersson,H. Nakatsuji, M. Hada, M. Ehara, K. Toyota, R. Fukuda, J. Hasegawa,M. Ishida, T. Nakajima, Y. Honda, O. Kitao, H. Nakai, M. Klene, X. Li, J. E. Knox, H. P. Hratchian, J. B. Cross, V. Bakken, C. Adamo, J. Jaramillo, R. Gomperts,R. E. Stratmann, O. Yazyev, A. J. Austin, R. Cammi, C. Pomelli,J. W. Ochterski, P. Y. Ayala, K. Morokuma, G. A. Voth, P.

Salvador, J. J. Dannenberg, V. G. Zakrzewski, S. Dapprich, A. D. Daniels, M. C. Strain, O. Farkas, D. K. Malick, A. D. Rabuck, K. Raghavachari, J. B. Foresman, J. V. Ortiz, Q. Cui, A. G. Baboul, S. Clifford, J. Cioslowski, B. B. Stefanov, G. Liu, A. Liashenko, P. Piskorz, I. Komaromi, R. L. Martin, D. J. Fox, T. Keith, M. A. Al-Laham, C. Y. Peng, A. Nanayakkara, M. Challacombe, P. M. W. Gill, B. Johnson, W. Chen, M. W. Wong, C. Gonzalez, J. A. Pople, "Gaussian Program Suite" in *Gaussian 03*; Gaussian, Inc.: Wallingford, CT, **2004**.

[46] J. Y. Salpin, S. Guillaumont, J. Tortajada, L. MacAleese, J. Lemaire, P. Maitre, *ChemPhysChem*, **2007**, *8*, 2235−2244.

[47] J. M. Bakker, J. Y. Salpin, P. Maitre, *Int. J. Mass Spectrom.*, **2009**, *283*, 214-221.

[48] A. Filippi, C. Fraschetti, L. Guidoni, F. Rondino, S. Piccirillo, V. Steinmetz, M. Speranza, submitted.

[49] B. Botta, C. Fraschetti, F. R. Novara, A. Tafi, F. Sacco, L. Mannina, A. P. Sobolev, J. Mattay, M. C. Letzel, M. Speranza, *Org. Biomol. Chem.*, **2009**, *7*, 1798-1806.

[50] J. M. Bakker, R. K. Sinha, T. Besson, M. Brugnara, P. Tosi, J. Y. Salpin, P. Maitre, *J. Phys. Chem. A*, **2008**, *112*, 12393-12400.

[51] J. R. Roscioli, L. R. McCunn, M. A. Johnson, *Science*, **2007**, *316*, 249-254.

[52] J. S. Prell, M. Demireva, J. Oomens, E. R. Williams, *J. Am. Chem. Soc.*, **2009**, *131*, 1232−1242.

[53] J. Oomens, J. D. Steill, B. Redlich, *J. Am. Chem. Soc.*, **2009**, *131*, 4310−4319.

[54] J. S. Prell, T. M. Chang, J. A. Biles, G. Berden, J. Oomens, E. R. Williams, *J. Phys. Chem. A*, **2011**, *115*, 2745-2751.

[55] P. Hurtado, F. Gamez, S. Hamad, B. Martinez-Haya, J. D. Steill, J. Oomens, *J. Phys. Chem. A*, **2011**, *115*, 7275-7282.

[56] J. Oomens, B. G,. Sartakov, G. Meijer, G. von Helden, *Int. J. Mass Spectrom.*, **2006**, *254*, 1-19.

[57] J. D. Steill, J. Oomens, J.. *J. Am. Chem. Soc.*, **2009**, *131*, 13570−13571.

[58] J. Lemaire, P. Boissel, M. Heninger, G. Mauclaire, G. Bellec, H. Mestdagh, A. Simon, S. L. Caer, J. M. Ortega, F. Glotin, P. Maitre, *Phys. Rev. Lett.*, **2002**, *89*, 273002/1-273002/4.

[59] a) F. Maseras, K. Morokuma, *J. Comput. Chem.*, **1995**, *16*, 1170-1179; b) S. Humbel, S. Sieber, K. Morokuma, *J. Chem. Phys.*, **1996**, *105*, 1959-1967; c) M. Svensson, S. Humbel, R. D. J. Froese, T. Matsubara, S. Sieber, K. Morokuma, *J. Phys. Chem.*, **1996**, *100*, 19357-19363; d) M. Svensson, S. Humbel, K. Morokuma, *J. Chem. Phys.*, **1996**, *105*, 3654-3661; e) S. Dapprich, I. Komromi, K. S. Byun, K. Morokuma, M. J. Frisch, *J. Mol. Struct.*, **1999**, *462*, 1-21.

[60] a) M. M. Francl, W. J. Pietro, W. J. Hehre, J. S. Binkley, M. S. Gordon, D. J. Defrees, J. A. Pople, *J. Chem. Phys.*, **1982**, *77*, 3654-3665; b) W. J. Hehre, R. Ditchfield, J. A. Pople, *J. Chem. Phys.*, **1972**, *56*, 2257-2261; c) P. C. Hariharan, J. A. Pople, *Theor. Chim. Acta*, **1973**, *28*, 213-222.

[61] A. K. Rappe , C. J. Casewit, K. S. Colwell, W. A. Goddard III, W. M. Skiff, *J. Am. Chem. Soc.*, **1992**, *114*, 10024-10035.

4. Basket resorc[4]arenes/nucleoside complexes in solution

4.1 Introduction

Nucleosides[1] are glycosylamines consisting of a nucleobase (often referred to simply base) bound to a ribose or deoxyribose sugar. In the cell, they can be phosphorylated by specific kinases on the primary alcohol group of the sugar, producing nucleotides, which are the molecular building blocks of DNA and RNA. Nucleotides possess also several other biological functions: they can be used as source of energy like ATP, which produces free energy making a lot of reactions thermodynamically favoured; they are also essential components of different co-factors which are necessary to metabolism, such as NAD^+, FAD and coenzyme A. Instead, nucleosides play key roles in biological environment as neuromodulators. For instance, adenosine is an ubiquitous purine nucleoside, essential in the regulation of cardiovascular physiological functions.[2,3]

The therapeutic use of nucleoside analogues as antimetabolites in many kinds of human cancers is actually very widespread: they act as prodrugs, being phosphorylated in vivo and yielding nucleotides analogues; these latter species are involved in the termination of the synthesis of the nucleic acids chains.

Some examples of pyrimidine analogues are cytarabine, a natural product deriving from marine source,[4] and gemcitabine,[5,6] a pyrimidine synthetic nucleoside analogue of 2'-deoxycytidine where the hydrogen atoms on the 2' carbon are replaced by fluorine atoms. Gemcitabine is indicated as first-line therapy for locally advanced or metastatic adenocarcinoma of the pancreas.[7]

In a large number of pathological conditions, the application of antimetabolites is often characterised by low selectivity against damaged cellular aggregates. The possible use of a soluble carrier for drugs in physiological environment is one of the most central trouble of the pharmaceutical technique, so that it can make lower the IC_{50} (half maximal inhibitory concentration) of some formulations. Encapsulation into suitable molecular carriers could be a plausible way to remove limitations in the use of chemotherapeutic agents.[8]

We recently found that bis(diamido)-bridged basket resorc[4]arene (*all-S*)-**6** (Chart 4.1) and its (*all-R*) enantiomer are capable of selectively encapsulating amino acids,[9] chiral amines,[9] amphetamine[10] and vinca alkaloids[11] in the gaseous phase, i.e., under conditions where the phenomenon is not influenced by solvation and ion pairing effects. More recently, we showed that proton-bound diastereomeric complexes of the above mentioned hosts with pyrimidine nucleosides in the gas phase behave as supramolecular "chiroselective logic gates", by releasing the nucleoside depending on the resorc[4]arene configuration.[12]

Therefore, we believed it is useful to investigate the interactions allowing the encapsulation of nucleoside analogues **12**–**15** (Chart 4.1) in (*all-S*)-**6** and (*all-R*)-**6** hosts by NMR methods, including NMR DOSY experiments, for the detection of translational diffusion and determination of heteroassociation constants. Molecular modeling was performed at the end to support the findings obtained and give an exhaustive picture of the complexation phenomena.

4.2 Results and Discussion

4.2.1 Choice of the resorc[4]arene hosts

We chose as a suitable molecular carrier for nucleoside analogues **12**–**15** (Chart 4.1) the previously described bis(diamido)-bridged basket resorc[4]arene (*all-S*)-**6** (Chart 4.1), whose synthesis is reported in chapter 2.[9] The host contains two rigid 1,2-diphenylethylenediamine bridges, built by reaction of the acid chloride functionalities of two adjacent substituents with (1*S*,2*S*)-(–)-1,2-diphenylethylendiamine (DPEDA).

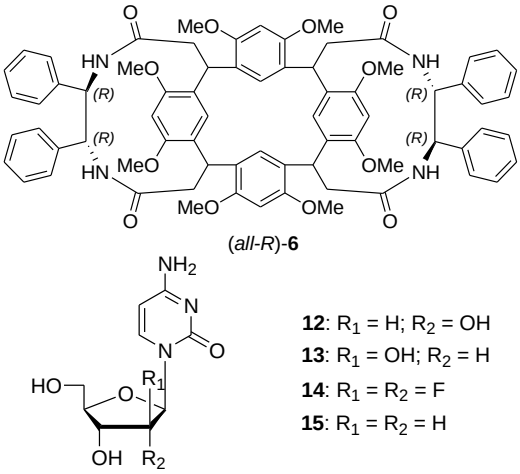

Chart 4.1. Structures of bis(diamido)-bridged basket resorc[4]arene (*all-R*)-**6** and of nucleoside analogues cytidine (**12**), cytarabine (or cytosine-β-d-arabinofuranoside) (**13**), gemcitabine (or 2',2'-difluoro-deoxycytidine) (**14**), and 2'-deoxycytidine (**15**).

With regard to the basket resorc[4]arenes conformation, we already found that the aromatic rims assumed the expected *flattened cone* arrangement, whereas two different conformations, tentatively designated as "open wings" and "folded wings", were attributed to the 1,2-diphenylethylenediamine bridges according to molecular modelling studies.[9] In particular, the "open wings" arrangement proved to be the lowest energy conformer in the gas phase for resorc[4]arene **6** host, where the minor distortions of the aromatic rim were ascribed to strains induced by the 1,2-diphenylethylenediamine bridges. Such previous modelling

predicted also: (*i*) the existence of a couple of intramolecular hydrogen bonds between opposite amido groups of the two side wings of the resorc[4]arene, and (*ii*) a conformational dependence on the solvent. Thus, we believed it useful to compare such results with NMR measurements performed in solution, where solvation effects on the amido groups of the two wings could play a role in the conformational features of the host.

4.2.2 Conformation of the resorc[4]arene hosts in solution

We decided to investigate the conformational features of macrocycle (*all-S*)-**6** and guest **15** (Chart 4.1) in solution measuring intermolecular dipolar interactions by 2D ROESY-NMR spectroscopy. Since both host and guest showed very low solubility in most organic solvents, with the exception of polar aprotic ones such as dimethyl sulfoxide (DMSO), NMR studies were performed in DMSO-d_6 at a 40 mM concentration. Interpretation of 2D ROESY map (Figure 4.1) of resorc[4]arene (*all-S*)-**6** enabled us to attribute the relative positions of both aromatic rings and of the diamido chains. In fact, the trace corresponding to methine protons H-2/14 (Figure 4.1e), which are located on the resorcarene bridge, showed more intense ROE effects at the frequency of aromatic protons H-25/27 which belong to A/C aromatic rings than those on the H-26/28 aromatic protons of B/D rings.

These effects, which are unexpected on the basis of a predominant *flattened cone* conformation, strongly suggest that a *1,3-alternate*-like is the prevalent conformation in solution. Reciprocal dipolar interactions at the frequencies of the methoxyl (OMe) protons (3.31 ppm and 3.39 ppm), which cannot be intra-ring, clearly confirmed that B and D aromatic rings are faced and the detected effects are due to OMe-4'/OMe-18' and/or OMe-6'/OMe-16' pairs. Very small chemical shifts differentiation of the methoxyl groups of A/C

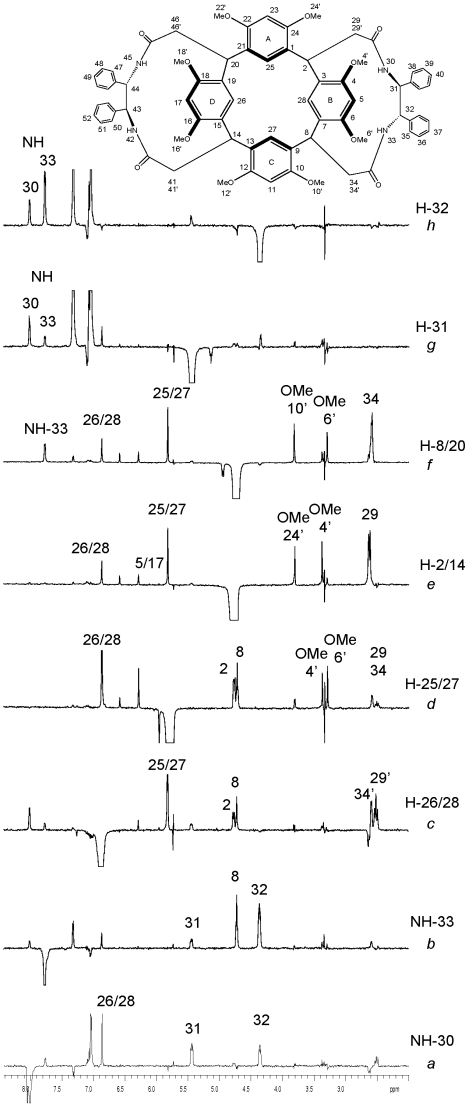

Figure 4.1. 2D ROESY traces of (*all-S*)-**6** protons (600 MHz, DMSO-d_6, 298 K, 0.6 s mixing time).

rings did not allow us to get similar information regarding the expected facing of A/C aromatic rings.

H-2 methine proton showed strongly different vicinal *J* coupling constants with diastereotopic methylene protons H-29 and H-29': 4.4 Hz for $^{3}J_{H2H29}$ and 12.6 Hz for $^{3}J_{H2H29'}$. Furthermore, H-2 proton gave a relevant ROE effect at the frequency of H-29 (Figure 4.1e), whereas any dipolar interaction was not detected with H-29' proton, indicating that H-2 proton was *gauche* to H-29 and *trans* to H-29'. Thus, among the two pairs of dihedral angles calculated from each vicinal coupling constant, the values of 90° and 180° were selected for the dihedral angles H_2-C-C-H_{29} and H_2-C-C-$H_{29'}$, respectively.

H-29' methylene proton, which was *trans* to H-2, gave ROE effects with H-26 aromatic proton, whereas the trace corresponding to H-29 proton did not reveal any dipolar interaction with the same H-26 aromatic proton. Therefore, H-29 proton, which is *gauche* to H-2, points at the outside of the diamido chain. Notably, since any significant inter-ROE H-2-NH-30 effect was not detected, NH-30 bond must be directed faraway from H-2, pointing at the inside of the diamido chain. Accordingly, the NH-30 trace (Figure 4.1a) showed a relevant ROE effect at the frequency of H-26 aromatic proton. In this way, if we assume a *transoid* H-N-C=O relative stereochemistry, the carbonyl group bound to NH-30 should point at H-29 proton, leading to the relevant high frequency shift of H-29 relative to H-29'.

NH-30 proton gave nearly equivalent ROE effects at the frequencies of H-31 and H-32 methine protons (Figure 4.1a). Thus, we can conclude that the above mentioned amide proton, which points at the inside of the diamido chain, is nearly halfway from the two H-31 and H-32 methine protons. Between the two 139° and 29° values of dihedral angles, calculated from the vicinal $^{3}J_{NH30H31}$ coupling constant (6.6 Hz), the first one was selected on the basis of the ROE data. Vicinal $^{3}J_{H31H32}$ coupling constant (11.6 Hz) gave the value of 175° for the corresponding H_{31}-C-C-H_{32} dihedral angle. Nearly equivalent inter-ROEs NH-33/H-32 and NH-33/H-8 were detected (Figure 4.1b), which are in agreement with the dihedral angle of 22°, calculated from the $^{3}J_{NH33CH32}$ coupling constant of 7.5 Hz. Very small dipolar interactions between NH-33 and H-26 aromatic proton and NH-30 were detected (Figure 4.1b), which suggested an average prevailing conformation in which NH-33 points at the external of the diamido bridge and at H-8 proton.

Finally, with regard to the CH_8-$CH_{34}H_{34'}$ fragment, very high intensity ROE effect at the frequency of H-25 was detected for H-8 (Figure 4.1f), which confirms that the *1,3-alternate*-like is the prevalent conformation in solution.

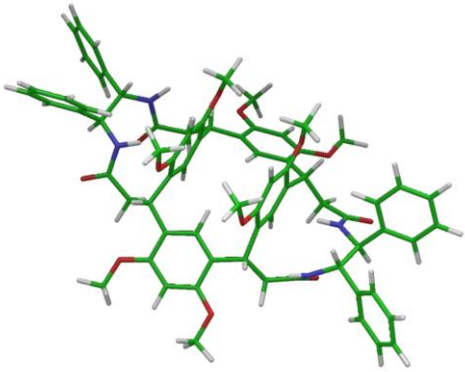

Figure 4.2. Schematic representation of (*all-S*)-**6** conformation in DMSO-d_6.

We can conclude that resorcarene (*all-S*)-**6** preferentially adopts, in DMSO-d_6, the *1,3-alternate*-like conformation whereby B/D and A/C rings are faced (Figure 4.2). The diamido chain bridging the resorcarene structure at its outside creates a large *cone*-like arrangement defined by the two aromatic A and C rings and by the two diamido arms, inside which extensive hydrophobic and hydrophilic interactions can be simultaneously pre-organized.

The same results were obtained by changing the solvent from DMSO-d_6 to pyridine-d_5.

4.2.3 Determination of heteroassociation constants for diastereoisomeric [(*all-S*)-6•15] and [(*all-R*)-6•15] complexes

Heteroassociation constants of [(*all-S*)-**6•15**] and [(*all-R*)-**6•15**] diastereoisomeric complexes were obtained from diffusion data in

DMSO-d_6 by single point measurements, and from ^{1}H NMR chemical shifts dilution data, by means of non-linear fitting of concentration-chemical shifts dependence.

Diffusion coefficients (D), measured by NMR DOSY experiments,[13] can be correlated by the hydrodynamic radius (R_H) to the molecular size, on the basis of the Stokes-Einstein equation, which strictly holds for spherical molecules (Eq. 1):

$$D = \frac{kT}{6\pi\eta R_H} \quad (1)$$

where k is the Boltzmann constant, T is the absolute temperature, and η is the solution viscosity. The resort to NMR DOSY in the study of complexation phenomena is justified by the fact that complexation processes originate species with increased sizes, and hence with lower diffusion coefficients. In fast exchange conditions, i.e., when diffusion of free and complexed species is coincident, the measured diffusion coefficient (D_{obs}) represents the weighted average of the value corresponding to the uncomplexed (D_f) and complexed (D_c) forms (Eq. 2).

$$D_{obs} = D_f x_f + D_c x_c \quad (2)$$

where x_f and x_c are the molar fractions of uncomplexed and complexed forms, respectively, with $x_f + x_c = 1$.

Molar fractions of complexed species (x_c), and, hence, association constant K, can be obtained from Eq. 3.

$$x_c = \frac{D_{obs} - D_f}{D_c - D_f} \tag{3}$$

When complexation phenomena involve species with significantly different sizes, it can be assumed that, in the complex, translational diffusion is mainly controlled by the larger molecules; thus, D_c can be put equal to the diffusion coefficient of the largest molecule. In this way, from a single point measurement, the complexed molar fraction can be easily obtained from Eq. 3.

Diffusion coefficient of uncomplexed (*all-S*)-**6** or (*all-R*)-**6** hosts was 0.90×10^{-10} m^2s^{-1}, and proved to be not influenced by the presence of guest **15**. On the contrary, diffusion coefficient of **15**, that was 2.04×10^{-10} m^2s^{-1} in the pure compound, decreased to 1.73×10^{-10} m^2s^{-1} in the presence of (*all-S*)-**6** and to 1.76×10^{-10} m^2s^{-1} in the presence of (*all-R*)-**6**. Thus, on the basis of Eq. 3, nearly equal bound molar fractions of about 0.25 were calculated. The above two values yielded very similar association constants (K ranging from 11 to 13 M^{-1}) for the two diastereoisomeric [(*all-S*)-**6•15**] and [(*all-R*)-**6•15**] complexes (see Table 4.1).

Table 4.1. Diffusion coefficients (D)[a] calculated for guest **15** (40 mM), uncomplexed (*all-R*)-**6**/(*all-S*)-**6** hosts (40 mM), and for their equimolar mixtures. Bound molar fractions (x_c) of **15** in the mixtures and heteroassociation constants K (M^{-1}) are also given.

	guest **15**	host **6**	[(*all-S*)-**6•15**]	[(*all-R*)-**6•15**]
D[a]	2.04	0.90	1.73	1.76
x_c	–	–	0.27	0.25
K	–	–	12.7	11.1

[a] $\times 10^{10}$ m^2s^{-1}, 600 MHz, DMSO-d_6, 298 K.

The heteroassociation constants were also determined by employing the non-linear fitting of ^{1}H NMR chemical shifts dilution data (in the 40–0.1 mM range) of equimolar mixtures.[14]

In the fast exchange conditions, the measured chemical shift (δ_{obs}) represents the weighted average of the values corresponding to the uncomplexed (δ_f) and complexed (δ_c) forms (Eq. 4).

$$\delta_{obs} = \delta_f x_f + \delta_c x_c \tag{4}$$

Data were fitted by Eq. 5, obtained as a combination of Eq. 4 with the equation of the association constant for 1:1 complexes.

$$C_0 = \frac{1}{K} \frac{(\delta_{obs} - \delta_f)(\delta_c - \delta_f)}{(\delta_c - \delta_{obs})^2} \tag{5}$$

Experimental data and their fitting curves, based on the chemical shifts of the two typologies of hydroxyl protons available for **15** (i.e., primary, OH-h, and secondary, OH-i), are reported in Figure 4.3 and Figure 4.4 for the two diastereoisomeric [(*all-S*)-**6•15**] and [(*all-R*)-**6•15**] complexes, respectively.

Also in this case, similar and quite low heteroassociation constants were found for the two diastereoisomeric complexes (see Table 4.2), in good agreement with the values obtained from DOSY measurements (*vide supra*), even though in a more complicated way.

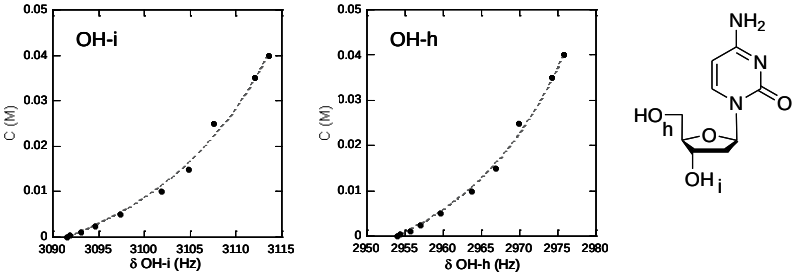

Figure 4.3. Dilution data and fitting curves for the two OH protons of **15** in the presence of an equimolar amount of (*all-S*)-**6**.

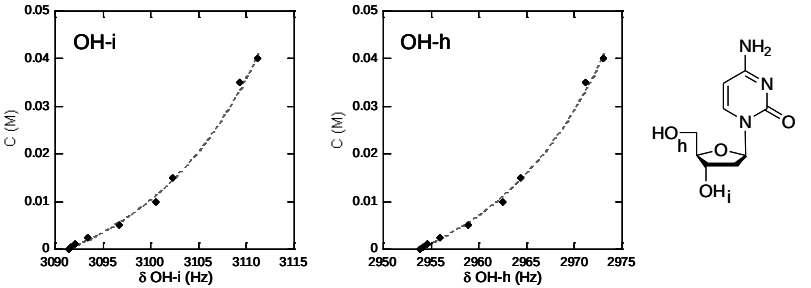

Figure 4.4. Dilution data and fitting curves for the two OH protons of **15** in the presence of an equimolar amount of (*all-R*)-**6**.

Table 4.2. Heteroassociation constants K (M^{-1})[a] obtained by non-linear fitting (see Eq. 5) of ^{1}H NMR chemical shifts of the two OH protons of **15**.

	[(*all-S*)-**6**•**15**]	[(*all-R*)-**6**•**15**]
OH-i	21.1 ± 3.9	20.5 ± 3.2
OH-h	19.9 ± 3.2	19.4 ± 3.0

[a] 600 MHz, DMSO-d_6 (40–0.1 mM), 298 K.

The heteroassociation phenomena were also investigated in pyridine-d_5, where the solubility of both host and guest allowed lower concentrations (up to 5 mM) with respect to DMSO. The heteroassociation constants calculated from diffusion measurements by single point determinations, even in this solvent, were fairly low, but more differentiated than in DMSO (see Table 4.3), the more stable complex being [(*all-S*)-**6•15**]. Also in this case, diffusion coefficient of uncomplexed (*all-S*)-**6** or (*all-R*)-**6** hosts proved to be not influenced by the presence of guest **15**.

Table 4.3. Diffusion coefficients (D)[a] calculated for guest **15** (5 mM), uncomplexed (*all-R*)-**6**/(*all-S*)-**6** hosts (5 mM), and for their equimolar mixtures. Bound molar fractions (x_c) of **15** in the mixtures and heteroassociation constants K (M^{-1}) are also given.

	guest **15**	host **6**	[(*all-S*)-**6•15**]	[(*all-R*)-**6•15**]
D[a]	5.05	2.82	4.82	4.94
x_c	–	–	0.10	0.05
K	–	–	24.7	11.1

[a] $\times 10^{10}$ m^2s^{-1}, 600 MHz, pyridine-d_5, 298 K.

4.2.4 Characterisation of diastereomeric [(*all-S*)-6•15] and [(*all-R*)-6•15] complexes

Since quite similar heteroassociation constants were obtained for the two diastereoisomeric [(*all-S*)-**6•15**] and [(*all-R*)-**6•15**] complexes by non-linear fitting of ^{1}H NMR chemical shifts (see Table 4.2), selective proton relaxation rates (SPRR) measurements[15] were made to significantly distinguish the two complexes. Such a method proved, in fact, a very sensitive probe for the study of complexation

phenomena occurring in solution. Thus, we measured the selective relaxation rates of almost all protons of pure **15** (see Chart 4.2) and in the presence of the two enantiomeric resorc[4]arene hosts.

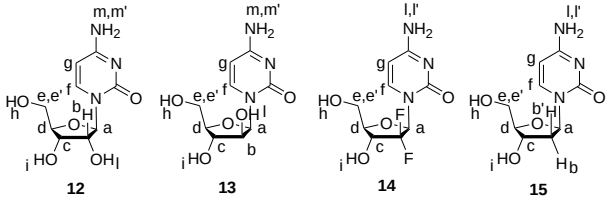

Chart 4.2. Protons labelling in **12**–**15** guests.

Due to the occurrence of complexation phenomena, relaxation rates of **15** increased in the two diastereoisomeric mixtures in comparison to the pure compound, but the increase was slightly higher in the presence of (*all-S*)-**6** host. The complexation induced variations ($\Delta R = R_{mix} - R_{free}$, see Table 4.4) were normalized with respect to the values measured for the pure guest **15** ($\Delta R/ R_{free}$) and, in this way, we could also obtain information about the nature of the interactions capable of stabilising the two complexes. As a matter of fact, greater variations were detected in both mixtures for the two hydroxyl protons (OH-i and OH-h) and for the H-g proton adjacent to the NH_2 group of **15** (see Chart 4.2). Among the protons of **15**, the H-a proton, which is *cisoid* to the OH-i group, underwent the largest variations as well as the H-b proton, *cisoid* to OH-i, was more perturbed with respect to H-b'. The most relevant difference in the two mixtures was found for the H-d proton, whose relaxation rate was nearly unaffected by the presence of (*all-R*)-**6**, whereas

underwent a significant increase in the presence of (*all-S*)-**6**. The behaviour of the H-d proton is in agreement with the trend obtained for the selective relaxation rates of the secondary hydroxyl proton OH-i, which seemed to be more extensively involved in the interaction with (*all-S*)-**6** than with its (*all-R*)-enantiomer.

Table 4.4. Selective relaxation rates (s^{-1}) of protons nuclei of free guest **15** (R_{free}) (40 mM) and in the presence of equimolar amounts of (*all-S*)-**6** or (*all-R*)-**6** hosts (R_{mix})[a]. Complexation induced variations ($\Delta R = R_{mix} - R_{free}$) and normalized complexation variations ($\Delta R/R_{free}$) are also given.

		H-a	H-b	H-b'	H-c	H-d	H-g	H-h	H-i
R_{free}		0.47	1.22	1.42	0.79	0.63	0.47	1.19	1.11
R_{mix}	[(*all-S*)-**6**•**15**]	0.61	1.43	1.55	0.91	0.74	0.69	10.85	9.75
	[(*all-R*)-**6**•**15**]	0.54	1.40	1.53	0.84	0.64	0.61	9.78	6.82
$R_{mix} - R_{free}$	[(*all-S*)-**6**•**15**]	0.14	0.21	0.13	0.12	0.11	0.22	9.66	8.64
	[(*all-R*)-**6**•**15**]	0.07	0.18	0.11	0.05	0.01	0.14	8.59	5.71
$\Delta R/R_{free}$	[(*all-S*)-**6**•**15**]	0.30	0.17	0.09	0.15	0.17	0.47	8.12	7.78
	[(*all-R*)-**6**•**15**]	0.15	0.15	0.08	0.06	0.02	0.30	7.22	5.14

[a] 600 MHz, DMSO-d_6, 298 K

Thus, we can conclude that both hydrogen bond donor groups of **15** are extensively involved in the interaction with (*all-S*)-**6**, whereas the interaction of the secondary hydroxyl group is more hindered in the presence of (*all-R*)-**6**.

Notably, during the SPRR measurements we observed an interesting role played by the small amount of water contained in the deuterated solvent. In other words, water changed its diffusion coefficient D from 8.13×10^{-10} m^2s^{-1} (in pure DMSO-d_6) to 7.76×10^{-10} m^2s^{-1} and 7.08×10^{-10} m^2s^{-1}, in the presence of pure guest **15** and uncomplexed resorc[4]arene **6**, respectively. The value decreased yet again in the presence of the diastereoisomeric [(*all-S*)-**6**•**15**] complex (up to 5.33

$\times 10^{-10}$ m^2s^{-1}), to reach the unexpected value of 2.59×10^{-10} m^2s^{-1} in the presence of the diastereoisomeric [(*all-R*)-**6•15**] complex. This means that water is involved in strongly differentiated exchange processes with the hydrogen bond donor groups of both resorc[4]arene **6** and guest **15** in a cooperative way. In [(*all-R*)-**6•15**] complex, such kind of processes are more effective. Thus, water could represent a very sensitive probe for the interaction of **15** with (*all-R*)-**6** host.

In order to achieve a deeper insight into the stereochemical features of the two diastereoisomeric solvates, we analysed the 1D ROESY spectra of [(*all-S*)-**6•15**] and [(*all-R*)-**6•15**] complexes. In the first case, several protons of **15** gave ROE effects on both aromatic protons of the A/C moieties, whereas only the H26/28 protons of the B/D rings showed proximity constraints with protons of **15** (Figure 4.5).

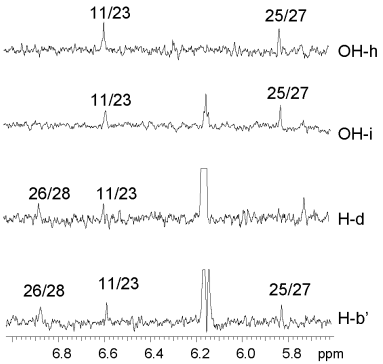

Figure 4.5. 1D ROESY spectra corresponding to the inversion of selected protons of **15** (40 mM) in the presence of one equivalent of (*all-S*)-**6** (600 MHz, DMSO-d_6, 298 K).

No dipolar interaction was detected at the frequency of the H5/17 aromatic protons. On these basis, we can conclude that guest **15** interacts at the larger rim of the *1,3-alternate* structure of (*all-S*)-**6**, as confirmed by molecular mechanics (MM) and quantum mechanics (QM) calculations (*vide infra*).

A completely different pattern of dipolar interactions was detected for the diastereoisomeric [(*all-R*)-**6•15**] complex: only the methoxyl groups of the rings B/D were in proximity of guest **15** protons, together with the ortho protons of the phenyl rings of the diamido bridge (Figure 4.6). Interestingly, the ROE effects at the water traces frequency was observed (Figure 4.6), suggesting that the external pockets of (*all-R*)-**6** between the B/D aromatic rings and the diamido bridges are involved in the interaction with **15**, which are also the interaction sites for residual water. In this way, the above mentioned remarkable lowering of the diffusion coefficient of water observed during its interaction with **15** can be justified.

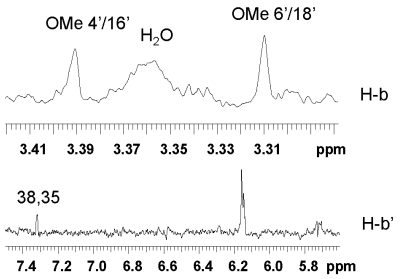

Figure 4.6. 1D ROESY spectra corresponding to the inversion of proton H-b (top) and H-b' (bottom) of **15** (40 mM) in the presence of one equivalent of (*all-R*)-**6** (600 MHz, DMSO-d_6, 298 K).

4.2.5 Characterisation of diastereomeric [(*all-S*)-6•12–14] and [(*all-R*)-6•12–14] complexes

We performed an analogous investigation in the presence of cytidine (**12**), cytarabine or cytosine-β-D-arabinofuranoside (**13**), and gemcitabine (**14**) (Chart 3.1). Cytarabine is an epimer of cytidine, while gemcitabine is the *gem*-difluoro derivative of 2'-deoxycytidine. Among these guests, only **12** proved able to interact to some detectable extent with the two resorcarene stereoisomers. As a matter of fact, relaxation rates of all hydroxyl protons were significantly perturbed in both [(*all-S*)-**6•12**] and [(*all-R*)-**6•12**] mixtures with a larger effect on the two secondary hydroxyl groups with respect to the primary ones (Table 4.5). Notably, in the case of guest **15**, the primary hydroxyl group was more significantly perturbed with respect to the secondary one, especially in the [(*all-R*)-**6•15**] mixture (see Table 4.4).

Table 4.5. Selective relaxation rates (s^{-1}) of protons nuclei of free guest **12** (R_{free}) (40 mM)[a]. Normalized complexation induced variations ($\Delta R/R_{free}$, with $\Delta R = R_{mix} - R_{free}$) are calculated in the presence of equimolar amounts of (*all-S*)-**6** or (*all-R*)-**6** hosts.

		H-a	H-e	H-e'	H-f	H-g	H-h	H-i	H-l
R_{free}		0.40	1.66	1.60	0.73	0.55	0.80	0.81	0.84
$\Delta R/R_{free}$	[(*all-S*)-**6•12**]	0.19	~ 0	0.02	0.08	0.13	2.82	3.90	3.94
	[(*all-R*)-**6•12**]	0.25	0.01	0.01	0.18	0.20	3.26	4.02	4.65

[a] 600 MHz, DMSO-d_6, 298 K.

Probably, in the case of guest **12**, the presence of two secondary hydroxyl functions located on the same side of the furanose ring

favours their interaction with the resorcarene at the expense of the primary group. Furthermore, any significant effect on the diffusion coefficients of the residual water located on the diamido bridges at the external of the resorcarene structure was not detected in the two [(*all-S*)-**6•12**] and [(*all-R*)-**6•12**] mixtures. Thus, it can be supposed that guest **12** interacts with both resorcarene enantiomers at their larger cavity, which is farther from the stereogenic centres of the cyclic host, and hence a minor discrimination of the two diastereoisomers is detected with respect to guest **15**. Accordingly, the association constants, as calculated by single point determinations from the diffusion data, were not only scarcely differentiated, but also very low ($K < 3\ M^{-1}$, see Table 4.6).

Table 4.6. Diffusion coefficients $(D)^{[a]}$ calculated for guest **12** (40 mM), uncomplexed (*all-R*)-**6**/(*all-S*)-**6** hosts (40 mM), and for their equimolar mixtures. Bound molar fractions (x_c) of **12** in the mixtures and heteroassociation constants K (M^{-1}) are also given.

	guest **12**	host **6**	[(*all-S*)-**6•12**]	[(*all-R*)-**6•12**]
$D^{[a]}$	1.95	0.90	1.92	1.86
x_c	–	–	0.03	0.09
K	–	–	0.8	2.7

[a] $\times 10^{10}\ m^2s^{-1}$, 600 MHz, DMSO-$d_6$, 298 K.

Even weaker intermolecular interactions were detected by proton relaxation rates measurements in the presence of both **13** and **14** guests (see Tables 4.7 and 4.8, respectively), and again the residual water did not reveal any perturbation due to the presence of the substrates.

Table 4.7. Selective relaxation rates (s^{-1}) of protons nuclei of free guest **13** (R_{free}) (40 mM)[a]. Normalized complexation induced variations ($\Delta R/R_{free}$, with $\Delta R = R_{mix} - R_{free}$) are calculated in the presence of equimolar amounts of (*all-S*)-**6** or (*all-R*)-**6** hosts.

		H-a	H-b	H-c	H-d	H-f	H-g	H-h
R_{free}		0.50	0.87	0.81	0.64	0.56	0.54	3.24
$\Delta R/R_{free}$	[(*all-S*)-**6**•**13**]	0.11	0.10	0.05	0.08	0.05	0.12	0.46
	[(*all-R*)-**6**•**13**]	0.14	0.09	0.09	0.07	0.07	0.12	0.29

[a] 600 MHz, DMSO-d_6, 298 K.

Table 4.7. Selective relaxation rates (s^{-1}) of protons nuclei of free guest **14** (R_{free}) (40 mM)[a]. Normalized complexation induced variations ($\Delta R/R_{free}$, with $\Delta R = R_{mix} - R_{free}$) are calculated in the presence of equimolar amounts of (*all-S*)-**6** or (*all-R*)-**6** hosts.

		H-a	H-b	H-c	H-d	H-f	H-g	H-h
R_{free}		0.60	0.57	0.88	0.71	1.68	6.08	5.31
$\Delta R/R_{free}$	[(*all-S*)-**6**•**14**]	0.15	0.17	0.04	0.15	0.05	~ 0	0.05
	[(*all-R*)-**6**•**14**]	0.10	0.14	0.02	0.13	0.04	0.03	0.07

[a] 600 MHz, DMSO-d_6, 298 K.

In the case of guest **15**, a good balance between hydrophobic and hydrophilic interactions is probably obtained within the external pocket for the (*all-R*)-**6** resorcarene, where water molecules mediate the hydrophilic interactions (*vide infra*). A similar balance is obtained in the presence of (*all-S*)-**6** resorcarene within the larger cavity. The presence of additional hydrogen bond donor or acceptor groups as in guests **12**–**14** probably drives the interaction towards the larger rim of the resorcarene, where the substrate is farther from the stereogenic centres of the resorcarene, thus causing a lower degree of diastereoisomeric discrimination.

4.2.6 Conformation of the resorc[4]arenes 6 hosts by MM and QM studies

A preliminary MM global conformational search was performed on (*all-S*)-**6** host after having imposed the whole set of NMR torsional constraints on the two diamido wings and chosen a 100 kJ/mol energy window over the global minimum for saving generated output structures. Such a search was primarily expected to assess all the relative orientations in 3D space of the four aromatic rings of the resorcarene rim, geometrically consistent with the NMR, without paying special attention to the corresponding relative steric energy. Four conformations of the rim were obtained: the *flattened cone* (FC), the *1,3-alternate*, and two already described types of *flattened partial cone* (namely, type 1 and type 2).[16] All the structures showed a similar orientation of the diamido wings. Considering that, in apparent disagreement with the NMR results, the MM steric energy values suggested only the *flattened cone* conformation to be populated at room temperature ($E_X - E_{FC} \geq 30$ kJ/mol, $X \neq FC$); the output structures *flattened cone*, *1,3-alternate* conformation and *flattened partial cone 1* were all optimized by *ab initio* Hartree-Fock (HF) calculations performed in vacuum. This step was chosen to ascertain both gas phase energy and degree of accuracy of each MM calculated geometry (*vide supra*). Owing to the large number of atoms of (*all-S*)-**6** host, the 6-31G*++ basis set was used (1888 basis functions). Unexpectedly, the HF optimization of all three structures outputted the *flattened cone* structure. This result confirmed that the

diamido wings could effectively perturbate the potential energy surface of the host, so that only a *flattened cone* conformation was a real minimum energy geometry of the resorcarene rim. Force field based molecular dynamics simulations confirmed the conformational collapse towards FC (data not shown).

The global minimum of (*all-S*)-**6**, picked out by the MM conformational search and consistent with the NMR constraints (alternatively: "the MM global minimum" or MM-FC), was superimposed to its HF optimized counterpart (HF-FC), in order to evaluate the similarity between the two modeled structures. A R.M.S.D. of 0.27 Å was calculated without considering non polar hydrogen atoms, therefore ascertaining the interchangeability of the two structures for docking calculations of **15**. MM-FC is shown in Figure 4.7.

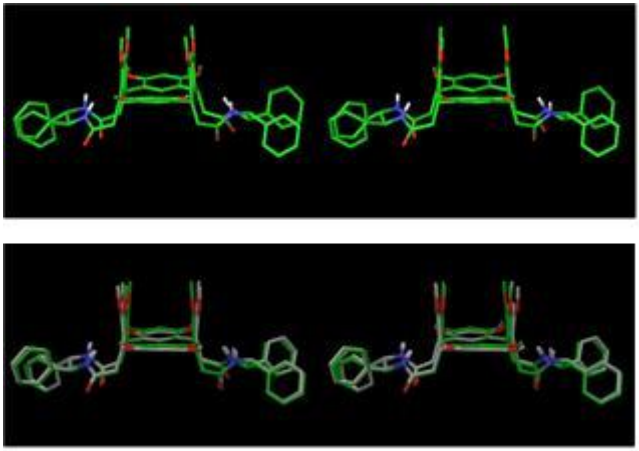

Figure 4.7. Crossed stereoview of MM-FC (top) and of MM-FC (bottom, green carbons) superimposed to HF-FC (grey carbons) for (*all-S*)-**6** host.

On the other hand, the frames collected during HF minimization of the *1,3-alternate* conformation (*vide supra*) allowed to evaluate which geometry of the upper rim would have been consistent, ignoring thermal motion, with the NMR measurements. The ratio between the following distances: (*i*) from methine protons H-2/14 to aromatic protons H-28/26 (named D1), and (*ii*) from methine protons H-2/14 to aromatic protons H-25/27 (named D2) was measured to this purpose. This value had been estimated to be roughly 1.1–1.2 from the intensities of the corresponding ROE effects (*vide supra*). The changing values of D1, D2, of the dihedral angle between the plane of aromatic ring B and the plane defined by C-28, C-8 and H-8 (named DH1) and of the distance between carbon atoms C-32 (C-31) and C-6 (C-4) (named D3) were calculated (data not shown). All these structural details are displayed as functions of the angle (named A^C) formed by each plane of opposite aromatic rings A and C with the plane defined by carbons C-2, C-8, C-14 and C-20, that is with the "horizontal orientation" roughly adopted by HF-FC. What emergs from these pictures is that the NMR measured distance ratio roughly corresponds to an A^C value of about 140 degrees. Notably, DH1 value increases towards 180 degrees when A and C rings move down and this effect might increase the intensity of the ROE peak 25/27 with respect to peak 26/28 (see Figure 4.1e) at values of A^C larger than 140 degrees. Accordingly to all these structural details, the structure proposed by NMR studies (*vide supra*) represents an

average of several geometries associated to some flexibility of the *flattened cone* resorcarene rim, and due to an up and down motion of A and C rings, with a small prevalence of the down extension towards a proper *1,3-alternate* conformation or a type 1 *flattened partial cone.*

Notably, distance D3, measuring the roominess of the external pocket of (*all-S*)-**6**, was dependent on angle A^C, where such structural descriptor revealed a sort of "flight" motion of the two amido wings, related to the up and down libration of aromatic A and C rings. Accordingly, the two side chains closed towards aromatic B and D rings when A and C moved down to a proper *1,3-alternate* conformation, and widened out when A and C took the shape of *flattened cone*. As a consequence of this motion, the space available for external binding of a guest compound become available or unavailable (Figure 4.8). This finding was in agreement with the above mentioned structural collapse of (*all-S*)-**6** towards FC conformation.

With the aim to quantify the flexibility of the resorcarene ring, constrained HF minimizations in the gas phase were performed, on frames extracted from the *ab initio* minimizations of both *1,3-alternate* and *flattened cone* geometry, by freezing both opposite A^C angles at chosen values, simulating in such a way a symmetric libration motion.

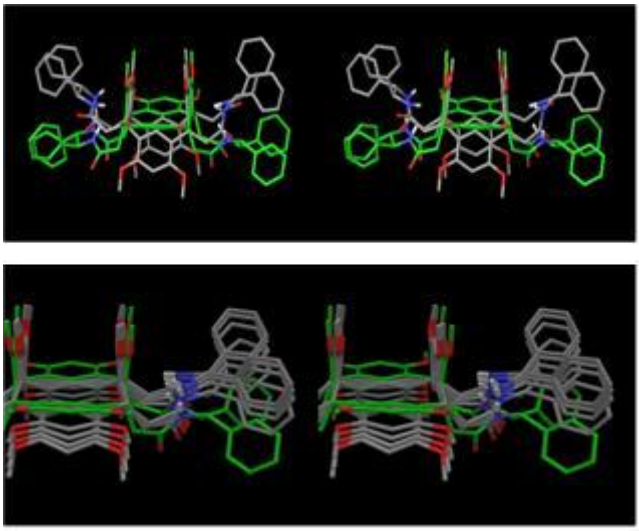

Figure 4.8. Superimposition (crossed stereoview) of HF-FC (green carbons) and *1,3-alternate* conformation of (*all-S*)-**6** (grey carbons, top); structural details of frames extracted from the minimization of a *1,3-alternate* conformation of (*all-S*)-**6** (grey carbons) and HF-FC (green carbons, bottom).

It came out from this calculation that the energy difference between HF-FC and such constrained geometries was less than 20 kcal/mol at least up to angle values of about 35–40 degrees below the horizontal orientation, confirming some flexibility of the host. Notably frames extracted from the minimization of the type 1 *flattened partial cone* conformation (this conformation symbolized a totally asymmetric libration motion) showed smaller ΔE values at A^C angles of, respectively 120° (-60°) and 140 (-40°). This difference is consistent with the assumed flexibility of the resorcarene rim, which can librate towards either a *1,3-alternate* or a type 1 *flattened partial cone* conformation.

A further calculation was carried out to verify the orientation of the two amido groups comprising, respectively, NH-30 and NH-42. The measured $^{3}J_{NH30H31}$ coupling constant value (*vide supra*), in fact, was consistent with two possible orientations of these groups: the up orientation (139°), inferable by the NMR data, and a down orientation (29°), previously predicted by MM based molecular modelling in the gas phase,[9] and yielding an intramolecular hydrogen bond between NH-30 and CO-34. An input structure with the down orientation was obtained by constrained minimization of MM-FC and the two geometries were subjected to HF optimization, both in the gas phase and in solvent models simulating either DMSO or water. Such optimizations (collected in Table 4.9) suggest that the solvation energy is a factor favouring the amide's up orientation.

Table 4.9. Calculated energy values ΔE (kcal/mol) of HF-FC and of a second FC geometry (namely, FC down) with down orientation of the two amido groups comprising, respectively, NH-30 and NH-42.[a]

Conformation	Gas phase	DMSO	Water
HF-FC	0.0	-44.3	-28.4
FC down	-9.6	-46.6 (-37.0)	-26.0 (-16.4)

[a] Obtained by *ab initio* calculation in the gas phase, DMSO, and water. The solvation energy contribution to the down conformation is given in parenthesis.

4.2.7 Docking simulations of diastereomeric [(*all-S*)-6•15] and [(*all-R*)-6•15] complexes

Docking simulations aimed at modelling the recognition of guest **15** by the bis(diamido)-bridged basket resorc[4]arene **6** host were

carried out choosing the MM-FC described by theoretical studies (*vide supra*) as the input structure. Both the two enantiomers of the host, namely (*all-S*)-**6** and (*all-R*)-**6**, were considered in turn as the host compounds. The MM global minimum of (*all-S*)-**6** was used to directly obtain its mirror image (i.e., the (*all-R*)-**6**) by application to the whole structure of the "Invert Chirality" command within Maestro 9.0 (see Experimental Section).

The complexation of guest **15** by (*all-R*)-**6** was simulated first. Characterisation of the diastereoisomeric [(*all-R*)-**6•15**] complex performed by NMR spectroscopy (*vide supra*) showed that **15** was preferably accommodated by this host not at the larger lower rim, but rather in the external pocket delimited by B/D rings and by the diamido arms (the wings). To shed some light on such a stereochemical preference, a first docking approach was chosen, which took into account the molecular flexibility of both partners (namely, flexible docking). A previously described MCMM/MOLS protocol was applied to this purpose.[17] Since MacroModel did not allow to simulate the solvation effects of DMSO, a couple of simulations, namely in the gas phase and in GB/SA water, was performed in parallel. None of the two flexible docking simulations, however, was successful either in reproducing the already characterised 3D structure of the host, or in predicting the recognition of **15** by (*all-R*)-**6**, as outlined by the NMR studies. The latter result, actually, was to be expected due to the coarseness of the

computational approach with respect to the small free energy differences (few kJ/mols) coming into play in chiral recognition processes like the one simulated here. Approximations of the method, among which the non accurate force field parameterization of some torsion parameters and of the atomic partial charges, coupled with exclusion of the solvent effect, caused a tangled picture of the host-guest interactions to be generated. Unsatisfactory results were obtained as well when the recognition of **15** by (*all-S*)-**6** was tackled.

Therefore, semirigid docking experiments were carried out in the gas phase, where the host geometry was maintained rigid in 3D space, while coupled rototranslations and conformational search of guest **15** were executed, according to the MCMM/MOLS protocol.[17] A couple of global searches was carried out at first, in which the 1D ROESY constraints (*vide supra*) were not used and the output geometries of both diastereomeric complexes were collected in order of increasing steric energy. Then, a second constrained docking (local search) was selectively carried out on the [(*all-R*)-**6•15**] complex; to collect geometries in which guest **15** was confined within the external pocket, cutoff distances were imposed between hydrogen atoms H-b/H-b' and both the methoxyl groups on B ring and hydrogens H35/38. In this case, while performing the conformational analysis of the five-membered sugar ring, the software was free to collect output geometries of **15** in which either

H-b or H-b' could be placed in front of aromatic ring B. For comparison purposes, such local search was performed also on the ([(*all-S*)-**6•15**] complex.

Unconstrained docking afforded a global minimum in which the guest was accommodated at the host lower rim: the sugar moiety was placed among A, B, C, and D aromatic rings, while the cytosine ring gave stacking interactions with carbonyl oxygen atoms of one wing. The steric energy difference between the two global minima was about 1.5 kcal/mol in favor of the [(*all-R*)-**6•15**] complex while, in general, no low energy complexes at the lower rim were detected, in which more than one intermolecular hydrogen bond involving the OH groups of **15** was formed. In the case of (*all-R*)-**6** host depicted in Figure 4.9, for instance, the global minimum displayed only one hydrogen bond between the secondary OH and one amidocarbonyl of the host.

The lowest energy output geometry obtained by the unconstrained docking, in which guest **15** was accommodated in the external pocket formed by each diamide arm of (*all-R*)-**6** host, was found at an energy value of about 1.5 kcal/mol over the global minimum. Accordingly, the steric energy values of this minimum and that of the global minimum of the [(*all-S*)-**6•15**] complex came out to be close each other, while all the calculated "external minima" of the complex between **15** and (*all-S*)-**6** possessed a further steric energy surplus of at least 2.5 kcal/mol.

The lowest energy external minima, however, did not show the set of host-guest distances expected from the NMR measurements of the [(*all-R*)-**6•15**] complex and concerning H-b and H-b' protons of **15**. The reason of such discrepancy may be ascribed to solvation, which is neglected by docking calculations.

Constrained dockings proved to be decisive: in the case of the [(*all-S*)-**6•15**] complex, the short host-guest distances detected by NMR for the [(*all-R*)-**6•15**] complex (i.e., between: (*i*) H-b and the methoxyl groups on aromatic B/D rings and (*ii*) H-b' and hydrogens H35/38, see Figure 4.6) were not found, whereas in the case of the [(*all-R*)-**6•15**] complex, several geometries consistent with NMR data were collected, within a sliding 15 kcal/mol energy window. The structure of the calculated "external" complex of guest **15** with (*all-R*)-**6** host is depicted in Figure 4.10. Its energy, in the gas phase, is about 7 kcal/mol higher than the global minimum at the lower rim, and solvation by DMSO might easily compensate such a ΔE. Notably, MacroModel estimated in about 43 kcal/mol the solvation energy of the whole complex in GB/SA chloroform and 23 kcal/mol in GB/SA water; moreover, in GB/SA chloroform (that is in the presence of the highest predicted solvation energy), the external complex was calculated to possess lower steric energy than the global minimum.

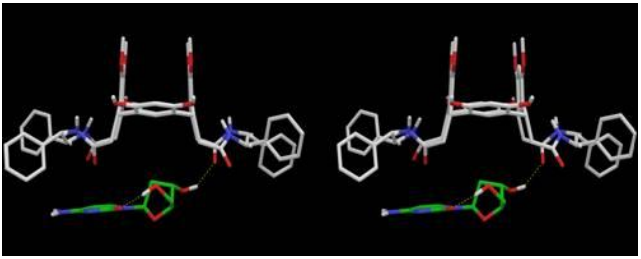

Figure 4.9. Crossed stereoview of guest **15** docked at the lower rim of (*all-R*)-**6** host. Non polar hydrogen atoms are not shown.

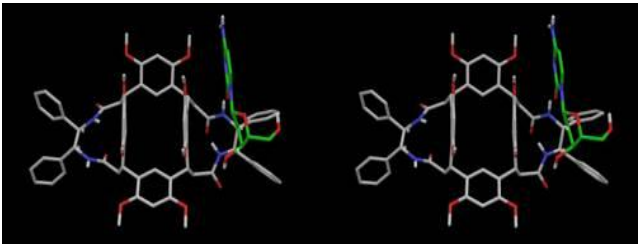

Figure 4.10. Crossed stereoview of the "external" complex between guest **15** and (*all-R*)-**6** host. Non polar hydrogen atoms are not shown. One hydrogen bond exists between the C=O group of cytosine and NH-30.

In conclusion, according to our simulations, guest **15** is profitably hosted externally only by (*all-R*)-**6** host (see Figure 4.10), since the two partners show reciprocal shape complementarity and can form an hydrogen bonding interaction between the cytosine carbonyl group and one amide NH, while the cytosine ring gives a stacking interaction with aromatic B/D rings; moreover, the secondary OH of the sugar is located among B/D rings, C/A rings and one of the phenyl rings of the wings and the primary OH is accommodated on top of the two facing phenyl rings. Due to the asymmetric shape of the hosting cavity, its mirror image (possessed by (*all-S*)-**6** host) is

not as much appropriate to host **15** (see Figure 4.11). The main reason of such an enantiodiscrimination is that, in an hypothetical external complex involving (*all-S*)-**6**, the hosting place of the two OH groups should be exchanged with respect to the diastereomeric complex so to direct the bulkier primary OH towards the resorcarene rim. As a consequence, the guest compound is better accommodated at the lower rim.

A semirigid docking of one water molecule was finally performed to calculate the most favorable spots available to this molecule, when interacting with the (*all-R*)-**6** host. These positions were estimated by MacroModel to be: (*i*) in front of the two facing CO at the lower rim so to give a couple of hydrogen bonds, (*ii*) in front of the NH-30/42 where the cytosine CO is accommodated, and (*iii*) in the region where the secondary OH of the furanose is hosted. Notably, the first and the third positions were compatible with the concurrent hosting of guest **15**. Moreover, when a water molecule was located in the third spot and minimized together with **15** in a ternary complex (see Figure 4.12), it formed an hydrogen bonding bridge between the secondary OH of **15** and one host CO (the one already described in the case of (*all-S*)-**6** host as pointing to H-29). The peculiar orientation of this carbonyl group was stabilised still further by such intermolecular interaction. These final returns are in agreement with the NMR experiments describing water diffusion.

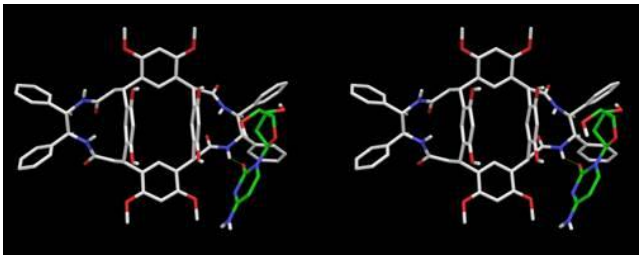

Figure 4.11. Crossed stereoview of an hypothetical "external" complex between guest **15** and (*all-S*)-**6** host. Non polar hydrogen atoms are not shown.

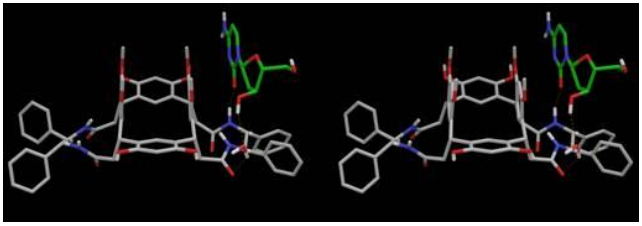

Figure 4.12. Crossed stereoview of a ternary complex formed by guest **15**, (*all-R*)-**6** host and one water molecule. A network of hydrogen bonds involving also the water molecule (bridge between the secondary OH of **15** and the CO group bound to NH-33) binds host and guest. Non polar hydrogen atoms are not shown.

4.3 Conclusions

We showed that bis(diamido)-bridged basket resorc[4]arene **6** behaves as an highly preorganized receptor for pyrimidine nucleosides by yielding several hydrogen bond and hydrophobic interactions. The combination protocol of NMR spectroscopic and molecular modelling methods that we successfully applied to detect such interactions can be easily extended to monitor the binding of

other small molecules to a macrocyclic receptor, besides pyrimidine nucleoside analogues. In such a way, NMR spectroscopy was confirmed to be a screening tool for the binding of potential antimetabolites to new drug carriers. In particular, we found that 2'-deoxycytidine **15** is hosted within two different interaction sites by chiral bis(diamido)-bridged basket resorc[4]arene **6**, depending on host configuration: (*all-R*)-**6** profitably hosts the nucleoside within an external pocket delimitated by one 3,5-dimethoxyphenyl group and its diamido arm (the wing); the two partners, in fact, show reciprocal shape complementarity and can form an hydrogen bond between the cytosine carbonyl group and one amide NH, whereas the cytosine ring gives a stacking interaction with B/D aromatic rings; moreover, the secondary OH of the five-membered sugar is located among B/D rings, C/A rings and one of the phenyl rings of the wings, while the primary OH is accommodated on top of the two facing phenyl rings. On the contrary, when the host has the *all-S* configuration (i.e., in the case of (*all-S*)-**6**), 2'-deoxycytidine is better accommodated at the larger lower cavity delimitated by two *syn* 3,5-dimethoxyphenyl moieties, as judged by ROE effects observed for both aromatic protons of the A/C moieties, whereas only the H26/28 protons of the B/D rings showed proximity constraints with the protons of **15**. Moreover, NMR data suggested that, whilst both hydrogen bond donor groups of **15** are extensively involved in the interaction with

(*all-S*)-**1**, the interaction of the secondary hydroxyl group is more hindered in the presence of (*all-R*)-**6** host.

Thus, although quite similar heteroassociation constants were obtained for the two diastereoisomeric [(*all-S*)-**6•15**] and [(*all-R*)-**6•15**] complexes, we were able to significantly distinguish them according to the stereochemical preference of guest **15**.

Notably, we observed an interesting role played by the small amount of water contained in deuterated DMSO: it is involved in strongly differentiated exchange processes with the hydrogen bond donor groups of both resorc[4]arene **6** and guest **15** in a cooperative way. In [(*all-R*)-**6•15**] complex, such kind of processes are more effective, since the external pockets are also the interaction sites for residual water. Thus, water could represent as well a sensitive probe for the discrimination of the above mentioned diastereomeric complexes.

The results presented in this chapter have been submitted for publication:

I. D'Acquarica, A. Calcaterra, F. Sacco, F. Balzano, F. Aiello, A. Tafi, N. Pesci, G. Uccello-Barretta, B. Botta, submitted to *Chemistry-A European Journal*.

4.4 Experimental Section

4.4.1 NMR experiments

NMR measurements were performed on a spectrometer operating at 600 MHz for ^{1}H nuclei. The temperature was controlled to ±0.1 °C. All ^{1}H NMR chemical shifts are referenced to TMS as internal standard. The 2D NMR spectra were obtained by using standard sequences with the minimum spectral width required. Proton 2D gCOSY (gradient COrrelated SpectroscopY) spectra were recorded with 128 increments of 2 scans and 2K data points. The relaxation delay was 3 s. 2D TOCSY (TOtal Correlation SpectroscopY) spectra were recorded by employing a mixing time of 80 ms. The pulse delay was maintained at 3 s; 256 increments of 4 scans and 2K data points each were collected. The 2D ROESY (Rotating-frame Overhauser Enhancement SpectroscopY) experiments were performed by employing a mixing time of 0.3 s or 0.6 s. The pulse delay was maintained at 5 s; 256 increments of 6 scans and 2K data points each were collected. Proton 1D ROESY spectra were recorded using selective pulses generated by means of the Varian Pandora Software. The selective 1D ROESY spectra were acquired with 1024 or 512 scans in 32K data points with a 5 s relaxation delay and a mixing time of 0.3 s or 0.6 s. DOSY (Diffusion Ordered SpectroscopY) experiments were carried out by using a stimulated echo sequence with self-compensating gradient schemes, a spectral

width of 6000 Hz and 64K data points. Typically, a value ranging from 100 to 400 ms was used for Δ, 1.5 ms for δ, and g was varied in 30 steps (2 transients each) to obtain an approximately 90–95% decrease in the resonance intensity at the largest gradient amplitude. The baselines of all arrayed spectra were corrected prior to processing the data. After data acquisition, each FID was apodized with 1.0 Hz line broadening and Fourier transformed. The data were processed with the DOSY macro (involving the determination of the resonance heights of all the signals above a pre-established threshold and the fitting of the decay curve for each resonance to a Gaussian function) to obtain pseudo two- dimensional spectra with NMR chemical shifts along one axis and calculated diffusion coefficients along the other. Heteroassociation constants for the two diastereoisomeric [(*all-R*)-**6•15**] and [(*all-S*)-**6•15**] complexes were determined using the dilution method. Non-linear fitting of the experimental data, obtained from the analysis of ^{1}H NMR chemical shifts of selected protons nuclei in a set of progressively diluted DMSO equimolar mixtures (ranging from 40 mM to 0.1 mM), was performed employing Kaleidagraph 4.0 program.

^{1}H-NMR signals of (*all-S*)-6

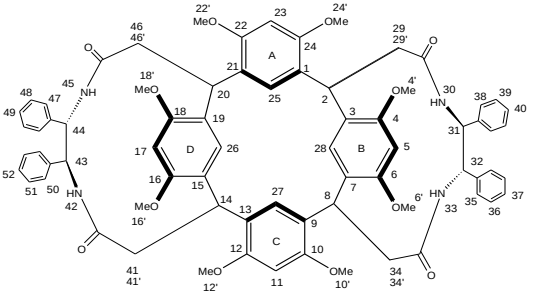

^{1}H NMR (600 MHz, 40 mM, DMSO, 298 K) δ (ppm): 8.01 (2H, H_{30}/H_{42}, d, $J_{30\text{-}31}$ = 6.6 Hz); 7.77 (2H, H_{33}/H_{45}, d, $J_{33\text{-}32}$ = 7.5 Hz); 7.32 (8H, H_{35}/H_{47} and H_{38}/H_{50}, d, J = 7.2 Hz); 7.01 – 7.10 (12H, H_{36}/H_{48}, H_{37}/H_{49}, H_{39}/H_{51} and H_{40}/H_{52}, m); 6.86 (2H, H_{26}/H_{28}, s); 6.58 (2H, H_{11}/H_{23}, s); 6.28 (2H, H_5/H_{17}, s); 5.82 (2H, H_{25}/H_{27}, s); 5.44 (2H, H_{31}/H_{43}, dd, $J_{31\text{-}32}$ = 11.6 Hz, $J_{31\text{-}30}$ = 6.6 Hz); 4.77 (2H, H_2/H_{14}, dd, $J_{2\text{-}29'}$ = 12.6 Hz, $J_{2\text{-}29}$ = 4.4 Hz), 4.72 (2H, H_8/H_{20}, t, $J_{8\text{-}34}$ = $J_{8\text{-}34'}$ = 8.2 Hz); 4.36 (2H, H_{32}/H_{44}, dd, $J_{32\text{-}31}$ = 11.6 Hz, $J_{32\text{-}33}$ = 7.5 Hz); 3.81 (6H, $MeO_{10'}/MeO_{22'}$, s); 3.80 (6H, $MeO_{12'}/MeO_{24'}$, s); 3.39 (6H, $MeO_{4'}/MeO_{16'}$, s); 3.31 (6H, $MeO_{6'}/MeO_{18'}$, s); 2.63 (2H, H_{29}/H_{41}, m); 2.59 (4H, H_{34}/H_{46} and $H_{34'}/H_{46'}$, m); 2.51 (2H, $H_{29'}/H_{41'}$, m).

^{1}H-NMR signals of 2'-deoxycytidine (15)

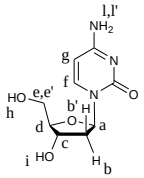

^{1}H NMR (600 MHz, 40 mM, DMSO, 298 K) δ (ppm): 7.76 (1H, H_f, d, $J_{f\text{-}g}$ = 7.4 Hz); 7.12 (1H, H_l, br s); 7.04 (1H, $H_{l'}$, br s); 6.13 (1H, H_a, dd, $J_{a\text{-}b'}$ = 7.3 Hz, $J_{a\text{-}b}$ = 6.0 Hz); 5.69 (1H, H_g, d, $J_{g\text{-}f}$ = 7.4 Hz); 5.16 (1H, H_i, d, $J_{i\text{-}c}$ = 4.3 Hz); 4.93 (1H, H_h, t, $J_{h\text{-}e}$ = $J_{h\text{-}e'}$ = 5.1 Hz); 4.17 (1H, H_c, m); 3.74 (1H, H_d, m); 3.54 (1H, H_e, ddd, $J_{e\text{-}e'}$ = 11.8 Hz, $J_{e\text{-}h}$ = 5.1 Hz, $J_{e\text{-}d}$ = 4.1 Hz); 3.50 (1H, $H_{e'}$, ddd, $J_{e'\text{-}e}$ = 11.8 Hz, $J_{e'\text{-}h}$ = 5.1 Hz, $J_{e'\text{-}d}$ = 4.0 Hz); 2.08 (1H, H_b, ddd, $J_{b\text{-}b'}$ = 13.1 Hz, $J_{b\text{-}a}$ = 6.0 Hz, $J_{b\text{-}c}$ = 3.2 Hz); 1.90 (1H, $H_{b'}$, ddd, $J_{b'\text{-}b}$ = 13.1 Hz, $J_{b'\text{-}a}$ = 7.3 Hz, $J_{b'\text{-}c}$ = 6.1 Hz).

^{1}H-NMR signals of cytidine (12)

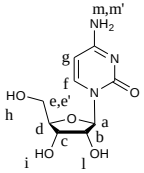

^{1}H NMR (600 MHz, 40 mM, DMSO, 298 K) δ (ppm): 7.81 (1H, H_f, d, $J_{f\text{-}g}$ = 7.5 Hz); 7.13 (1H, H_m, br s); 7.07 (1H, Hm', br s); 5.74 (1H, H_a, d, $J_{a\text{-}b}$ = 3.8 Hz); 5.68 (1H, Hg, d, $J_{g\text{-}f}$ = 7.5 Hz); 5.24 (1H, H_l, d, $J_{l\text{-}b}$ = 5.1 Hz); 5.00 (1H, H_h, t, $J_{h\text{-}e}$ = $J_{h\text{-}e'}$ = 5.2 Hz); 4.94 (1H, H_i, d, $J_{i\text{-}c}$

= 5.1 Hz); 3.91 (2H, H_c/H_b, m); 3.79 (1H, H_d, m); 3.63 (1H, H_e, ddd, $J_{e-e'}$ = 12.1 Hz, J_{e-h} = 5.2 Hz, J_{e-d} = 3.1 Hz); 3.52 (1H, $H_{e'}$, ddd, $J_{e'-e}$ = 12.1 Hz, $J_{e'-h}$ = 5.2 Hz, $J_{e'-d}$ = 3.6 Hz).

^{1}H-NMR signals of cytarabine (13)

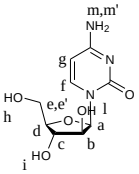

^{1}H NMR (600 MHz, 40 mM, DMSO, 298 K) δ (ppm): 7.55 (1H, H_f, d, J_{f-g} = 7.4 Hz); 7.04 (1H, H_m, br s); 6.96 (1H, $H_{m'}$, br s); 6.01 (1H, H_a, d, J_{a-b} = 4.2 Hz); 5.63 (1H, H_g, d, J_{g-f} = 7.4 Hz); 5.36 (1H, H_i, d, J_{i-c} = 4.2 Hz); 5.35 (1H, H_l, d, J_{l-b} = 5.0 Hz); 4.96 (1H, H_h, t, J_{h-e} = $J_{h-e'}$ = 4.9 Hz); 3.92 (1H, H_b, m); 3.86 (1H, H_c, m); 3.71 (1H, H_d, m); 3.57 (1H, H_e, m); 3.55 (1H, $H_{e'}$, m).

^{1}H-NMR signals of gemcitabine (14)

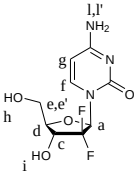

^{1}H NMR (600 MHz, 40 mM, DMSO, 298 K) δ (ppm): 9.89 (1H, $H_{l'}$, s); 8.79 (1H, H_l, s); 8.12 (1H, H_f, d, J_{fg} = 7.9 Hz); 6.21 (1H, H_g, d, J_{gf}

= 7.9 Hz); 6.08 (1H, H_a, m); 4.17 (1H, H_c, td, J_{cf} = 12.5 Hz, J_{cd} = 8.9 Hz); 3.89 (1H, H_d, ddd, J_{dc} = 8.9 Hz, J_{de} = 3.1 Hz, $J_{de'}$ = 2.3 Hz); 3.77 (1H, $H_{e'}$, dd, $J_{e'e}$ = 12.7 Hz, $J_{e'd}$ = 2.3 Hz); 3.62 (1H, H_e, dd, $J_{ee'}$ = 12.7 Hz, J_{ed} = 3.1 Hz).

4.4.2 Molecular modelling

Three-dimensional structure building and all molecular mechanics (MM) calculations including conformational analyses and docking simulations were carried out on an IBM workstation with Linux operating system running Maestro 9.0 and Macromodel 9.7 programs (Schrödinger, LLC, New York). Conformers were generated in MacroModel using the implemented MM2* force field with selection of the constant dielectric treatment (ε = 1.0), in the gas phase, GB/SA water or GB/SA chloroform, depending on the calculation. No cutoff was used for nonbonded interactions and the force field partial atomic charges were chosen. Molecular energy minimizations were performed using the PRCG method with 5000 maximum iterations and 0.0001 gradient convergence treshold. The conformational searches were carried out by application of the Monte Carlo Multiple Minimum (MCMM) torsional sampling method. The preliminary MCMM search was performed on the eight rotatable bonds of the resorcarene rim (according to the default setup options) after having imposed the following torsional constraints on

the two diamide arms (the values listed hereafter refer to the wing on the right side of Figure 4.1, the left wing has been constrained as well according to the C_{2v} symmetry of the resorcarene host): H2-C2-C29-H29 180° (target value 180°, force constant 100.0 kJ/mol); H2-C2-C29-H29' (target value -60°, force constant 100.0 kJ/mol); H29'-C29-C30=O30 (target value 0°, force constant 100.0 kJ/mol); H30-N30-C31-C32 (target value 140°, force constant 100.0 kJ/mol); H31-C31-C32-H32 (target value 180°, force constant 100.0 kJ/mol) set to 0°; H32-C32-N33-H33 (target value -22°±10°, force constant 100.0 kJ/mol); improper dihedral H33-N33-C8-H8 (target value 0°±15°, force constant 100.0 kJ/mol). All unique geometries within a 100 kJ/mol energy window over the global minimum were collected (distance cutoff for redundant conformers equal to 1.0 Å). The *ab-initio* calculations were carried out on a Intel Xeon powered cluster running Jaguar 7.6 program starting from minimized geometries obtained from molecular mechanics. The structures were optimized at the Hartree-Fock (HF) 6-31G*++ level of theory, using the Schlegel guess as initial Hessian and testing optimization in vacuum or in solution using solvent model DMSO or water. The following parameters were selected to control SCF convergence: accurate accuracy level, 1e-07 hartree as maximum energy change, while default values were leaved unchanged for all the remaining parameters. The protocol applied to perform the docking global searches has been previously described in details.[17] In this study, a

semirigid docking was performed, in which the input host geometry was frozen according to BatchMin FXAT command. Docking local searches were carried out by setting BatchMin MCMM arg4 to the value of 1. In this way, each Monte Carlo step began with the original structure, in which guest **15** was accommodated within the external pocket.

4.5 References

[1] D. Voet, J. G. Voet C. W. Pratt, *Fundamentals of Biochemistry*, John Wiley & Sons, Inc., New York, **1999**.

[2] H. Van Belle, *Cardiovasc. Res.*, **1993**, *27*, 68-76.

[3] S. A. Baldwin, J. R. Mackey, C. E. Cass, D. J. Young, *Mol. Med. Today*, **1999**, *5*, 216-224.

[4] A. B. Da Rocha, R. M. Lopes, G. Schwartsmann, *Curr. Opin. Pharmacol.*, **2001**, *1*, 364-369.

[5] H. Anderson, P. Hopwood, R. J. Stephens, N. Thatcher, B. Cottier, M. Nicholson, R. Milroy, T. S. Maughan, S. J. Falk, M. G. Bond, et al., *Br. J. Cancer*, **2000**, *83*, 447–453.

[6] P. Huang, W. Plunkett, *Cancer Chemother. Pharmacol.*, **1995**, *36*, 181-188.

[7] A. Gelibter, P. Malaguti, S. Di Cosimo, E. Bria, E. M. Ruggeri, P. Carlini, F. Carboni, G. M. Ettorre, M. Pellicciotta, D. Giannarelli, E. Terzoli, F. Cognetti, M. Milella, *Cancer*, **2005**, *104*, 1237-1245.

[8] a) A. D. Adema, I. V. Bijnsdorp, M. L. Sandvold, H. M. Verheul, G. J. Peters, *Curr. Med. Chem.*, **2009**, *16*, 4632-4643; b) L. Hajdo, A. B. Szulc, B. Klajnert, M. Bryszewska, *Drug. Dev. Res.*, **2010**, *71*, 383-394.

[9] B. Botta, I. D'Acquarica, L. Nevola, F. Sacco, Z. Valbuena Lopez, G. Zappia, C. Fraschetti, M. Speranza, A. Tafi, F.

Caporuscio, M. C. Letzel, J. Mattay, *Eur. J. Org. Chem.*, **2007**, 5995-6002.

[10] B. Botta, A. Tafi, F. Caporuscio, M. Botta, L. Nevola, I. D'Acquarica, C. Fraschetti, M. Speranza, *Chem. Eur. J.*, **2008**, *14*, 3585-3595.

[11] B. Botta, C. Fraschetti, F. R. Novara, A. Tafi, F. Sacco, L. Mannina, A. P. Sobolev, J. Mattay, M. C. Letzel, M. Speranza, *Org. Biomol. Chem.*, **2009**, *7*, 1798-1806.

[12] B. Botta, C. Fraschetti, I. D'Acquarica, F. Sacco, J. Mattay, M. C. Letzel, M. Speranza, *Org. Biomol. Chem.*, **2011**, *9*, 1717-1719.

[13] a) C. S. Johnson Jr., *Prog. Nucl. Magn. Reson. Spectrosc.*, **1999**, *34*, 203; b) G. A. Morris, Diffusion-ordered spectroscopy (DOSY). In: *Encyclopedia of Nuclear Magnetic Resonance*, Vol. 9 (Eds: D. M. Grant, R. K. Harris), John Wiley, Chichester, **2002**, pp. 35-44.

[14] L. Fielding, *Tetrahedron*, **2000**, *56*, 6151-6150.

[15] a) D. Neuhaus, M. P. Williamson, *The Nuclear Overhauser Effect in Structural and Conformational Analysis*, WILEY-VCH, New York, **1989**; b) G. Valensin, G. Sabatini and E. Tiezzi, In: *Advanced Magnetic Resonance Techniques in Systems of High Molecular Complexity* (Eds: N. Niccolai, G. Valensin), Birkhauser, Boston, **1986**, pp. 69-76.

[16] B. Botta, M. C. Di Giovanni, G. Delle Monache, M. C. De Rosa, E. Gacs-Baitz, M. Botta, F. Corelli, A. Tafi, A. Santini, E. Benedetti, C. Pedone, D. Misiti, *J. Org. Chem.*, **1994**, *59*, 1532-1541.

[17] B. Botta, F. Caporuscio, I. D'Acquarica, G. Delle Monache, D. Subissati, A. Tafi, M. Botta, A. Filippi, M. Speranza, *Chem. Eur. J.*, **2006**, *12*, 8096-8105.

5. Gas-phase enantioselective reactions of basket resorc[4]arenes

5.1 Introduction

The study of the forces involved in the interactions that occurs in nature, for example between proteins and small organic molecules, is the first step toward a deeper knowledge of the mechanisms on wich life is based. Molecular recognition, infact, plays a keyrole in most of biological processes. Chirality is another fundamental aspect to be taken in consideration. Virtually all biological processes involve chiral molecules of appropriate shape and size holding suitable functionalities in specific positions. Their shape-specific interactions with suitable dissymmetric receptors are at the basis of chiral recognition and biocatalysis. The remarkable catalytic proficiency of natural and synthetic receptors is because of a combination of the following: (i) shape-specific intermolecular interactions between functionalities located on the host/guest complementary surfaces, which severely limit their translational and (overall) rotational motion, and (ii) the rate acceleration because of partial desolvation of the functionalities themselves in the host cavity.[1] Thus, solvation/desolvation phenomena may strongly affect chiral recognition and rate acceleration of biological processes and complicate the understanding of the underlying principles. For this

reason mass spectrometry (MS) represents a suiable technique to investigate these systems, because interference from the solvent and the counterion is safely excluded.[2] Although MS is traditionally regarded as a "blind" tool for stereochemical analysis, a body of evidence is nowadays available witnessing the potential of such a technique for structural and stereochemical studies.[3-14] At the same time, the ability of MS to characterize diastereomeric complexes in the absence of perturbing environmental factors and to measure with high sensitivity and reproducibility ion abundance differences make it particularly attractive when small energetic differences between diastereomeric complexes have to be determined.

Chiral recognition by MS is usually based on the measurement of following: (i) the relative abundance of noncovalent diastereomeric adducts between a chiral host and the two enantiomers (one isotopically labeled) of a guest;[5,9,15] (ii) the relative stability of diastereomeric adducts by equilibrium measurements[10,12,16] or by collision-induced dissociation (CID) experiments (Cooks' kinetic method) (thermodynamic enantioselectivity),[6,17-24] and (iii) the rates of ion/molecule reactions between diastereomeric adducts and suitable chiral or achiral reactants (kinetic enantioselectivity).[11,25-29]

In this studies, we focus our attention on the last methodology which provides precious information not only on the relative stability of diastereomeric ion-molecule complexes, but also on the dynamics and kinetics of their evolution during guest exchange processes.

Therefore we considered proton bound complexes of both enantiomers of resorc[4]arene **10** with several guests like aminoacids and dipeptides (see chart 5.1). These diasteromeric complexes generated in the gas phase were allowed to react with a chiral organic base and it was observed a reaction of displacement of the guest by the base. Some consideration about reactivity of diasteromeric complexes can be done, moreover the kinetic enantioselectivity showed by the reaction can be razionalized depending on the configuration of the host, and the guest.

5.2 Results and Discussion

5.2.1 Choice of the hosts and of the guests

We chose to explore the chiral features of the host-guest interactions involving both enantiomers of the new bis(diamido)-bridged basket resorc[4]arene **10**, (whose synthesis is reported in chapter 2) with some simple guests (see chart 5.1).

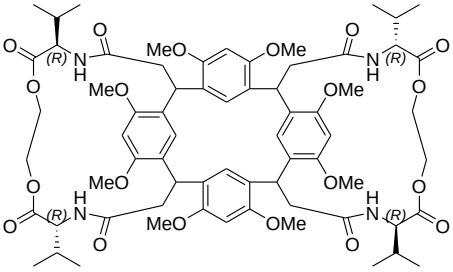

(*all-R*)-**10**

L-Phe
L-Tyr
L,L-AlaAla
L,L-AlaPhe

Chart 5.1. Host and guests considered.

Preliminary ESI-CID-MS/MS studies indicated that host **10** could form quite stable proton bound complexes with several aminoacids, especially with the aromatic ones, and these systems represent a good model of the drug-receptor interaction.

We chosed as guests: L-Phe and L-Tyr, two aromatic aminoacids wich differ only for the presence of an hydroxyl group on the aromatic ring in the tyrosine; L,L-AlaAla and L,L-AlaPhe, which are structurally similar dipeptides. For this reasons we decided to investigate the kinetic enantioselectivity of proton-bound $[M•H•A]^+$ complex between the chiral hosts (*all-R*)-**10** or (*all-S*)-**10** and the guests indicated in chart 5.1 by measuring the reaction rates of the displacement of the guest from the complex by an organic base ((*R*)-(–)-2-butylamine). At the state of the arts we only performed ESI-FTICR studies and we do not posses any theoretical calculations data. In future we will perform QM and MD calculations in order to better interpretation the experimetal data.

5.2.2 Methodology

The methodology, employed for measuring the kinetic enantioselectivity in the gas phase, is based on the generation of a proton-bound $[M•H•A]^+$ complex between a chiral host M and a chiral guest A by electrospray ionization (ESI) of suitable M/A mixtures. Typically, 1×10^{-5} M methanolic solutions containing equimolar amounts of M and A were electrosprayed through a heated

capillary (130°C) into the external source of the FTICR mass spectrometer. The proton-bound $[M•H•A]^+$ complex is transferred into the resonance cell of a Fourier-transform ion cyclotron resonance mass spectrometer (FT-ICR-MS) by a system of potentials and lenses and quenched by collisions with an inert gas (e.g., methane) pulsed into the cell through a magnetic valve. Then, the complex is isolated by broad-band ejection of the accompanying ions and allowed to react in the presence of an externally introduced chiral or achiral reagent B present in the cell at a fixed pressure (from 10^{-8} to 10^{-7} mbar depending on its reactivity) (eq. 1).

$$[M•H•A]^+ + B \rightarrow A + [M•H•B]^+ \quad (1)$$

The rate constant of the guest exchange reaction 1 is extracted based on the decay of the isolated ion $[M•H•A]^+$ as a function of time *t*. If *I* is the intensity of complex $[M•H•A]^+$ at the delay time *t* and I_0 is the sum of the intensities of $[M•H•A]^+$ and $[M•H•B]^+$, a mono-exponential $\ln(I/I_0)$ versus *t* plot is often obtained whose slope provides the pseudo-first-order rate constant *k'* for reaction 1 (Fig. 5.1).

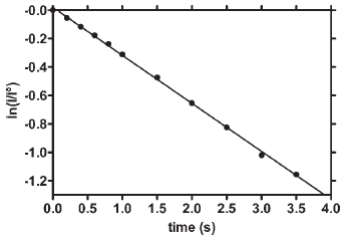

Figure 5.1. Mono-exponential kinetic plot of the gas-phase reaction between $[M•H•A]^+$ and B.

The corresponding second-order rate constants *k* are calculated from the ratio between the slope of the first-order plots and the B concentration ($k = k'/[B]$). If their values are compared with the relevant collision rate constants (k_C), estimated according to Su's trajectory calculation method,[34] a direct extimation of the efficiency of the reaction ($eff = k/k_C$) can be obtained.

In some instances, the $\ln(I/I_0)$ versus *t* plot is not linear and presents a curvature which denotes the occurrence of bi-exponential kinetics (upper curve of Fig. 5.2). This is because of the coexistence of at least two stable isomeric structures for $[M•H•A]^+$, one less reactive (denoted with the slow subscript) and the other more reactive (denoted with the fast subscript).[15,28–33] The time dependence of $[M•H•A]^+_{fast}$ (open circles in Fig. 5.2) can be inferred from the overall $[M•H•A]^+$ decay (solid circles in Fig. 5.2) after subtracting the first-order decay of $[M•H•A]^+_{slow}$ (upper line in Fig. 5.2). The Y-intercepts of the first-order decay of $[M•H•A]^+_{slow}$ and $[M•H•A]^+_{fast}$ provide an estimate of their relative distribution. In contrast, any mono-exponential kinetics is generally attributed to the occurrence of a single structure or, alternatively, of several stable isomers, but with comparable reactivity toward B.

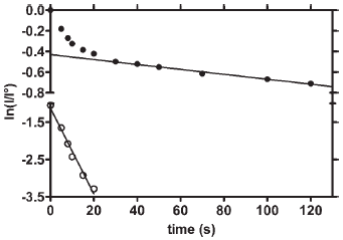

Figure 5.2. Bi-exponential kinetic plot of the gas-phase reaction between $[M•H•A]^+$ and B.

Kinetic enantioselectivity of reaction 1 is obtained by comparing the second-order rate constants *k* for the same reaction involving the diastereomeric $[M_R•H•A]^+$ and $[M_S•H•A]^+$ complexes. When the host and the guest in the complex have the same configuration (L-aminoacids have *S*- configuration), the rate constant is denoted as k_S; when instead they have opposite configurations (i.e. M_R host has *R*-configurtion, because the guest has fixed *S*- configuration), the rate constant is denoted as k_R. The enantioselectivity factor ρ is expressed by the k_S/k_R ratio. When the guest exchange 1 involves a chiral reactant B (either B^S or B^R), another enantioselectivity factor ξ can be extracted from the kinetic results, based on the rate constant ratio of the same reaction involving B^R (k_{BR}) and B^S (k_{BS}), namely $\xi = k_{BR}/k_{BS}$. A $\rho > 1$ value indicates that the reactant B displaces the guest from the homochiral (host and guest with *S*- configuration) complex faster that the guest from the heterochiral one (host with *R*-configuration and guest with *S*-). The opposite is true when $\rho < 1$. A $\rho = 1$ value corresponds to equal displacement rates. Analogously, a $\xi > 1$ value indicates that the displacement of the A guest from a

given $[M•H•A]^+$ diastereomer is faster with B^R than with B^S. Again, the opposite is true when $\xi < 1$. A $\xi = 1$ value corresponds to equal displacement rates. In these preliminary studies we used just one enantiomer of a chiral amine as reactant gas, therefore for now we will not take into consideration the ξ factor. In the future we will perform the same gas phase reactions showed in this chapter, using (*S*)-(+)-2-butylamine as reactant gas B. With these more data we will be able also to evaluate the ξ factor.

5.2.3 Determination of the exchange rate constants

On the base of the methodology indicated we calculated the exchange rate constants for reaction 1 between $[M•H•A]^+$ complexes and (*R*)-(–)-2-butylamine. For all the complexes the raction showed bi-exponential kinetic plots (Figure 5.3) that indicates the presence of two populations of complexes, one of wich reacts faster than the other which reacts slower. The k_S/k_R ratio provided also ρ factors, which give information about enantioselectivity of the reaction. The results are reported in Table 5.1. Molar fractions (x_{fast}, x_{slow}, see Table 5.1) of $[M•H•A]^+_{slow}$ and $[M•H•A]^+_{fast}$ were extimated from Y intercepts of linear fitting of the experimental data (Figure 5.3). Their values indicate that $[M•H•A]^+_{fast}$ are more aboundant than $[M•H•A]^+_{slow}$ (about 6:4) when A is a simple aminoacid. On the other hand, an inversion of the population occur when A is a dipeptide, infact the $[M•H•A]^+_{slow}$ complex becomes the most aboundant with a x_{slow} of about 0.60 or higher (see Table 5.1).

Table 5.1. Exchange rate constants ($k \times 10^{-10}$ cm^3 molecule^{-1} s^{-1}) for reaction 1 between $[M•H•A]^+$ complexes and (*R*)-(–)-2-butylamine ($P_B = 2.8 \times 10^{-10}$ mbar), molar fractions (x_{fast}, x_{slow}) of $[M•H•A]^+_{slow}$ and $[M•H•A]^+_{fast}$ complexes, ρ factors are also given.

Host (M)	Guest (A)	x_{fast}	k_{fast}	x_{slow}	k_{slow}	ρ_{fast}	ρ_{slow}
(*all-R*)-**10**	L-Phe	0.64	6.52±1.17	0.36	1.54±0.28	1.32±0.33	0.98±0.25
(*all-S*)-**10**	L-Phe	0.63	8.60±1.54	0.37	1.51±0.28		
(*all-R*)-**10**	L-Tyr	0.65	3.03±0.42	0.35	0.41±0.06	0.57±0.11	0.20±0.04
(*all-S*)-**10**	L-Tyr	0.56	1.72±0.24	0.44	0.08±0.01		
(*all-R*)-**10**	L,L-AlaAla	0.26	1.13±0.25	0.74	0.010±0.002	3.88±0.88	25.0±4.0
(*all-S*)-**10**	L,L-AlaAla	0.40	4.38±0.20	0.60	0.26±0.02		
(*all-R*)-**10**	L,L-AlaPhe	0.32	0.37±0.04	0.68	0.003±0.001	1.80±0.30	22.5±6.0
(*all-S*)-**10**	L,L-AlaPhe	0.38	0.66±0.09	0.62	0.059±0.008		

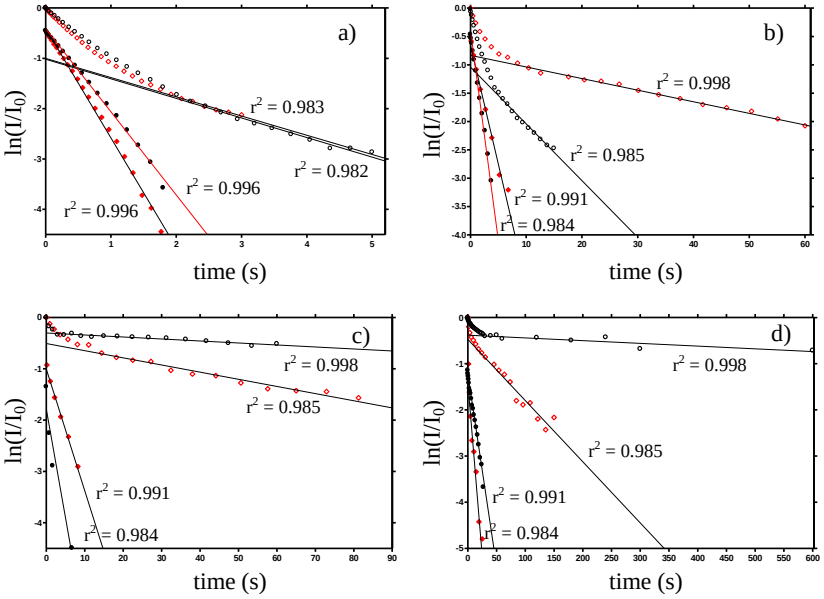

Figure 5.3. Semilogarithmic kinetic plots of reaction 1 between (*R*)-(–)-2-butylamine ($P_B = 2.8 \times 10^{-10}$ mbar) and respectively: a) $[$**10**•H•L-Phe$]^+$, b) $[$**10**•H•L-Tyr$]^+$, c) $[$**10**•H•L-AlaAla$]^+$, d) $[$**10**•H•L-AlaPhe$]^+$, black dots = [(*all-R*)-**10**•H•A]$^+$, red dots = [(*all-S*)-**10**•H•A]$^+$.

If we look at the ρ factors we can see that that the reaction 1 does not show any enantioselectivity (ρ = 0.98) for the $[M•H•L\text{-}Phe]^+_{slow}$ diasteromeric complexes, and low selectivity for $[(all\text{-}S)\text{-}\mathbf{10}•H•L\text{-}Phe]^+_{fast}$ which reacts moderately faster than $[(all\text{-}R)\text{-}\mathbf{10}•H•L\text{-}Phe]^+_{fast}$ (see Table 5.1). The presence of the phenolic OH group in L-tirosine determines a dramatic effect on the diasteromeric complexes. Enatioselectivity, in fact, increase for both slow and fast complexes, but in this case $[(all\text{-}R)\text{-}\mathbf{10}•H•L\text{-}Tyr]^+_{fast}$ and $[(all\text{-}R)\text{-}\mathbf{10}•H•L\text{-}Tyr]^+_{slow}$ have the higher exchange rate constants. This inversion of selectivity is quite curious and it was observed only for the complexes containing L-tyrosine as guest. Future theoretical calculations could explain why such a small modification (the OH group in L-tyrosine) can lead to an inversion of tendence on enantioselectivity.

Complexes containg L-AlaAla compared with $[M•H•L\text{-}Phe]^+$ shows a very high increase of the enantioselectivity. Infact $[(all\text{-}S)\text{-}\mathbf{10}•H•L\text{-}AlaAla]^+_{fast}$ reacts with B about four time faster than $[(all\text{-}R)\text{-}\mathbf{10}•H•L\text{-}AlaAla]^+_{fast}$, moreover enantioselectivity rises surprisingly to 25 (see Table 5.1), if we consider the ρ_{slow}. This means that $[(all\text{-}S)\text{-}\mathbf{10}•H•L\text{-}AlaAla]^+_{slow}$ reacts with B twenty-five times faster than $[(all\text{-}R)\text{-}\mathbf{10}•H•L\text{-}AlaAla]^+_{slow}$. This effect appars to be due to the presence of dipeptides as guest, indeed a similar trend can be found for $[M•H•L\text{-}AlaPhe]^+$ complexes. Also in this case a good enantioselectivity for $[(all\text{-}R)\text{-}\mathbf{10}•H•L\text{-}AlaPhe]^+$ was found (ρ_{fast} = 1.80, ρ_{slow} = 22.5), it is

interesting to note that changing the guest from L-Phe to L,L-AlaPhe enantioselectivity rises up, especially considering the slow complexes. It is possiblible that the differences between the exchange rate constants depend on structural differences between the diastereoisomeric complexes. This structural details can be put in light by computational calculation.

5.3 Conclusion

We saw as both enantiomer of bis(diamido)-bridged basket resorc[4]arene **10** can behave as an highly preorganized receptor capable to interact with aminoacids and dipeptides forming proton bound complexes. These diastereoisomeric complexes, generated in gas phase by electrospray ionization, were allowed to react with (*R*)-(–)-2-butylamine and in all cases bi-exponential kinetic plots were obtained. This means that there are at least to populations of each diasteromeric complex $[M•H•A]^+_{fast}$ and $[M•H•A]^+_{slow}$, one of which reacts faster than the other one. The k_S/k_R ratio provided ρ factors which gave information about the enantioselectivity of the exchange reaction. In most cases homochiral complexes (*all-S*- configuration of the host **10**) show higer reactivity, moreover if we consider $[M•H•A]^+_{slow}$ complexes enantioselectivity is considerably increased. $[M•H•L\text{-}Phe]^+$ complexes show low selectivity, but when L-Tyr is used as guest the enantioselectivity grows up, but favouring the

reaction of [(*all-R*)-**10**•H•L-Tyr]$^+$ for both slow and fast complexes. This effect can be attributed to the presence of the hydroxyl group in L-tirosine and it is notable that a small structural difference can lead to such a big difference between the reactivity of the diasteromeric complexes. Considering the complexes involving L,L-AlaAla and L,L-AlaPhe as guest, in both cases the exchange reaction with B resuts to be faster when the complex involve (*all-S*)-**10** enantiomer. In particular the [(*all-S*)-**10**•H•L-AlaAla]$^+_{slow}$ complex reacts more than twenty times faster than [(*all-R*)-**10**•H•L-AlaAla]$^+_{slow}$. The same trend was found for [$M_{R/S}$•H•L-AlaPhe]$^+_{slow}$ complexes. This experimental observation indicate that there is a remarkable difference between the stability of the diasteromeric complexes. Probably they assume different structures, depending on the configuration of the resorcarene **10** host and of the guest. As we saw in the previous chapters, the host have different pockets with which the guest can interact forming the complex, therefore different *in* or *out* structures can be generated with different relative stability. We want to perform MD and QM calculations on these systems in order to predict the relative stability of each complex and to deeply understand the interactions involving the formation of the diasteromeric complexes.

5.4 Experimental Section

General Remarks. All reagents and solvents were purchased from Sigma-Aldrich and used without further purification. FTICR experiments were performed with an APEX III (7 T Magnet) FTICR mass spectrometer equipped with an Apollo ESI source (Bruker Daltonik GmbH, Bremen).

FTICR experiments. All Stock solutions (5.0×10^{-5} M in CH_3OH) of either (*all-R*)-**10** or (*all-S*)-**10** containing a ten fold excess of guest were electrosprayed through a heated capillary (T = 130 °C) into the external source of the FTICR mass spectrometer, and the resulting positive ions were transferred into the analyzer cell. Abundant signals corresponding to the natural isotopomers of the proton-bound complex $[M•H•A]^+$ were monitored and isolated by broad-band ejection of the accompanying ions. When a background pressure of about 2.8×10^{-8} mbar of the chiral amine (*R*)-(–)-2-butylamine was introduced into the FTICR cell, the exchange reaction [Equation (1)] exclusively took place. The appearance of the exchanged product $[M•H•B]^+$ was monitored as a function of time. All the exchange reactions represented by Equation (1) obey bi-exponential pseudo-first-order kinetics. This indicates that the $[M•H•A]^+$ complexes were thermalized in their reactions with B. The corresponding second-

order rate constants k_{fast} and k_{slow} were calculated from the ratio between the slopes of the first-order plots and the B pressure.

5.5 References

[1] F. Hollfelder , A. J. Kirby, D. S. Tawfik, *Nature*, **1996**, *383*, 60-63.

[2] A. Filippi, F. Gasparrini, M. Pierini, M. Speranza, C. Villani, *J. Am. Chem. Soc.*, **2005**, *127*, 11912.

[3] A. Filippi, A. Giardini, S. Piccirillo, M. Speranza, *Int. J. Mass. Spectrom.*, **2000**, *198*, 137-163.

[4] M. Speranza, *Int. J. Mass. Spectrom.*, **2004**, *232*, 277-317.

[5] M. Sawada, *Mass. Spectrom. Rev.*, **1997**, *16*, 73-90.

[6] W. A. Tao, R. G. Cooks, *Anal. Chem.*, **2003**, *75*, 25A-31A.

[7] M. G. Finn, *Chirality*, **2002**, *14*, 534-540.

[8] J. S. Splitter, F. Turecek, *Applications of mass spectrometry to organic stereochemistry*, New York: VCH Publishers; **1994**.

[9] M. Sawada, Chiral mass spectrometry, in: T. Matsuo, R. M. Caprioli, M. L. Gross, T. Seyama, editors. *Biological mass spectrometry: present and future*. [Proc. Kyoto '92 Int. Conf.] New York: Wiley, **1994**.

[10] C. A. Schalley, *Int. J. Mass. Spectrom.*, **2000**, *194*, 11-39.

[11] C. B. Lebrilla, *Acc. Chem. Res.*, **2001**, *34*, 653-661.

[12] D. V. Dearden, Y. Liang, J. B. Nicoll, K. A. Kellersberger, *J. Mass. Spectrom.*, **2001**, *36*, 989-997.

[13] K. A. Schug, W. Lindner, *J. Sep. Sci.*, **2005**, *28*, 1932-1955.

[14] P. Dwivedi, C. Wu, L. M. Matz, B. H. Clowers, W. F. Seims, H. H. Hill, *Anal. Chem.*, **2006**, *78*, 8200-8206.

[15] E. N. Nikolaev, E. V. Denisov, V.S. Rakov, J. H. Futrell, *Int. J. Mass Spectrom.*, **1999**, *182/183*, 357-368.

[16] Y. Liang, J. S. Bradshaw, D. V. Dearden, *J. Phys. Chem. A.*, **2002**, *106*, 9665-9671.

[17] K. Vékey, G. Czira, *Rapid Commun. Mass Spectrom.*, **1995**, *9*, 783-787.

[18] W. A. Tao, L. Wu, R. G. Cooks, *Chem. Commun.*, **2000**, 2023-2024.

[19] W. A. Tao, D. Zhang, E. N. Nikolaev, R.G. Cooks, *J. Am. Chem. Soc.*, **2000**, *122*, 10598-10609.

[20] W. A. Tao, R. G. Cooks, *Eur. J. Mass Spectrom.*, **2002**, *8*, 107-115.

[21] W. A. Tao, R. L. Clark, R. G. Cooks, *Anal. Chem.*, **2002**, *74*, 3783-3789.

[22] W. A. Tao, R. G. Cooks, *Angew. Chem. Int. Ed. Engl.*, **2001**, *40*, 757-760.

[23] W. A. Tao, F. G. Gozzo, R. G. Cooks, *Anal. Chem.*, **2001**, *73*, 1692-1698.

[24] L. Wu, R. G. Cooks, *Anal. Chem.*, **2003**, *75*, 678-684.

[25] J. Ramirez, F. He, C. B. Lebrilla, *J. Am. Chem. Soc.*, **1998**, *120*, 7387-7388.

[26] J. Ramirez, S. Ahn, G. Grigorean, C. B. Lebrilla, *J. Am. Chem. Soc.*, **2000**, *122*, 6884-6890

[27] J. F. Gal, M. Stone, C. B. Lebrilla, *Int. J. Mass Spectrom.*, **2003**, *222*, 259-267.

[28] S. Ahn, J. Ramirez, G. Grigorean, C. B. Lebrilla, *J. Am. Soc. Mass Spectrom.*, **2001**, *12*, 278-287.

[29] G. Grigorean, C. B. Lebrilla, *Anal. Chem.*, **2001**, *73*, 1684-1691.

6. Acknowledgements

Ringrazio il Prof. Antonello Filippi, il Prof. Maurizio Speranza per l'opportunità che mi hanno offerto lavorando con loro e per la loro disponibilità. Ringrazio la Dott.ssa Caterina Fraschetti per il prezioso aiuto pratico e morale, per avermi fatto compagnia a Bielefeld, e per essermi stata vicino nei momenti difficili. Ringrazio il Prof. Bruno Botta per avermi dato l'opportunità di collaborare con il suo gruppo. Grazie a tutto il laboratorio del Prof. Botta nel quale negli anni ho visto diversa gente andare e venire, in particolare: Fabiola Sacco, Francesca Ghirga, Carmela Molinaro, Roberta Torge, Antonella Cerreto, Alessandra Mascarello, Violeta Markovic, Sevgi Sahin, Sara Toscano, Deborah Quaglio, Cinzia Ingallina, Luca Santi, Patrizio Ghirga, Virginia Vighi, Palma Notarantonio e la mia amica di vecchia data Valentina Iovine. A lei un grazie particolare per la sua amicizia e per avermi sempre aiutato. Grazie anche a Dorina Kotoni per essere sempre così carina, gentile e disponibile nei miei confronti. Ringrazio il Prof. Pierini per il suo costante buon umore, la sua disponibilità e le ottime caramelle e cioccolatini. Grazie alla Dott.ssa Ilaria D'Acquarica per i suoi consigli e aiuti. Ringrazio la Dott.ssa Alessia Ciogli per i presiosi consigli sull'HPLC. Grazie a Simona per l'allegria e i suoi ottimi tiramisù. Grazie a Patrizia e Rocchina per la loro straordinaria simpatia e allegria, e in particolare a Rocchina per le analisi MS, ti sono debitore! Grazie al Prof. Giancarlo Fabrizi e a tutto il suo laboratorio per il loro prezioso aiuto

con l'NMR. Ringrazio la Prof. Gloria Uccello-Barretta, la Dott.ssa Federica Aiello e la Dott.ssa Federica Balzano per l'opportunità di collaborare con loro. Ringrazio il Prof. Andrea Tafi e il Dott. Nicolò Pesci per i calcoli computazionali. Thanks to Prof. Harald Groeger and Prof. Jochen Mattay for giving me the opportunity to work with FTICR at Bielefeld University. Thanks to Dr. Matthias Letzel for his precious and needful help with FTICR. Thanks to Christian for enjoying my stay in Bielefeld. Ringrazio i miei genitori e la mia famiglia per avermi sempre aiutato, incoraggiato e sopportato. Ringrazio Carlos, Luca, Valeria, Davide, Paolo, Sara e tutti i miei amici per essermi stati sempre vicino.